NICKEL POWDER PRECIPITATION BY HIGH-PRESSURE HYDROGEN REDUCTION

by

Freeman Ntuli

Thesis Presented for the Degree of

DOCTOR OF PHILOSOPHY

in the Department of Chemical Engineering
Faculty of Engineering and the Built Environment
UNIVERSITY OF CAPE TOWN

August 2008

ABSTRACT

The effect of impurities on the precipitation behaviour of nickel powder produced by high-pressure hydrogen reduction was investigated in order to determine the factors responsible for the formation of powder with undesirable morphology. In nickel precipitation by hydrogen reduction, two product morphologies have been observed: the spherical, open powder (desirable) and the spherical, closing/closed powder (undesirable). Two major impurities were studied namely; a morphology modifier (a polyacrylic acid derivative) used as an additive and iron which is an inherent impurity. Reduction experiments to investigate the effects of the morphology modifier were conducted on a pilot-plant scale using a 75 L autoclave with modifier dosages in the range of 0.25-5 vol %. Experiments to investigate the effects of iron were conducted on a laboratory scale using a 0.5 L autoclave fitted with a Teflon reaction beaker. Both autoclaves were fitted with a double impeller configuration consisting of an upper axial impeller and lower Rushton turbine. Iron was added to the reduction solution as ferrous sulphate solution (acidified to pH 2.5 to prevent oxidation) to give reduction solutions with Fe^{2+} concentrations of 6, 20 and 200 mg/L. Reduction was conducted at a temperature between 180-190 ^{o}C and 2800 kPa pressure using a nickel ammine sulphate solution (free NH_3:Ni^{2+} and $(NH_4)_2SO_4$:Ni^{2+} molar ratios of 2.0-2.1 and 2.2 respectively). Nickel powder samples were collected from the autoclaves after each successive batch reduction (densification) within a cycle. The powder was then separated from the mother liquor before being washed and dried for subsequent analysis. The concentration of the nickel before and after reduction was also measured to establish the nickel depletion rate.

The effects of the selected impurities were investigated by analysing the nickel depletion rates, SEM micrographs, powder purity and transforming the particle size distribution (PSD) data of the powder samples into moments. The evolution of the moments, volume or mass moment mean size (*D(4.3)*), number based mean size ($\overline{L}_{1.0}$) and BET surface area were used to generate information on the particle rate processes responsible for powder formation. These findings were validated by means of mathematical models based on the moment form of the population balance equation.

The morphology modifier was found to act as a growth inhibitor, thus, decreasing the aggregation rate and making the powder more prone to breakage. Iron was found to induce surface nucleation, thus, creating more growth sites on the particle surface leading to an increase in the growth rate. Based on mathematical modelling results and evidence from SEM micrographs, the spherically shaped nickel powder particles were proposed to be formed through the formation of a pre-cursor by secondary aggregation followed by spherulitic growth. The degree of compactness of the spherulites (open or closed formation) was proposed to be determined by the number of active growth sites on the nickel particle surface. The morphology modifier was found to decrease the number of growth sites as a result of growth inhibition leading to the production of more open spherulites which are more prone to shear-induced breakage. Iron was found to increase the number of growth sites as a result of surface nucleation leading to more compact spherulites which are more resistant to shear-induced breakage. Based on these findings a modifier dosage of less than 1 vol % and Fe levels of less than 6 mg/L are recommended if spherical, open particles are desired. Thus, by characterising the effect of any impurity on growth it is possible to predict its impact on particle morphology.

ACKNOWLEDGEMENTS

Appreciation is expressed to my supervisor, Prof. Alison Emslie Lewis for her sustained interest and guidance in carrying out this research project and in the preparation of this thesis.

Appreciation is also expressed to Impala Platinum Refineries for granting me an opportunity to work in their plant and make use of their pilot plant and other materials and equipment during the course of the project. Their financial support and provision of material and information used in this project is greatly appreciated. Special thanks to Hurbert Ramagwede and Hans Grobbeller who were instrumental in assisting me to conduct the experiments and integrating me within the company.

The author also gratefully acknowledges the grant-holder bursary offered by the National Research Foundation of South Africa and the Department of Chemical Engineering at UCT.

Many thanks to Melinda Waldron of the Electron Microscope Unit (EMU) at UCT for her assistance in using the SEM and Helen Davy for helping with the laser diffraction technique, BET measurements and nickel analysis.

Appreciation is also expressed to the former and current work colleagues in the Crystallisation and Precipitation Unit at UCT for their support and encouragement in the course of this project namely; Mfandaedza, Christian, Fran, Rob, Thebe, Yifei, Ochieng, Cello, Jeeten and Christine.

To my wife, Faith and son Mthabisi thank you for your emotional and moral support.

Lastly I thank God, without whose guidance and sustenance, this work would never have succeeded.

NOTATION

A_s	surface area of the nickel particles (m^2)
B	birth rate ($m^{-1}.m^3.s^{-1}$)
B^o	nucleation rate ($\#.s^{-1}m^{-3}$)
$\overline{B_j}$	moment form of the birth rate ($m^{-j}.m^3.s^{-1}$)
c	actual local concentration (M)
c^*	saturation concentration (M)
Δc	concentration driving force (M)
D	death rate ($m^{-1}.m^3.s^{-1}$)
$\overline{D_j}$	death rate ($m^{-j}.m^3.s^{-1}$)
D_{max}	upper limiting agglomerate size (μm)
E	activation energy ($J.mol^{-1}$)
G	growth rate when linear dimension is used as a measure of size ($m.s^{-1}$)
F	Faraday's constant
k_1	rate constant ($mol.s^{-1}.rpm^{-1}.Pa^{-1}.m^{-2}$)
k_2 ; k_4	rate constant ($mol.s^{-1}.m^{-2}.Pa^{-1}$)
k_3 ; k_6	rate constant (s^{-1})
k_5	rate constant ($Pa^{-1}.K^{-1}.\ s^{-1}$)
k_7	rate constant ($s^{-1}.Pa^{-1}$)
k_{bo}	size independent factor of the breakage frequency (s^{-1})
k_b	breakage frequency (s^{-1})
m_j	jth moment of the number length distribution ($\#.m^{j-3}$)
l_o	characteristic size of appearance of nuclei (m)
L	particle size or linear dimension (m)
N	number of nuclei or particles per unit volume ($\#.m^{-3}$)
N_o	number of particles present per unit volume i.e. before aggregation ($\#.m^{-3}$)
n	number density per unit volume of suspension (m^{-4})
$[Ni^{2+}]$	concentration of nickel in solution ($mg.L^{-1}$)
P_{H_2}	partial pressure of hydrogen (Pa)
R	stirrer speed (rev/s)
R	molar gas constant ($kPa.m^3/kg\ mol.K$)
t	time (s)
T	temperature (K)
V	volume of solids in suspension (m^3)
V_m	molar volume of solid ($m^3.mol^{-1}$)

Greek Symbols

α	ratio of catalytically active surface area to actual surface area
β	symmetry factor
β_o	aggregation rate constant or kernel ($m^3.\#^{-1}.s^{-1}$)
λ	particle size, length (m)
ε	particle volume in PBE (m^3)
ε	applied potential (V)
ε_{eqm}	equilibrium potential (V)
$\Delta\varepsilon$	potential difference (V)
μ	chemical potential (J/mol)
η	overpotential (V)
i	current (A)
i_o	exchange current density in (A/m^2)
v	particle volume in PBE (m^3)
$v_{electrodic}$	rate of the electrochemical reaction ($moles/cm^2s^{-1}$)
ρ	density (kg/m^3)
τ	time constant

Superscripts

$\bar{}$	average
$'$	expressed as function of particle volume

Subscripts

a	due to aggregation
b	due to breakage

Acronyms

BET	Brunauer, Emmet and Teller
PBE	Population Balance Equation
PGM	Platinum Group Metals
PSD	Particle Size Distribution
SEM	Scanning Electron Microscope
SAFT	Surface Analyser for Trace Elements

TABLE OF CONTENTS

1 INTRODUCTION 1

1.1 MOTIVATION AND AIM 1
1.2 OUTLINE 3

2 LITERATURE REVIEW 4

2.1 CHEMISTRY OF HYDROGEN REDUCTION 4
2.2 REDUCTION KINETICS 7
2.3 PARTICLE RATE PROCESSES 10
2.3.1 Nucleation 11
2.3.2 Growth 11
2.3.3 Aggregation and breakage 12
2.3.4 Population Balance Modelling 13
2.4 FACTORS AFFECTING THE PRODUCT QUALITY 15
2.4.1 Foreign substances 15
2.4.2 pH 17
2.4.3 Hydrodynamics 17
2.4.4 Rate of Reaction and Temperature 18

3 EFFECTS OF IRON 20

3.1 INTRODUCTION 20
3.2 EXPERIMENTAL 22
3.2.1 Apparatus and reagents 22
3.2.2 Experimental programme 24
3.2.3 Procedure 25
3.3 RESULTS AND DISCUSSION 27
3.3.1 Repeatability studies 27
3.3.2 Nickel depletion rate 29
3.3.3 Evolution of the PSD of nickel powder in the presence of iron 29
3.3.4 Evolution of the moments in the presence of iron 31
3.3.5 BET surface area and SEM micrographs 36
3.3.6 Powder purity results 39
3.3.7 Population balance 39
3.3.8 Mechanisms of nickel precipitation in the presence of iron 40
3.4 CONCLUSION 41

4. EFFECTS OF A MORPHOLOGY MODIFIER 43

4.1 INTRODUCTION 43
4.2 EXPERIMENTAL 44
4.2.1 Apparatus and reagents 44
4.2.2 Procedure 45
4.3 RESULTS AND DISCUSSION 47
4.3.1 Attainable number of densifications 47
4.3.2 Nickel depletion rate 48
4.3.3 Evolution of PSD of nickel powder 48
4.3.4 Moments evolution 50
4.3.5 BET surface area 54
4.3.6 SEM and SAFT results 55
4.3.7 Proposed mechanism of action of the modifier 57
4.4 CONCLUSION 58

5. KINETIC MODELLING OF NICKEL REDUCTION 59

5.1 MATHEMATICAL MODELS 59
5.1.1 Aggregation 60
5.1.2 Aggregation and growth 60
5.1.3 Nucleation and aggregation 61
5.1.4 Nucleation and growth 61
5.1.5 Aggregation and breakage 62
5.2 RESULTS AND DISCUSSION 63
5.2.1 Reduction under standard operating conditions 64
5.2.2 Reduction in the presence of iron 66
5.2.3 Reduction in the presence of a morphology modifier 72
5.3 PARTICLE FORMATION 78
5.4 CONCLUSION 80

6. CONCLUSIONS 82

7 SUGGESTIONS FOR FUTURE WORK 86

8. REFERENCES 87

1 INTRODUCTION

1.1 Motivation and aim

The process of nickel precipitation by hydrogen reduction was pioneered by Schaufelberger in 1946 and developed for commercial purposes by Sherrit Gordon Mines between 1950 and 1960 (Schaufelberger and Yonkes, 1956; Evans, 1968). However, research on the fundamental aspects of the metal reduction has been limited (Evans, 1968). Most of the studies on hydrogen reduction of nickel have focused on finding the optimum conditions for commercial batch operations (Saarinen *et al*., 1998). Thus there has been little fundamental research carried out in the field to develop an understanding of the process and the detailed precipitation kinetics.

In nickel precipitation by hydrogen reduction, two types of product morphologies have been observed: the spherical, open powder "botryoidal" and the spherical, closed/closing powder. Typical examples of such particles are shown in Figure 1.1, which are nickel products produced on an industrial scale.

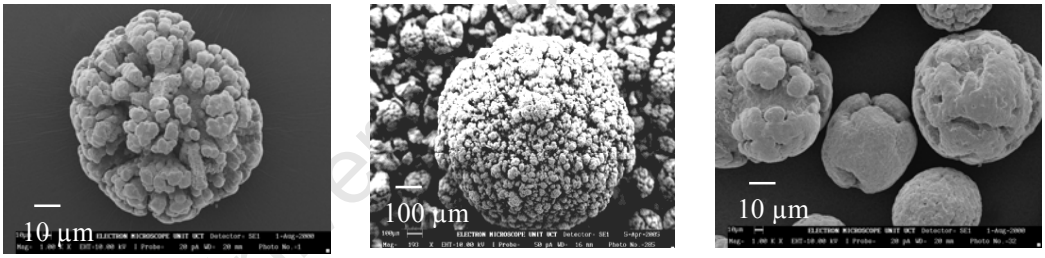

(a) **(b)** **(c)**

Figure 1.1 Morphology of nickel powder produced industrially, (a) open-desirable (b) closing undesirable and (c) closed- undesirable

The spherical, closed powder is undesirable because;

- It leads to longer reducing times (greater than 20 min). Reducing times are less than 10 min for the spherical, open powder;
- It is difficult to briquette;
- It wears out the impeller blades and the autoclave lining;
- It encapsulates impurities.

The factors that lead to the production of powder with undesirable morphology are not well understood. Furthermore, there is little understanding of the precipitation process itself, which makes it difficult to understand the effect of the mechanisms and kinetics of precipitation on the powder morphology.

The factors that have been identified as having some influence on the morphology of nickel particles are: temperature, pH, hydrogen partial pressure, presence and concentration of impurities and contamination of hydrogen by carbon monoxide (Lewis *et al.*, 2004; Lewis and Ntuli, 2005). Out of these factors, presence and concentration of impurities was identified as the most critical processing parameter influencing particle morphology.

Thus, the aim of this project was to investigate the effect of impurities on the mechanisms and kinetics of nickel precipitation with the objective of determining their impact on particle morphology.

The key question to be addressed was; how are particles with undesirable morphology formed?

Two major impurities were considered; a morphology modifier employed as an additive (intentionally added impurity) and iron which is present as an inherent impurity.

Based on the mass precipitated per batch reduction (i.e. densification), Mackiw *et al.*, 1957, postulated that the major size enlargement mechanisms in nickel reduction were aggregation (particle-particle cementation) in the early stages of a cycle (i.e. successive number of densifications) followed by growth (catalytic precipitation of metals from solution). Aggregation was found to cease after a certain critical size was reached, which was dependant mostly on the degree of agitation. However, since their conclusions were not based on actual measurements of the particle size distribution (PSD), it is the objective of this work to further study the precipitation kinetics based on the evolution of the PSD and nickel depletion rates.

The effect of additives on nickel particle morphology has also received considerable attention (Kunda *et al.*, 1965 and Kunda *et al.*, 1968). However, these studies were mainly based on scanning electron microscope (SEM) micrograph observations on the change in particle morphology obtained by using different additives, thus, could not provide adequate information on the precipitation kinetics. Change in particle morphology was mainly attributed to either particle surface activation or passivation by a particular additive.

In order to generate an understanding of the kinetics and mechanism of the precipitation process in the presence of impurities a more fundamental approach based on PSD evolution and population balance modelling is presented.

Based on these previous studies the underlying hypotheses of this project were;

- Aggregation is the dominant size enlargement mechanism in the first densifications until the limiting aggregate size (D_{max}=50μm) is reached; thereafter aggregation ceases and growth becomes the dominant size enlargement mechanism.
- Impurities that have a significant effect on morphology affect the molecular growth rate of nickel particles by changing the surface activity of the particles.

1.2 Outline

The thesis commences with an overview of the industrial process, chemistry and kinetics of nickel reduction. An overview of the precipitation kinetics and previous research done on nickel reduction is also covered.

Chapter 3 looks at the influence of iron on the precipitation behaviour of nickel based on laboratory scale studies.

Chapter 4 addresses pilot plant studies conducted on the effect of a morphology modifier on the precipitation behaviour of nickel.

A kinetic model of the nickel reduction process based on the moment form of population balance equation is presented in Chapter 5, including the mechanisms involved in particle formation.

Finally, an overall conclusion on the effect of these impurities and areas requiring further study are presented in Chapter 6 and suggestions for future work in Chapter 7.

2 LITERATURE REVIEW

The process of nickel powder precipitation by high pressure hydrogen reduction is conducted on an industrial scale in agitated vessels called autoclaves, operated in a semi-batch mode at temperatures between 180-190 ^{o}C and 2800 kPa. Nickel seed on which further reduction occurs is introduced by either by nucleation or seeding and is kept in suspension by agitation. Reduction of nickel ions from solution occurs on the surface of the suspended seed by introducing pressurised hydrogen gas until the reduction solution has been depleted of nickel. Agitation is then stopped and the nickel seed is allowed to settle. The depleted solution is then discharged leaving behind the nickel seed to catalyse subsequent batch reductions. A fresh reduction solution is then introduced and the process repeated until the nickel particles are too dense to be kept in suspension by the agitator. The powder and the final depleted solution are then discharged from the autoclave and separated by settling. Each batch reduction is termed a densification, and 50-60 densifications are conducted on an industrial scale before the powder is finally discharged. The nickel powder is then washed, dried, compacted into briquettes and then sintered in a hydrogen atmosphere to produce consolidated metal.

A brief overview of the reduction chemistry, reduction and precipitation kinetics and factors affecting the morphology of nickel particles is discussed in the sections below. Areas where further research is needed are also identified. Recent reviews of the subject are presented in the publications of Saarineen, Agrawal and their co-workers (Saarinen *et al.*, 1998; Agrawal *et al.*, 2006).

2.1 Chemistry of Hydrogen Reduction

The solution speciation of nickel ammine sulphate solutions was derived using an OLI thermodynamic simulation of the reduction solution components at 180 ^{o}C and 2800 kPa. The potential/pH diagram (Pourbaix) is shown in Fig 2.1 and helps identify the nickel complexes formed at different operational conditions. The thermodynamic driving force for this system can be visualised by superimposing E/pH curves for the hydrogen system on the nickel ammine sulphate Pourbaix diagram as a function of the NH_3/Ni molar ratio (Fig. 2.2). The optimum NH_3/Ni^{2+} ratio which minimises the amount of nickel ion concentration remaining in solution after reduction and gives the largest thermodynamic driving force for hydrogen reduction is around 2 (Fig. 2.2), (Meddings and Mackiw, 1964).

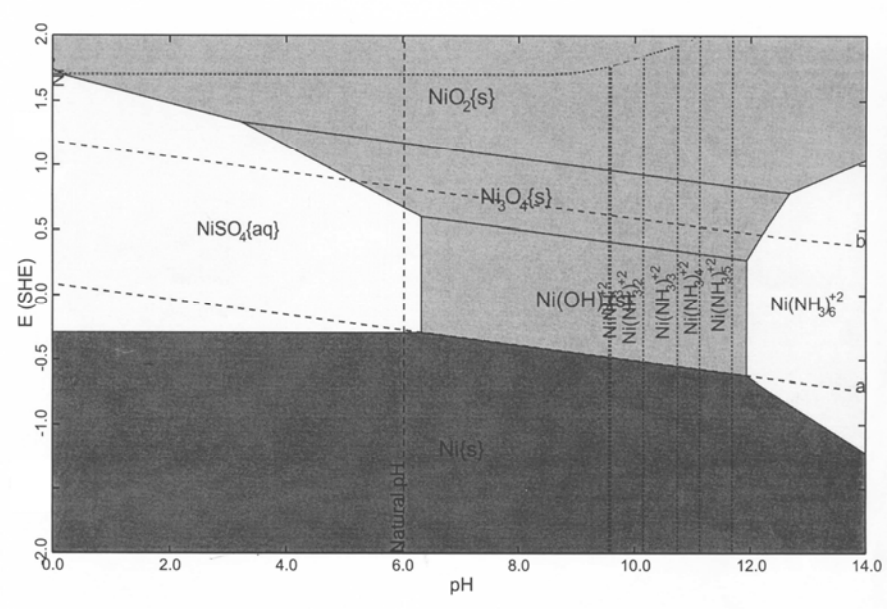

Figure 2.1 Pourbaix diagram for nickel ammine sulphate (OLI)

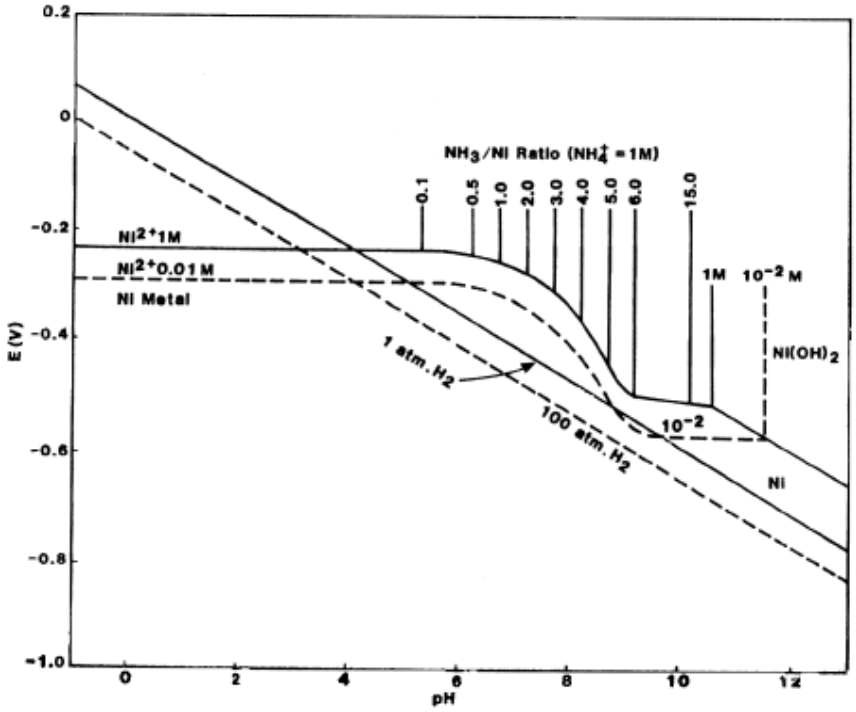

Figure 2.2 Thermodynamics of nickel ammine solutions (Meddings and Mackiw) (Copyright Gordon and Breach)

The overall precipitation reaction is given by equation 2.1.

$$Ni(NH_3)_nSO_4 + H_2 \longrightarrow Ni^0 + (NH_4)_2SO_4 + (n-2)NH_3 \qquad (2.1)$$

The reduction of nickel ions at active sites has been proposed to proceed according to the reaction scheme shown below (Kunda *et al.*, 1965).

$$Ni^0 + H_2 \longrightarrow \begin{matrix} H \\ Ni \\ H \end{matrix} \qquad \text{Chemisorption} \qquad (2.2)$$

$$Ni^0 + 1/2H_2 \longrightarrow Ni(H) \qquad \text{Dissolution} \qquad (2.3)$$

$$2Ni(H) + Ni^{2+} \longrightarrow 3Ni^0 + 2H^+ \qquad \text{Reduction} \qquad (2.4)$$

Both the chemisorbed and dissolved hydrogen are present in atomic form and are in an excited state because the nickel-hydrogen bonds are weak. Reduction of nickel ions or complexes in solution occurs through these excited hydrogen atoms.

In practice, the hydrogen ions generated by reduction (equation 2.4) are removed by addition of ammonia to the reduction solution which reacts with the hydrogen ions to form ammonium salts instead of the free acid. The addition of ammonia results in the formation of nickel ammine sulphate complexes which increases the solubility of nickel sulphate. However, this can lead to a reduction in the concentration of free nickel ions due to the complexing effect of ammonia, especially towards the end of the reduction reaction where the concentration of nickel ions is low.

Recent investigations suggest that the reaction mechanism is electrochemical in nature involving electron transfer between the anodic and cathodic sites on the metal surface as shown in Fig. 2.3 (Sobol, 1993; Osseo-Asare, 2003). The presence of two different potentials on the same surface represents a non-steady-state situation and, in order to achieve uniform potential, electrons flow through the surface of the metal particle, from anodic to the cathodic site.

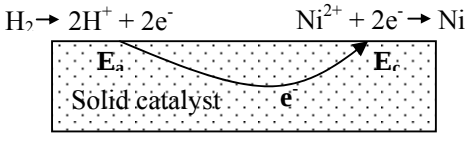

Figure 2.3 Electrochemical reduction of nickel ions on metal surface

The thermodynamic feasibility of the reduction reaction depends on the solution pH. According to equation (2.4), reduction generates H^+ ions, which can lower the pH below the equilibrium value, causing the reduction to cease. Below the critical pH value the reaction is not thermodynamically feasible. The critical pH value is given by equation (2.5) which is derived from the Nernst equation of the electrochemical reaction shown in equation 2.4, (Jackson, 1986).

$$pH = 4.2 - 0.002T \log P_{H_2} \left[Ni^{2+}\right] \qquad (2.5)$$

At standard temperature and pressure, nickel reduction is thermodynamically feasible at a pH above 5. However, in practise the reduction is not achieved due to kinetic factors, thus a catalyst (seed) is needed to initiate the reduction (Evans, 1968).

2.2 Reduction Kinetics

Studies of nickel reduction kinetics by hydrogen reduction were mainly based on two approaches: experimental precipitation studies and electrochemical experimental and modelling studies.

Experimental precipitation studies were mainly based on the work of Mackiw and co-workers (Mackiw *et al*., 1957). Their studies were carried out in a 4.5 L autoclave fitted with a downwards pumping axial flow impeller and a radial flow impeller.

Both impellers had a diameter of 0.064 m with an inter impeller spacing of 0.076 m. The radial impeller was placed above the axial flow impeller. A rotation speed of 730 rpm was used because it was found to be above the critical speed for this arrangement. This was done to ensure that mass transfer was not the rate-limiting step. Their rate equation is given by equation (2.6),

$$-\frac{d\left[Ni^{2+}\right]}{dt} = k_1 N P_{H_2}{}^{0.9} A_s \qquad (2.6)$$

The rate of reduction was found to be proportional to the surface area of nickel particles after a certain critical size was reached, which corresponded to the point where aggregation ceased and size enlargement occurred by molecular growth.

Needes and Burkin also noted that if the reaction solution is saturated with hydrogen, the rate of reduction becomes independent of hydrogen partial pressure and first order with respect to nickel in solution (Needes and Burkin, 1975). They also incorporated the dependence of rate on the molar ratio of free ammonia to nickel $f(R_A)_{Ni}$ in their rate equation, equation 2.7.

$$-\frac{d[Ni^{2+}]}{dt} = k_2 A_S P_{H_2} f(R_A)_{Ni} \qquad (2.7)$$

Based on their experimental precipitation studies, Dobrokhotov and Onuchkina found that the rate with respect to hydrogen partial pressure was 0.5 and in this respect differed with work of Mackiw, Needes and Burkin (Dobrokhotov and Onuchkina, 1962). Their rate expression is given in equation 2.8.

$$-\frac{d[Ni^{2+}]}{dt} = k_3[Ni^{2+}] + AP_{H_2}{}^{0.5} \exp\left[-\frac{E}{RT}\right] \qquad (2.8)$$

Experimental precipitation studies based on the evolution of the particle size distribution of nickel in successive densifications revealed that the rate of reaction depended not on the total surface area but on the active surface area (Zhang and Lewis, 2006). They introduced a parameter α (ratio of active surface area to total surface area) to account for the active surface area which was governed by the properties of the solid particle formed.

Their overall generalised kinetic expression is given in equation 2.9, where S represents the surface area and n ranges from 0.5-1 depending on the degree of agitation.

$$-\frac{d[Ni^{2+}]}{dt} = k_4 \alpha S P_{H_2}^n \qquad (2.9)$$

Experimental electrochemical studies were mostly based on electrochemical polarization studies conducted by Nagai and Sato which yielded a rate expression given in equation 2.10 (Nagai and Sato, 1972). A similar rate equation was obtained using electrochemical modelling studies, equation 2.11 (Osseo-Asare, 2003)

$$-\frac{d[Ni^{2+}]}{dt} = k_5 A \exp\left[-\frac{28800}{RT}\right](a_{Ni^{2+}})^{0.48} P_{H_2}{}^{0.5} - \{k_6[H^+] - [H^+]\} \qquad (2.10)$$

$$-\frac{d\left[Ni^{2+}\right]}{dt} = k_7\left[Ni^{2+}\right]^{1/2} P_{H_2}^{1/2} \qquad (2.11)$$

Sobol attributed the differences in the rate equations obtained through experimental precipitation studies to differences in the effectiveness of the mixing devices employed in the autoclaves (Sobol, 1993). It was noted that most authors did not give adequate information on their mixing devices and the intensity of mixing, an exception being the work of Mackiw and co-workers (Mackiw *et al.*, 1957).

Sobol noted that, at high intensity mixing, the reaction was kinetically controlled, while at low intensity mixing the reaction was diffusion controlled. Under diffusion conditions (low intensity mixing) he postulated that the rate was first order with respect to hydrogen partial pressure and independent of the concentration of nickel ions in solution, equation (2.7).

Under kinetic conditions (intensity mixing) he postulated that the rate with respect to hydrogen partial pressure was 0.5 and first order with respect to nickel concentration in solution, equation (2.8). However, this finding contradicted that of Mackiw and coworkers who carried their experiment under kinetic conditions and found the order to be 0.9 with respect to the partial pressure of hydrogen, equation (2.6). Thus it is important to study the reduction kinetics unhindered by mixing or mass transfer effects. This avoids polluting the kinetic factors with hydrodynamic effects.

Previous researchers have also noted that serious ambiguities in the measured metal ion and molecular hydrogen concentrations at the prevailing high temperature and pressure raises questions of the accuracy of the kinetics derived from experimental precipitation studies (Mason and Burkin, 1975).

Based on the study of the cathodic precipitation of cobalt, Sobol found that the order of reaction with respect to the activity of nickel ions was between 0.4- 0.48 (Sobol, 1993). This was in agreement with earlier work carried out by Nagai and Sato. Sobol postulated that this was due to the participation of a univalent nickel (either NiOH or Ni—H complex) in the preliminary reduction. This was believed to be the rate-limiting step. However, the existence of the univalent form has not been experimentally verified. Similar studies also proved that the rate equation (2.8) was valid in an acidic medium with a pH in the range of 0.5- 2.2.

Thus, more extensive electrochemical studies and experimental precipitation studies are needed in order to determine the exact rate equation and the mechanisms involved. Developments in high temperature sensors (e.g. for hydrogen, pH and potential) and mixing devices can greatly improve the accuracy of experimental precipitation studies.

2.3 Particle Rate Processes

Particle rate processes refers to the kinetic processes of nucleation, growth, aggregation and breakage which are responsible for the evolution of the PSD during a crystallisation process. The particle rate processes active during the precipitation of nickel by hydrogen reduction have been identified as nucleation, aggregation, growth and breakage (Lewis and Ntuli, 2005).

The thermodynamic driving force for crystallisation, $\Delta\mu$, is defined as the difference in chemical potential between the crystallising compound in the supersaturated solution and in the crystal (Söhnel and Garside, 1992).

In customary crystallisation calculations the driving force is normally expressed as supersaturation, in terms of concentration units by assuming unity activity coefficients. The absolute supersaturation and supersaturation ratio are defined by equations 2.12 and 2.13 respectively.

$$\Delta c = c - c^* \tag{2.12}$$

$$S = \frac{c}{c^*} \tag{2.13}$$

However, this definition of the driving force in terms of solubility has limited application in nickel reduction since the nickel metal precipitated is not soluble in the reduction solution. Thus, the driving force should be expressed in electrochemical terms and the overpotential which is the driving force in electrodic reactions is equated to supersaturation as in chemical reactions. The following definition based on the Butler-Volmer equation for electrodic reactions is suggested (equation 2.14 and 2.15), where the rate of the electrochemical reaction (υ-moles/cm^{2}s^{-1}) is expressed as a function of overpotential (η), (Bockris and Reddy, 1970).

$$v_{electrodic} = \frac{i}{F} = \frac{i_o}{F} e^{-\beta F\eta/RT} \tag{2.14}$$

$$\eta = \Delta\varepsilon - \varepsilon_{eqm} \tag{2.15}$$

The major challenge in this approach is to measure or calculate the exchange current density (i_o) of the nickel reduction system. Despite the challenge, this approach would yield a true measure of the driving force as compared to surface area especially in systems with impurities that can affect the surface activity of the particles.

2.3.1 Nucleation

Nucleation involves the formation of the smallest thermodynamically stable metal particle, commonly referred to as a nuclei or seed. Nucleation mechanisms are divided into two catergories, primary and secondary nucleation (Söhnel and Garside, 1992). Primary nucleation occurs either spontaneously from solution in the absence of solid particles (homogenous nucleation) or is catalysed by foreign solid phase (heterogeneous nucleation). Secondary nucleation is initiated by the presence of the solid phase of the crystallising substance.

The formation of nuclei is important for initiating reduction because nickel ions do not react homogenously with dissolved hydrogen to form metal precipitates (Sherritt Gordon Mines, 1958). In nickel reduction, nucleation occurs by either homogenous nucleation or heterogenous nucleation (Saarinen *et al.*, 1998). Homogenous nucleation involves the formation of metal atoms by chemical reduction in the bulk solution, while heterogenous nucleation involves the addition of foreign catalysts.

The homogenous nucleation agents that are commonly employed are either ferrous sulphate, aluminium sulphate or chromous sulphate used in conjuction with other organic catalysts mainly anthraquinone (Saarinen *et al.*, 1998). Previous plant studies have demonstrated the absence of nucleation under normal reduction conditions (Sherritt Gordon Mines, 1958).

The rate of primary nucleation (J) i.e. number of nuclei formed per unit volume and time is given by equation 2.16.

$$J(t) = \frac{1}{V}\frac{dN}{dt} \tag{2.16}$$

2.3.2 Growth

Growth involves the deposition of nickel atoms from the solution onto a metal surface (Evans, 1968). It involves the processes of diffusion, surface adsorption, chemical reaction, deposition and desorption (Schaufelberger, 1956). Growth can either be controlled by diffusion of molecules or ions from solution to the crystal surface or by surface intergration which involves incorporation of ions, atoms or molecules into the crystal lattice (Söhnel and Garside, 1992). For growth controlled by surface intergration, three mechanisms have been identified; growth by screw dislocation (spiral growth), growth by two-dimensional nucleation and rough growth (Mullin, 1997).

The crystal growth mechanism is not very well understood but previous investigations support the screw dislocation mechanism as opposed to the two-dimensional, surface nucleation viewpoint (Schaufelberger, 1956).

Growth can be defined in terms of the linear growth (G) or mass growth rate expressed by equations 2.17 and 2.18 respectively.

$$G = \frac{dL}{dt} \tag{2.17}$$

$$\frac{1}{A}\frac{dm}{dt} = 3\frac{k_v}{k_a}\rho G \tag{2.18}$$

2.3.3 Aggregation and breakage

Aggregation involves the clustering together of two or more metal particles to form an aggregate, which can be permanently cemented together by an overgrowth of metal (Schaufelberger, 1956).

In general two kinds of aggregation can be distinguished namely, primary and secondary aggregation (Jones, 1993).

Primary aggregation is a result of mal-growth of crystals as a result of impurity action or diffusion field limitations (especially at high growth rates) or surface nucleation. Secondary aggregation is a consequence of crystal/crystal aggregation due to hydrodynamic factors. It is normally difficult to identify by visual observation whether aggregates are primary or secondary (Jones, 1993).

Aggregation is normally undesirable in nickel reduction systems as it reduces the total area available for reaction ad thus the reduction rate. This results in plastering on the walls of the autoclave resulting in more equipment downtime to leach out the metal (Schaufelberger, 1956). However, in cases of slow growth, as is the case in nickel precipitation, it is the only mechanism available for the consolidation of small particles to metal powder course enough to prevent redissolution in subsequent washing steps or dusting during drying (Schaufelberger, 1956). Significant aggregation has also been found to reduce the deactivation of nickel particles during the precipitation process as opposed to breakage and crystal growth which decreased activation (Zhang and Lewis, 2006).

Breakage involves the disruption of the particle aggregate into smaller particles or fines and may occur by two modes namely, collisional mechanical break-up and turbulent fluid mechanical break-up (Jones, 1993). Breakage may give rise to fines if the mechanism of breakage involves surface erosion (attrition) resulting in a gradual change in size of the parent particle or fragments (smaller entities of significant size). Fragmentation results in the rapid disappearance of the original parent particles.

Evidence from SEM micrographs of nickel powder obtained from industrial autoclaves coupled with population balance modelling suggests that the nickel reduction process is dominated by aggregation and breakage (Lewis and Hounslow, 2005). Lewis and Hounslow (2005) used attrition as a breakage mechanism in their modelling work and assumed that the fragments formed are primary particles.

Previous studies suggest that during the early densification cycles, size enlargement occurs mainly by aggregation until a certain critical size (D_{max}- maximum value of *D(50)* achieved) is reached, after which aggregation ceases (Evans, 1968). It is however, proposed that aggregation does not cease but a balance between the aggregation and breakage rate is established creating a stationery state. The value of D_{max} has been shown to depend on the intensity of mixing according to equation 2.19 (Söhnel and Mullin, 1991). The value of the exponent *n* was found to vary between 0 and 3, depending on the Reynolds number.

$$D_{\max} \approx R^{-n} \tag{2.19}$$

2.3.4 Population Balance Modelling

Population balances are normally used to provide information on the number and size distribution of particles in precipitation processes. They can also be used to provide information on the particle rate processes in the reactor. The general population balance equation for a crystalliser assuming constant volume, no flow of particles into and out of the crystalliser (i.e. batch) and that crystal growth is not a function of size is given by equation (11), (Randolph and Larson, 1988).

$$\frac{\partial n}{\partial t} - G\frac{\partial n}{\partial L} = B - D \tag{2.20}$$

The term $\partial n/\partial t$ gives the change in number density with respect to time in the batch crystalliser, $G\,\partial n/\partial L$ describes the difference between crystals growing into and out of a size interval L to $L+dL$. The parameters B and D represent the birth and death rates respectively, due to nucleation, aggregation and breakage. The number density function is defined by equation 2.21 and can be calculated from a volume based histogram ($vol\%_i$ versus L_i), where i indicates the size sub-range and the particle concentration $\left(conc(vol\%)\right)$ using equation 2.22. If particles are spherical, a volume shape factor $\left(k_v\right)$ equal to $\pi/6$ is used.

$$n(L)=\frac{dN}{dL} \tag{2.21}$$

$$n(L)dL=\sum_i \frac{vol\%_i \times conc(vol\%)}{100}\cdot\frac{1}{k_v \overline{L}^3} \tag{2.22}$$

In cases where both growth and aggregation are active, a complete analytical solution to the population balance is not possible, thus, a moment form of the population balance can be used (Bramley *et al.*, 1996). The population balance, equation 2.20, is transformed into its moment form, equation 2.23, by multiplying all its terms by $L^p dL$ and integrating from 0 to ∞ (Randolph and Larson, 1988).

$$\frac{dm_j}{dt} - jGm_{j-1} = \overline{B_j} - \overline{D_j} \tag{2.23}$$

The *j*th moment of the number density function, *n(L)*, with respect to internal coordinate, *L*, the birth and death functions in equation 2.23 are defined as:

$$m_j = \int_0^\infty L^j n(L)dL \tag{2.24}$$

$$\overline{B_j} = \int_0^\infty L^j B(L)dL \tag{2.25}$$

$$\overline{D_j} = \int_0^\infty L^j D(L)dL \tag{2.26}$$

The particular forms of the birth and death function obtained after the moment transformation depends on the specific models chosen to model the active particle rate process.

2.4 Factors Affecting the Product Quality

For metallic powders, the properties of the individual particles (e.g. size, shape and microstructure) and the bulk properties (e.g. chemical composition, PSD, specific surface and apparent density) are important in powder metallurgy. All these parameters are determined by the overall precipitation kinetics which are governed by the relative rates and mechanisms of the kinetic processes of nucleation, growth, aggregation and breakage. The parameters that influence the morphology and PSD are: concentration of foreign substances, pH, hydrodynamics, temperature and rate of reaction (Söhnel and Garside, 1998).

2.4.1 Foreign substances

Foreign substances are considered as any material other than that of the crystallising compound. When intentionally added they are referred to as additives and when inherently present in the growth media they are referred to as impurities. However, it is common in crystallisation literature to classify both additives and impurities (as defined above) under the term impurities (Sangwal, 1996). In this thesis, the term impurities would be used to exclusively refer to inherently present foreign substances.

Sheritt Gordon Mines Research and Development Division conducted extensive investigations on the effect of available commercial additives on the physical properties of the nickel powder (Kunda *et al.*, 1965; Kunda and Evans, 1968).

The effect of fifty-five organic and inorganic additives on the physical properties of the nickel powder produced from both nickel ammine sulphate and nickel ammine ammonium carbonate solutions were investigated.

Additives were classified broadly into four categories namely: reduction catalysts; additives for preventing agglomeration; coating catalyst and flocculants and wetting agents (Kunda *et al.*, 1965). Evidence from electron scanning micrographs revealed that a specific additive affected nucleation or growth but not both.

Inorganic additives e.g. platinum and ferrous sulphate were found to act as nucleating and reduction catalysts due to their ability to adsorb hydrogen. However, aluminium sulphate acted only as a nucleating catalyst due to its electronic structure. The ability of iron and platinum to act as reduction catalysts is due to the presence of empty *d*-orbitals which enables them to adsorb hydrogen through electron transfer. Since aluminium is not a *d*-block element it can not adsorb hydrogen by chemisorption and therefore can not catalyse the reduction reaction.

Organic additives were found to affect the physical properties of the powder by either activating or passivating the particle surface. Activating agents e.g. anthraquinone and polyacrylic acid activate the entire surface of the particles by undergoing reversible hydrogenation reactions, leading to uniform deposition and spherical shaped particles. Passivating agents e.g. acrysol and stearic acid lack hydrogenation properties and simply coat the metal surface resulting in either preferential deposition and/or prevention of aggregation. This leads to irregularly shaped particles.

The effect of a morphology modifier widely used in industrial nickel reduction systems has also been investigated and the findings are reported in Chapter 3 of this thesis (Ntuli and Lewis, 2006).

In the nickel reduction, impurities are present in the hydrogen gas used for reduction and the reduction solution. Impurities in the reduction solution are generated during the leaching of the Ni-Cu matte to generate a nickel rich feed solution and a platinum group metal (PGM) residue.

Carbon monoxide, an impurity in the hydrogen gas, is usually converted to carbon dioxide, which decreases the partial pressure of hydrogen and limits the extent of reduction (Schaufelberger, 1956). However, since the process conditions are highly reducing carbon monoxide probably forms water vapour and carbon not carbon dioxide. In basic ammoniacal solutions, nickel forms nickel carbonyl with carbon monoxide, a toxic gas that must be safely vented. In acidic solutions the carbonyl is converted to a powder of poor quality (Schaufelberger, 1956).

The major impurities in the reduction solution are iron, cobalt and copper (Schaufelberger, 1956). Of these, iron has the most significant influence on particle morphology and its effect has been studied and the findings are presented in Chapter 4 of this thesis (Ntuli and Lewis, 2007).

Research into the effect of impurities has not been given much attention in the commercial production of nickel powder. Thus, the effect of these inherent impurities is unknown and their concentration is not well monitored during production.

2.4.2 pH

According to Saarinen *et al.*, (1998), the solution pH determines the reduction rate and morphology of the nickel particles to a greater degree than the other processing variables. However, this hypothesis has not been backed up with experimental studies, thus it is difficult to ascertain the exact effect of pH on the morphology and rate of reaction.

The solution pH also affects the chemical speciation of the solution. From the Pourbaix diagram of the ammoniacal nickel sulphate system (Fig 2.1), precipitation of basic salts or hydroxides is feasible above a pH of 6.5. Since hydrolysis slows down the reduction process, it is desirable to use a solution pH that is less than that at which a hydroxide or a basic salt will precipitate (Jackson, 1986).

However, in commercial production, the pH of the reduction solution is around 8 and hydrolysis is prevented by adding ammonium sulphate ($(NH_4)_2SO_4$:$NiSO_4$ molar ratio between 1.7- 5) to act as a buffer (Burkin, 1987; Saarinen *et al.*, 1998).

2.4.3 Hydrodynamics

Since nickel can only precipitate on the surface of existing solid particles, mixing is essential to ensure that the nickel particles are adequately suspended and dispersed during reduction (Boyd and Essen, 2000). Poor solid suspension reduces the surface area available for reduction; as a result the apparent density of the suspended particles rapidly increases and agitators are unable to suspend them. This factor limits the number of densifications that can be performed. Solid suspension should be more than merely off-bottom since a uniform dispersion optimises the chemical reaction (Ochieng and Lewis, 2006; Boyd and Essen, 2000)

Agitation is also essential to provide adequate gas-liquid mass transfer of hydrogen gas in the autoclave headspace into solution, since the rate of reaction is determined by the amount of hydrogen dissolved in solution (Boyd and Essen, 2000). Considering the above factors, it is clear that reduction can not proceed without agitation, which explains why hydrodynamics plays a crucial part in nickel reduction.

2.4.4 Rate of Reaction and Temperature

According to Mackiw *et al.*, (1957), the rate equation for the precipitation of nickel from ammoniacal sulphate solutions (equation 2.6) is proportional to the number of seed particles and hydrogen partial pressure. The quantity of seed added determines the product particle size distribution. The particle size decreases with increase in seed quantity because the same quantity of metal is distributed over a large number of particles (Boyd and Essen, 2000).

The hydrogen partial pressure and temperature determines the amount of dissolved hydrogen in solution, which represents the amount of hydrogen available for the reaction (Boyd and Essen, 2000). However, hydrogen solubility studies have revealed that temperature has the greatest effect on hydrogen solubility, as opposed to pressure (Schaufelberger, 1956). The increase in solubility with increasing temperature above 80 ^{o}C is nearly exponential; while increasing the pressure only gradually increases the hydrogen solubility. The solubility of hydrogen in aqueous solution varies with temperature and increases rapidly above 80 ^{o}C, Fig. 2.4 (Jackson, 1986). The hydrogen solubility in ammine sulphate solutions has been shown to be much higher than that obtained in pure water e.g. at 222 ^{o}C and equilibrium hydrogen pressure of 3447 kPa the hydrogen solubility was 0.059 M in pure water as compared to 0.392 M in ammine sulphate solutions (Needes and Burkin, 1975). However, the hydrogen solubility values are largely dependant on the degree of agitation employed, thus these values only serve as a guideline.

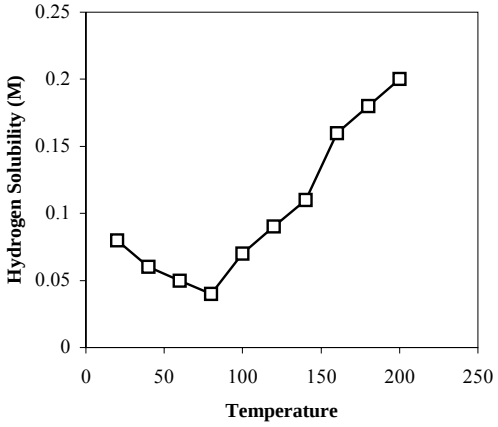

Figure 2.4 The variation of H_2 solubility with temperature under a pressure of 2.03 MPa

Temperature has also been found to have a great influence on nucleation, growth rate of crystals, precipitation rate, crystal size and shape (Söhnel and Garside, 1998). The precipitation rate and the primary nucleation rate have been shown to increase with temperature. The rate controlling step in crystal growth i.e. diffusion or surface integration and the shape and size of crystals have also been found to be altered by increases in temperature.

3 EFFECTS OF IRON

3.1 Introduction

The effect of iron on the precipitation behaviour of nickel powder was investigated on a laboratory scale using 0.5 L autoclave fitted with a Teflon reaction beaker and a double impeller configuration. While iron exists as an impurity (inherently present) in industrial nickel reduction plants, its effect was studied as an additive, since it was intentional introduced to the reduction solution in order to study its effects on the precipitation process. Research into the effect of impurities has not been given much attention in the commercial production of nickel powder. Thus, the effect of these impurities is unknown and their concentration is not well monitored during production. As a result, it is difficult to identify the factors leading to the unpredictable production of nickel powder not meeting quality specifications in terms of purity and morphology.

Most of the impurities are introduced into the reduction solution during the leaching of the Ni-Cu matte to generate a nickel-rich feed solution and a platinum group metals (PGM) residue. Ni-Cu matte has been found to have the following typical chemical composition; 47.9 % Ni, 27.6 % Cu, 21.4 % S, 0.7 % Co, 0.6 % Fe, Se 0.05 % the remaining portion being the PGM and Au fraction (Brugman and Kerfoot, 1986). Of the constituents present in appreciable amounts only iron (converted to ferrous sulphate during leaching) is not recovered for commercial purposes but is removed from the nickel feed solution by jarosite precipitation. At Impala Platinum Refineries in South Africa, the maximum allowable concentration of iron in the nickel reduction solution after jarosite precipitation is 9 mg/L although in most instances the levels are below 3 mg/L. Since the presence of iron in concentrations above the allowable limit has been associated with the production of undesirable powder, it was necessary to investigate the effect of ferrous sulphate on the precipitation behaviour of nickel.

Numerous studies have been carried out on the use of ferrous sulphate as an additive to induce nucleation and this reagent has been widely used for this purpose in nickel reduction (Mackiw *et al*., 1957; Kunda and Evans, 1968; Elmarghani and Sliepcevich, 1986). However, currently it is being replaced by other inorganic salts namely, aluminium sulphate and chromium sulphate used in conjunction with organic catalysts (Saarinen *et al*., 1998).

This is because ferrous sulphate has been found not to be suitable for the production of extra high purity powders required for special applications (Zubrycki *et al*., 1969). When used as a nucleation agent, ferrous sulphate in concentrations between 200- 500 mg/L produced a very fine nickel powder with an average size of 1- 2 μm (Zubrycki *et al*., 1969; Kunda and Evans, 1968). This powder acted as an autocatalyst on which further reduction of nickel from solution occurred. Ferrous sulphate (100 mg/L Fe^{2+}) was also found to activate nuclei produced from aluminium sulphate which is not a reduction catalyst (Kunda and Evans, 1968). The reduction rate during nucleation was increased by a factor of 3 and the powder became considerably finer when ferrous sulphate (200 mg/L of Fe^{2+}) was used in conjunction with organic additives (Kunda and Evans, 1968).

Although the exact mechanism of nucleation is still not clear, it is thought to occur through the precipitation of a mixed Fe(II)- Ni(II) hydroxide or basic sulphate (Saarinen et al., 1998). The activity of ferrous sulphate as a nucleation catalyst was found to decrease with increasing solution concentration of ammonium sulphate and no nucleation was observed at a molar ratio of $(NH_4)_2SO_4$:$NiSO_4$ of 2.2 (Mackiw *et al*., 1957; Elmarghani and Sliepcevich, 1986). Later studies revealed that a $(NH_4)_2SO_4$:$NiSO_4$ molar ratio between 1.7 and 5 was effective in preventing hydrolysis and the precipitation of basic sulphates (Burkin, 1987; Saarinen, 1998). Thermodynamic calculations have also verified that at 180 ^oC and molar ratio of $(NH_4)_2SO_4$:$NiSO_4$ between 1- 11, precipitation of hydroxides or basic sulphates was not feasible (Kolhenen and Jalkanen, 2005). Of the iron added during nucleation only 10 % remained in the nickel powder (Kunda and Evans, 1968). Thus, in commercial production, nucleation is conducted in the absence of ammonium sulphate (unbuffered solution) and subsequent batch reductions (densifications) are conducted with solutions buffered with ammonium sulphate (molar ratio of $(NH_4)_2SO_4$: $NiSO_4 \approx 2.8$) to ensure that only metallic nickel is precipitated and no further nucleation occurs.

The objective of this study was to investigate the effect of ferrous sulphate on the precipitation behaviour of nickel during the densification stage. Previous plant data has shown that iron does not have an appreciable effect on the precipitation behaviour of nickel when present at a concentration below 3 mg/L (Lewis and Ntuli, 2005). Thus, the concentrations of iron selected for use in this study were 6 mg/L, 20 mg/L and 200 mg/L. The concentrations were selected on the following basis:

- 6 mg/L: the maximum allowable concentration (level where action needs to be taken to reduce Fe levels) but above the standard value of less than 3 mg/L;
- 20 mg/L: the maximum concentration of iron in the reduction solution observed in industrial practice and
- 200 mg/L: the concentration normally used for nucleation in industrial practice.

This range was deemed adequate to cover the expected range of iron levels in industrial practice.

The effect of iron on the active particle rate processes during nickel reduction was identified by transforming the PSD data into moments (Hounslow *et al*., 1988) de-normalised based on the liquor mass balance. Scanning electron micrographs and BET measurements were used to verify the identified active particle rate processes and observe the powder morphology.

3.2 Experimental

3.2.1 Apparatus and reagents

Experiments were conducted in a 0.5 L stainless steel autoclave fitted with a Teflon reaction beaker and a detachable mixer head (Fig. 3.1). A pressure gauge, thermocouple, safety valve venting at 3500 kPa, dip pipe, vent valve and impeller shaft were attached to the detachable mixer head (Fig. 3.1). Heating was achieved by inserting the reactor in an electrically heated stainless steel mantle fitted with a thermocouple and mounted on an autoclave stand. Both thermocouples were controlled by a DTH-101 brainchild digital temperature controller. A 6-blade Rushton turbine (impeller diameter 0.02629 m) was used as the lower impeller and a 4- blade axial impeller (impeller diameter 0.03738 m) was used as the upper impeller. Inter-impeller spacing and impeller offbottom clearance were 0.007 and 0.0031 m respectively. A motor mounted on the autoclave stand was used to transmit power to the impeller shaft. Agitation rate was set and controlled using a variable speed controller. Agitation speed, temperature inside the reactor and of the heating mantle were displayed on the control panel fitted on the autoclave stand.

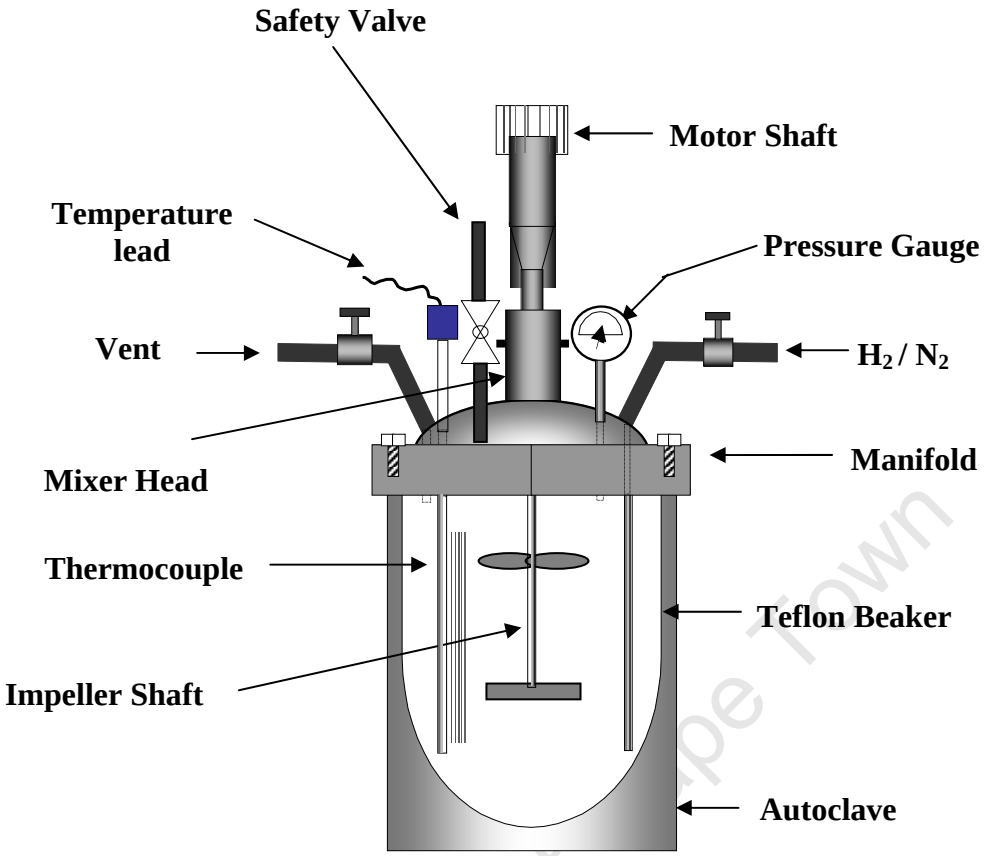

Figure 3.1 Autoclave configuration

The reduction solution was prepared by dissolving 45 g of analytical grade nickel sulphate hexahydrate and 50.25 g of analytical grade ammonium sulphate in 0.9 L of hot distilled water. The solution was kept hot and stirred with a magnetic stirrer on a magnetic hot plate. Approximately 25 mL of 29.7 % ammonium solution was then added and the solution was made up to 1 L by adding demineralised water. The nickel concentration was then measured using atomic absorption (AAS, Model Varian 110) and the free ammonia measured by titration with 0.1 N sulphuric acid (standardised against 0.1 N $NaCO_3$) using a screened methyl orange indicator. The reduction solution contained 10.05 g/L Ni^{2+} and a molar ratio of $(NH_4)_2SO_4$: Ni^{2+} and free NH_3: Ni^{2+} of 2.2 and between 2.0-2.1 respectively. Free NH_3: Ni^{2+} molar ratio was adjusted by addition of either analytical grade ammonia solution or sulphuric acid. High purity hydrogen gas (minimum assay 98.8% H_2) was used for reduction and nitrogen gas (minimum assay 99% N_2) was used for purging.

A 200 mL ferrous sulphate stock solution (10 g/L Fe^{2+}) was made by dissolving 10.057 g of analytical grade ferrous sulphate ($FeSO_4.7H_20$) in distilled water (adjusted to pH 2.5 using concentrated sulphuric to avoid the oxidation of ferrous to ferric). Modifier N9300 (a polyacrylic acid derivative) supplied by Chermserve Technical Products was used as an additive. The additive is used as an anti-agglomerating agent, thus it acts as a reduction catalyst by maintaining the surface area needed for reduction. This makes it possible to run more densifications on a cycle before the particles become too dense to be kept in suspension by the agitator. Nickel seed (*D(4.3)*=43.3±6.9 μm) was supplied by Impala Platinum Refineries. The seed morphology is shown in Fig. 3.8(a).

Scanning electron micrographs (SEM) and powder purity were captured and measured using a Leica electron optics (Leo) scanning electron microscope (Model SS 440) and sigma software was used for elemental analysis. A laser diffraction Malvern Mastersizer (Model S –Long bench) was used to measure PSD and BET specific surface area was measured using a BET instrument (Model Micromeritics Tristar).

3.2.2 Experimental programme

The experimental programme was divided into two phases; the repeatability studies and the experimental studies. Due to the scale of operation, sampling between batch reductions would significantly reduce the amount of powder in the autoclave. This tends to mask the effect of process dependant particle rate processes, thus, studying the precipitation process in the absence of sampling between batch reductions was preferred. However, to get a deeper understanding of the precipitation process it is necessary to know what happens at each batch reduction. In order for this to be done it was necessary to prove that under similar reduction conditions, independent batch reduction experiments were repeatable. This would enable results obtained from different sets of successive batch reductions conducted under similar experimental conditions to be combined into a single cycle with minimum error. The experimental studies focussed on the effect of iron on the precipitation behaviour of nickel powder.

3.2.3 Procedure

20 g of seed and 400 mL of reduction solution were used for the repeatability studies and 15 g of seed and 320 mL of solution were used in the experimental phase. The required amount of seed and reduction solution was weighed and measured using an analytical balance and a volumetric flask respectively. The reduction solution and seed were then transferred into the autoclave and a predetermined amount of modifier was added. For the repeatability studies, 2.8 mL (0.7 vol %) of modifier was added in the first densification and thereafter 1.4 mL (0.35 vol %) for each subsequent densification. For the experimental studies 1.92 mL (0.6 vol %) was added in the first densification and thereafter 0.96 mL (0.3 vol %) was added for each subsequent densification. A double modifier dosage was used in the first densification to prevent excessive aggregation of seed in the initial stages of the cycle. For the experimental phase 0.19 mL, 0.64 mL and 6.4 mL of the ferrous sulphate stock solution were added to give reduction solutions with Fe concentrations of 6 mg/L, 20 mg/L and 200 mg/L respectively.

After the autoclave was placed in the heating mantle, the mixer head was then attached to the autoclave and the two components bolted together by use of two stainless steel manifolds. Heating was then commenced by switching on the heating system and setting the temperature controller of the heater to 280 ^{o}C. The motor shaft was then engaged to the mixer head shaft and agitation was commenced by switching on the agitator and gradually increasing the speed using the control knob until it reached 72 rpm on the speed dial. This setting corresponded to a shaft speed of 1075 rpm as measured by an EB16 tachometer. When the internal temperature of the autoclave reached 50 ^{o}C, agitation was stopped and the vent valve was one-quarter opened. The autoclave was then purged for 1 min with nitrogen gas at 700 kPa to expel oxygen, after which the vent valve was closed. Agitation was then resumed for 2 min and purging was then repeated with hydrogen at 1000 kPa for 1 min using the same procedure as for the nitrogen purge.

Heating and agitation were continued until the internal temperature of the autoclave was 165 ^{o}C. The autoclave was then pressurised with hydrogen at a pressure of 2000 kPa and the starting time of reduction was noted. In order to avoid saturation of the headspace with steam and to ensure there was a continuous flow of hydrogen into the autoclave, the vent valve was kept one-eighth open during reduction. This setting ensured that the total pressure inside the autoclave was approximately 2800 kPa in the absence of hydrogen consumption.

The temperature rose rapidly to 180 ^{o}C during reduction and was maintained between 180 and 190 ^{o}C until reduction was complete.

In the course of reduction, the total pressure in the autoclave fluctuates because of hydrogen utilisation during nickel reduction and stabilises at approximately 2800 kPa as soon as reduction is complete because there is no further consumption of hydrogen. This factor was used to indicate that reduction was complete and the time taken to reach this point was taken as the reduction time. When reduction was complete, the hydrogen valve was closed and agitation and heating were stopped. The motor shaft was then disengaged and the autoclave (coupled to the mixer head) was removed from the heating mantle, depressurised by slightly opening the vent valve and allowed to cool to around 70 ^{o}C. After cooling, the autoclave was opened by unbolting the manifold and removing the mixer head.

During cooling, the dense nickel seed particles settle to the bottom of the reaction beaker and are separated from the reduction end solution by decantation. Subsequent batch reductions were then performed by addition of fresh reduction solution to the initial seed particles using the procedure described above. The volume and nickel concentration of the reduction end solution were then measured using a volumetric flask and by atomic absorption spectroscopy respectively. When the desired number of batch reductions had been completed, the nickel powder was separated from the reduction solution by filtration. The powder was then washed three times with hot water and dried in an oven at 80 ^{o}C. Before starting another cycle the autoclave was leached with dilute nitric acid at 80 ^{o}C for 15min to ensure that no nickel is left to act as seed for subsequent reduction cycles. A sample of the nickel seed (15 g) in water at 80 ^{o}C was also subjected to similar agitation conditions in the autoclave for 20 min to account for seed breakage due to hydrodynamic factors.

The PSD and BET specific surface area of the seed and powder were then measured using a laser diffraction technique (Malvern Mastersizer S) and BET instrument, respectively, while the morphology and purity were observed/measured using SEM.

3.3 Results and discussion

3.3.1 Repeatability studies

Results for the repeatability studies for zeroth moment (m_0), second moment (m_2), third moment (m_3), number based mean size ($\overline{L}_{1.0}$) and the volume or mass moment mean *D(4.3)* are shown in Fig. 3.2.

The mean ($\overline{x}$) and standard deviation (s) for the *D(4.3)* are shown in Table 3.1. The relative standard deviation was less than 0.19 with the exception of D4 where it was 0.28. Grubbs' test showed that extreme values are not outliers at α=0.05.

Thus, it can be seen that combining densifications conducted in separate experiments into one single cycle does not affect the trends in the evolution of the derived moments and the conclusions drawn from these trends with 95% confidence. The relative standard deviation of each of the parameters shown in Fig. 3.2 was used to compute the error associated with each measurement in the experimental phase.

Table 3.1
Variation of the D(4.3) in the repeatability experiments

Parameter	*D(4.3)* for particular densification					
	Seed	D1	D2	D3	D4	D5
$\overline{x}$	42.2	45.3	58.4	151.8	154.0	216.6
s	6.9	5.4	7.9	5.4	42.8	39.3

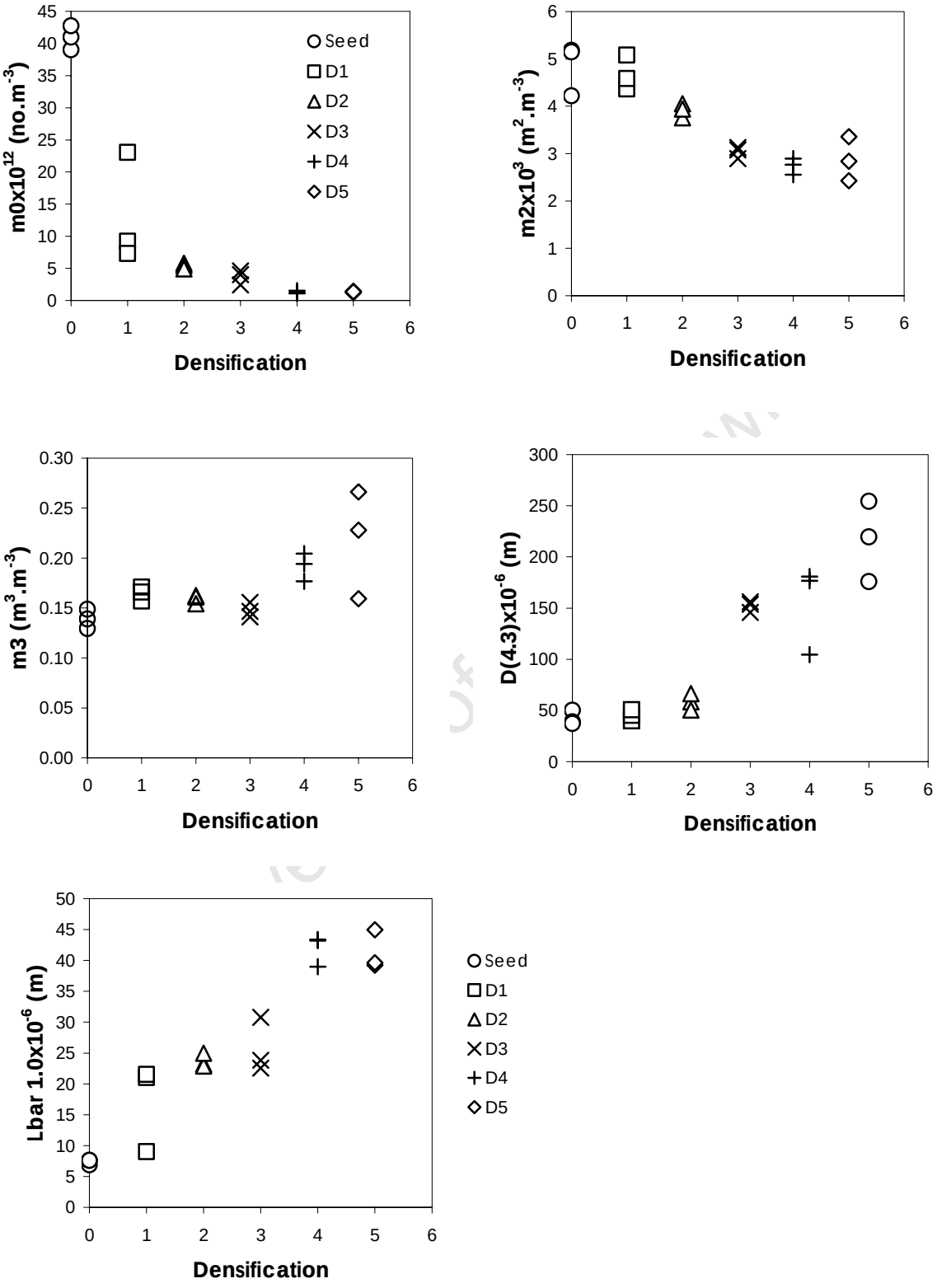

Figure 3.2 *m0, m2, m3, D(4.3)* and $\overline{L}_{1.0}$, for the repeatability studies

3.3.2 Nickel depletion rate

The average rate of nickel depletion from solution at different Fe concentrations is shown in Table 3.2. The average reduction time per batch was 7±2 min in the absence of Fe and 6±1 min in the presence of Fe. There was an increase in average depletion rate as the concentration of Fe was increased, although there was no significant difference in the depletion rate at Fe=6 and Fe=20 mg/L. The nickel depletion rate has been known to be increased by an increase in the active seed surface area (Zhang and Lewis, 2006) and addition of additives promoting growth (Kunda and Evans, 1968).

Table 3.2
Nickel depletion rate at different Fe concentrations

Iron concentration	Average depletion rate (g Ni/L. min)
Fe =0 mg/L	1.13±0.13
Fe =6 mg/L	1.19±0.19
Fe =20 mg/L	1.24±0.07
Fe =200 mg/L	1.34±0.12

3.3.3 Evolution of the PSD of nickel powder in the presence of iron

The evolution of the complete particle size distribution on a volume percentage basis at different Fe levels is shown in Fig. 3.3. The PSD was monomodal at Fe=0 and 200 mg/L and showed a gradual shift in the modal size to larger sizes, indicating particle size enlargement. At Fe=6 and 20 mg/L the PSD became bimodal at D6 with the appearance of a peak at larger sizes.

Based on the mass deposition rates and since the particles are nearly spherical, the maximum particle size that could be achieved by molecular growth alone can be calculated from equation 3.1 (Söhnel and Mullin, 1991).

$$d_{\max} = 2\left(3V_m \Delta c / 4\pi N_o\right)^{1/3} \qquad (3.1)$$

Inserting the appropriate values into equation 3.1 i.e. $V_m = 6.6 \times 10^{-3}$ m^3 mol^{-1}, $\Delta c = 0.76$ mol m^{-3} (based on total mass deposited over six densifications) and $N_o \sim 6.22 \times 10^{12}$ m^{-3} (estimated from Fig. 3.4a), the calculated d_{max} value is 11.5 μm.

Thus, it is highly unlikely that the particles at the 100 μm modal size were formed as a result of molecular growth alone, therefore aggregation played a major role in the formation of these particles.

A more detailed investigation of the particle size enlargement and reduction mechanisms follows and hereafter the particle size distributions are represented in their moment forms only.

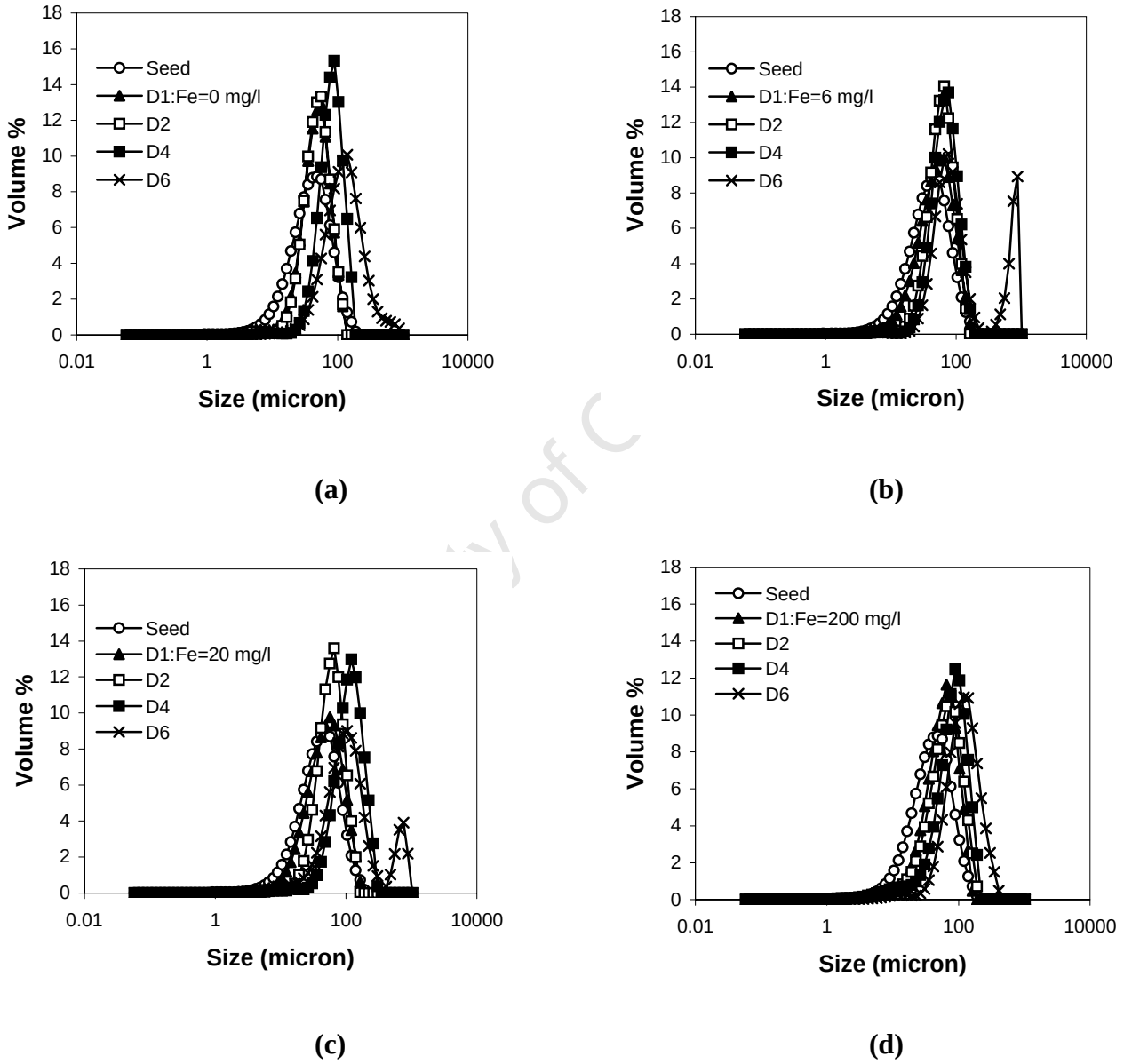

Figure 3.3 Evolution of the PSD in volume %: (a) Fe=0mg/L; (b) Fe=6mg/L; (c) Fe=20mg/L and (d) Fe=200mg/L

3.3.4 Evolution of the moments in the presence of iron

The evolution of the zero[th] moment (m_0- equivalent to particle number) and the number based mean size ($\overline{L}_{1.0}$) at different concentrations of iron (Fe) is shown in Fig. 3.4. In both cases the precision was much lower at D1 relative to the other densifications. Since the Malvern cuts out the lower size tail during deconvolution it is very inaccurate for calculating the number of particles below 10 μm, this factor reduces the accuracy of the m_0 and $\overline{L}_{1.0}$.

(a)

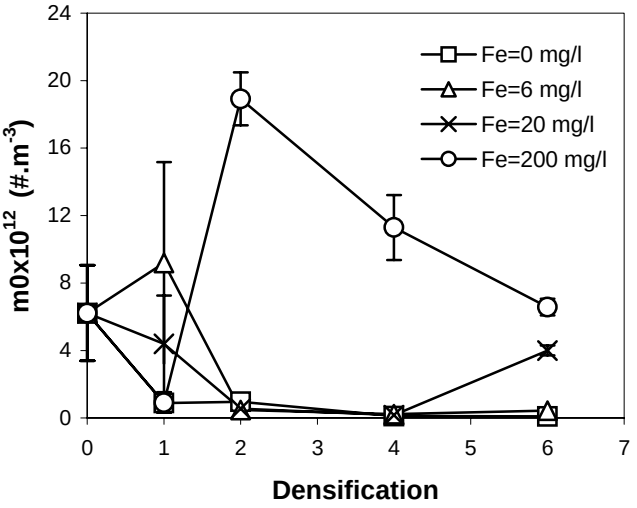

(b)

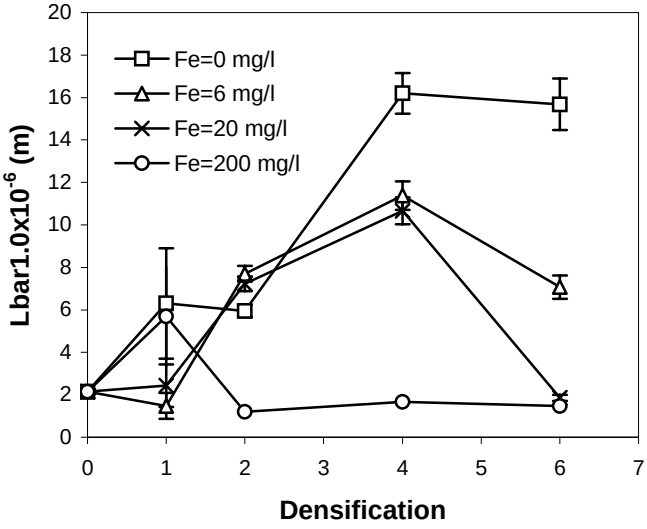

Figure 3.4 Evolution of the m_0 (a) and $\overline{L}_{1.0}$ (b) at different concentrations of iron

In the absence of iron (Fe=0 mg/L), there was an initial sharp decrease (approximately six-fold) in m_0 followed by a gradual decrease from D2 to D6.

At Fe levels of 6 mg/L, there was an initial increase in m_0 followed by a significant decrease at D2; thereafter there was a gradual decrease and increase between D2-D4 and D4-D6 respectively.

At 20 mg/L Fe, there was an initial drop in m_0; thereafter the trend was similar to that in the presence of 6 mg/L Fe with the exception of a sharp rise in m_0 at the end of the cycle.

For 200 mg/L Fe, the initial decrease in m_0 was similar to that in the absence of iron; however, there was a significant increase in m_0 at D2. Thereafter, there was a steady decrease in the m_0 until the end of the cycle.

As far as the particle rate processes are concerned, decrease in m_0 would constitute evidence of aggregation while an increase in m_0 would be due to breakage and/or nucleation. In the absence of iron, the evolution of the m_0 shows that aggregation was the dominant particle rate process and that the extent of aggregation decreased as the $\overline{L}_{1.0}$ increased (Fig. 3.4).

Previous plant studies have demonstrated the absence of nucleation under normal reduction conditions (Sherrit Gordon Mines, 1958). In the presence of iron, the magnitude of the increase in m_0 could not be attributed to breakage alone. This was tested by separate experiments carried out in water using the same shear rate and seeds as in the reduction experiments, and in which breakage was not evident. Thus, the increase in m_0 is evidence of nucleation. While previous studies demonstrated the absence of homogenous nucleation in the presence of ferrous sulphate in buffered nickel ammine sulphate solutions (Mackiw *et al*., 1957; Elmarghani and Sliepcevich, 1986), heterogeneous nucleation has been demonstrated to occur in the presence of nickel seed even in buffered solutions. Since nucleation is thought to occur through the formation of mixed hydroxides of Fe(II)- Ni(II), this suggests that the nickel seed surface promotes the hydrolysis of the basic sulphate salts of iron and nickel.

The magnitude of the sharp increase in m_0 increased with increase in the level of Fe in the reduction solution, however, sharp increases were noted earlier in the cycle at Fe levels of 6 and 200 mg/L and towards the end at Fe=20 mg/L (Fig. 3.4a).

Aggregation was also dominant at other points in the cycle in the presence of Fe as evidenced by decreases in m_0 (Fig. 3.4a) at D2 (6 mg/L), D1 (20 mg/L) and D1 and from D2 (200 mg/L).

Since the extent of aggregation is a function of m_0, the magnitude of the $\overline{L}_{1.0}$ (weighted to particle number) would be influenced by the relative rates of nucleation and aggregation. Thus, at Fe levels of 6 mg/L and 20 mg/L, aggregation occurs faster than nucleation between D1 and D4 and thereafter nucleation dominates (Fig. 3.4). The decrease in the rate of aggregation in the later stages of the cycles confirms earlier studies that found that, above a certain critical size, aggregation ceases (Evans, 1968).

In this study, the critical value has been found to be an $\overline{L}_{1.0}$ of approximately 10 μm in the presence of iron and $\overline{L}_{1.0}$ = 16 μm without. This is a logical conclusion since the critical size can change with changes in process conditions (Söhnel and Mullin, 1991). At Fe=200 mg/L the rates of aggregation and nucleation between D2 and D6 were nearly balanced and thus the $\overline{L}_{1.0}$ was almost constant (Fig. 3.4b).

Evolution of the (m_3- equivalent to total particle volume) and the *D(4.3)* at different Fe levels is shown in Fig. 3.5. Precision in the *D(4.3)* was low as from D4 and that of the m_3 at D6. There were no significant differences in the m_3 in the presence or absence of added Fe.

The *D(4.3)* at the end of each of the cycles increased from Fe=0 mg/L reaching a maximum at Fe=6 mg/L and decreasing thereafter, reaching a minimum at Fe=200 mg/L (Fig. 4.5b). Since the *D(4.3)* was measured based on a volume distribution, volume/mass would be the most significant particle parameter. Thus, the *D(4.3)* conveys information about the larger particles of the PSD. The sharp increase in the *D(4.3)* at the end of each cycle can not be attributed to molecular growth alone as this is inconsistent with the mass increase of less than 30% per densification. Thus, the increase in the *D(4.3)* can only be attributed to aggregation of large particles. The m_3 did not show any significant change because all the experiments were conducted until reduction was complete, thus, the amount precipitated is almost equal in all cases.

(a)

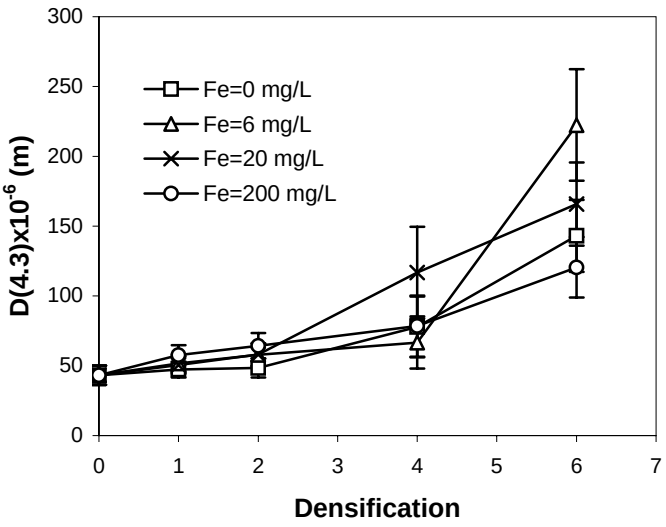

(b)

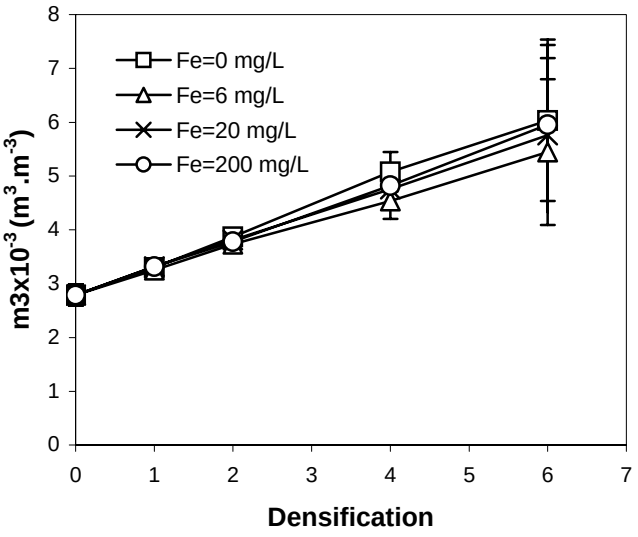

Figure 3.5 Evolution of the m_3 (a) and *D(4.3)* (b) at different concentrations of iron

Evolution of the (m_2- equivalent to surface area) is shown in Fig. 3.6. In the absence of iron there was a decrease in m_2 with the exception of an increase from D1 to D2. At Fe=6 mg/L there was an initial decrease until D2, thereafter there was no significant change in m_2. A steady decrease until D4 followed by a sharp rise thereafter was noted at Fe=20 mg/L, while an increase between D1 and D4 was followed by a sharp decrease thereafter at Fe=200 mg/L.

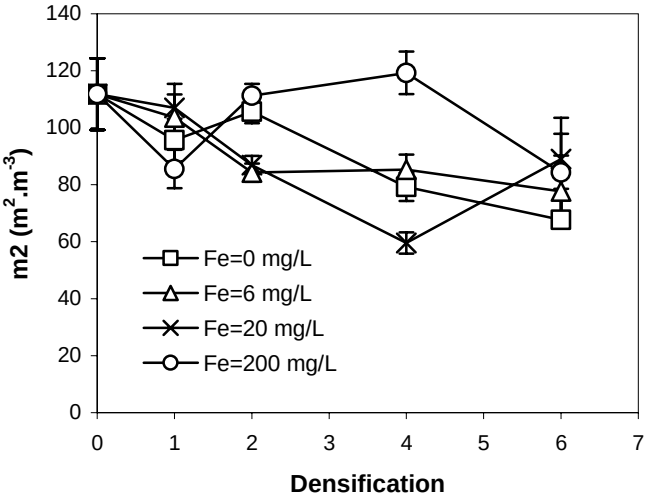

Figure 3.6 Evolution of the m_2 at different concentrations of iron

In crystallisation systems, surface area increases as a result of breakage, nucleation or molecular growth and decreases as a result of aggregation. Nucleation and breakage result in the creation of more small particles which contribute additional surface area to the system. The magnitude of the increase is greater in the case of nucleation since a large number of smaller particles are created as compared to breakage. Aggregation results in a decrease in surface area as a result of cementation between particles which minimises the available surface area. Since growth occurs by deposition of metal on an existing surface, the change in surface area will depend on the mass deposited. It has been shown that, for spherical particles, doubling the mass of the particles results in an approximately 60 % increase in surface area (Mackiw *et al*., 1957). Since the increase in mass per densification was less than 30 % in this particular study (Fig. 3.5a) and considering that the particles were not spherical, growth would not result in significant changes in surface area.

Thus, from the evolution of the m_2 at Fe=0 mg/L, it appears that aggregation and breakage were the major particle rate processes. The magnitude of increase between D1 and D2 is too small to be attributed to nucleation; furthermore there is no significant change in m_0 during the same period.

Nucleation and aggregation were the major particle rate process at Fe levels of 20 and 200 mg/L. At Fe=6 mg/L aggregation was dominant until D2 and thereafter growth was the dominant size enlargement mechanism since there is no significant difference in m_2 from D2 to D6.

Furthermore, the increase in depletion rate in the presence of Fe can not be solely attributed to increase in surface area due to nucleation. The m_2 in the absence of Fe is much higher than that at Fe=200 mg/L as from D2-D4 and comparable to that at Fe=6 mg/L as from D4-D6. This suggests that Fe acted as a growth promoter.

Since the overall mass increase was approximately 100%, this implies that molecular growth would result in a 60% increase in surface area. Hence, the significant decrease in surface area noted in Fig. 3.6 can only attributed to aggregation of larger particles.

3.3.5 BET surface area and SEM micrographs

The BET surface area results at specified densifications in a cycle are shown in Fig. 3.7. There was an increase in the BET surface area at the end of each cycle with increases in Fe concentration.

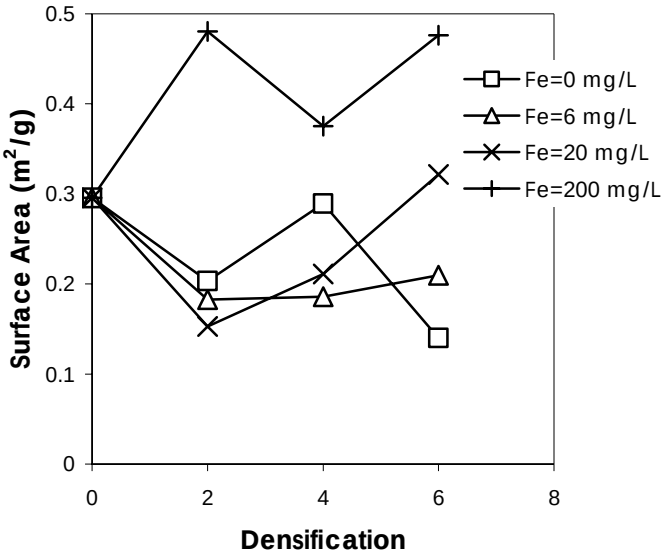

Figure 3.7 Evolution of BET surface area at different concentrations of iron

Since valid conclusions on whether particle formation was due to growth or aggregation cannot be based on SEM micrographs alone, the interpretation of the particle morphology is based on evidence from the evolution of the moments and the PSD.

SEM micrographs of the seed and powder produced after six densifications at magnification of 2000x and 1000x are shown in Fig. 3.8.

At Fe=0 mg/L, Fe=20 mg/L and Fe=200 mg/L the powder consisted of aggregated small spherical particles, becoming finer at higher Fe concentrations. However, at Fe=6 mg/L the particles were compact and the aggregating particles were less visible as compared to powder produced in other cycles. Comparison of the seed particles with those obtained at D6 in all the cycles does show the presence of particles smaller than those observed in the seed particles at Fe=20 and 200 mg/L, suggesting the presence of nucleation (Fig. 3.8). No significant differences were noted in the absence of iron and the particles at Fe=6 mg/L were compact and could not be compared with the seed particles.

These findings are consistent with the BET measurements which showed that the final BET surface area for each cycle increased with increasing Fe concentration, suggesting the presence of nucleation, which creates new particles thus, additional surface area.

The surface morphology of the powder at Fe=6 mg/L (Fig. 3.8) and the nearly constant BET surface area from D2 to D6 suggests that growth played a role as a size enlargement mechanism in this stage of the cycle.

(a)

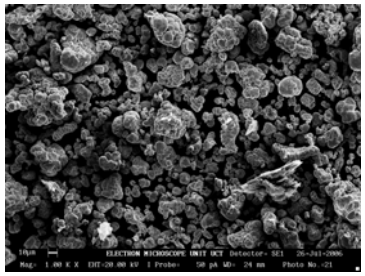

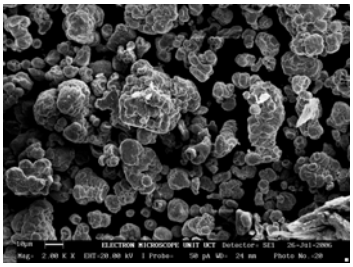

(b)

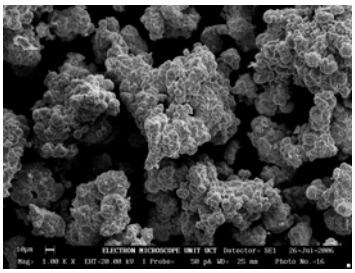

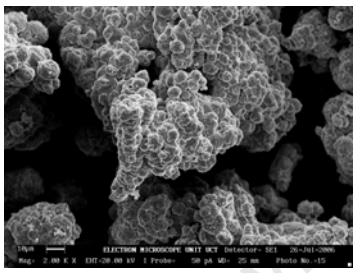

(c)

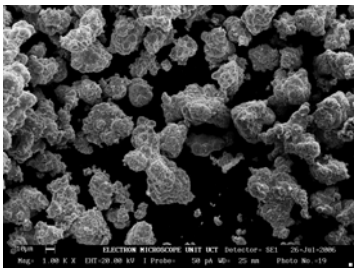

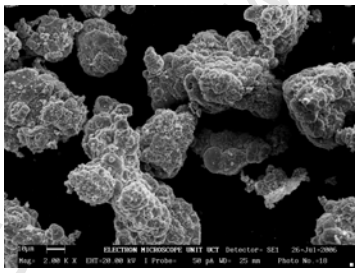

(d)

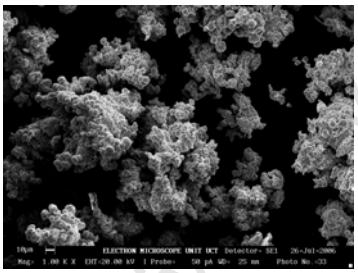

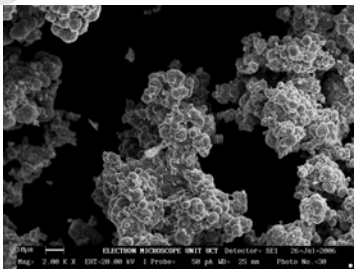

(e)

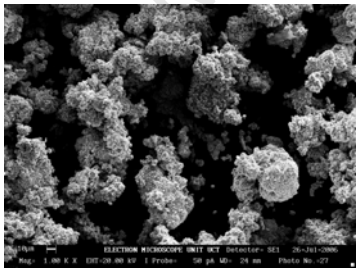

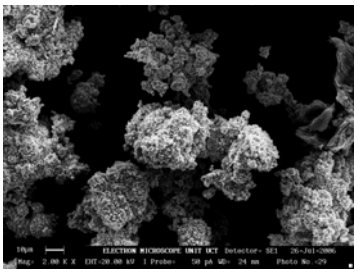

Left: Magnification 1000x
Scale: _10 μm

Right Magnification 2000x
Scale: _10 μm

Figure 3.8 SEM micrographs of the seed and powder at D6 (b) Fe= 0 mg/L (c) Fe=6 mg/L (d) 20 mg/L (e) Fe= 200 mg/L

3.3.6 Powder purity results

The nickel content of the seed and powder at the end of each cycle is shown in Table 3.3.

Table 3.3
Nickel content of the seed and powder obtained at D6

Densification stage	Nickel content (wt %)
Seed	99.82±0.15
D6 (Fe =0 mg/L)	99.85±0.54
D6 (Fe =6 mg/L)	99.85±0.61
D6 (Fe =20 mg/L)	99.82±0.63
D6 (Fe =200 mg/L)	99.38±0.49

Iron was the major impurity in the powder and a greater proportion of the iron in the powder came from the seed rather than that added to the solution. There was no significant change in the average purity of the powder in the absence of iron up to Fe=20 mg/L, thereafter there was drop in the average purity at Fe=200 mg/L.

Thus, though the precipitation of metallic iron is thermodynamically feasible under reduction condition (Evans, 1968), these studies reveal that only minute quantities of iron are reduced to metallic iron up to an iron concentration of 200 mg/L. Previous studies reveal that the iron hydroxides initial formed on nucleation dissolve into ferrous sulphate as reduction proceeds due to the increase in the concentration of $(NH_4)_2SO_4$ as the reaction proceeds (Mackiw *et al*., 1957).

3.3.7 Population balance

The population balance for a well mixed crystallizer, assuming size independent growth, aggregation and no breakage is given by equation 3.1 and 3.2 (Randolph and Larson, 1988):

$$\frac{\partial n(L,t)}{\partial t} + G_L \frac{\partial n(L,t)}{\partial L} = r_A(L,t) \qquad (3.1)$$

$$r_A(v,t) = \beta\left[\frac{1}{2}\int_0^{\infty} n(v,t)n(v-u,t)du - n(v,t)\int_0^{\infty} n(v,t)du\right] \qquad (3.2)$$

By combining equation 3.1 and 3.2 and following the treatment of Hulburt and Katz (1964), the population balance is transformed to its moment form to yield the molecular growth rate (G_0), agglomeration kernel (β) and aggregation rate (R_a) as given by equations 3.3, 3.4 and 3.5 respectively (Chen *et al*. 2003):

$$G_0 = \frac{\Delta m_3}{3\overline{m}_2 \Delta t} \tag{3.3}$$

$$\beta = \frac{\Delta m_2}{\left(\overline{m}_1\right)^2 \Delta t} - 2\frac{G_0}{\overline{m}_1} \tag{3.4}$$

$$R_a = -\beta m_0^2 / 2 \tag{3.5}$$

These expressions were used to calculate G_0, β and R_a from the cycle with Fe=0 mg/L and Fe=6 mg/L as from D2-D6, where aggregation and growth were found to be the major size enlargement mechanisms.

The average G_0 at Fe=0 mg/L was found to be 4.7(±0.01) x 10^{-9} m/s while at Fe=6 mg/L it was 4.8(±0.01) x 10^{-9} m/s. These values are consistent with increase in the depletion rate in the presence of iron (Table 3.2) and show that Fe increases the molecular growth rate.

The calculated aggregation rates at Fe=0 mg/L were in the range of 2x10^8-1.7x10^7 #.m^3/s and 9.4x10^7- 2.2x10^7 #.m^3/s at Fe=6 mg/L. These values are at best approximate estimates because the effects of breakage and nucleation (in the presence of Fe) have been neglected.

3.3.8 Mechanisms of nickel precipitation in the presence of iron

It is now well understood that for an impurity to influence the growth of crystals in solution it has to be adsorbed on the surface of the growing crystal (Sangwal, 1996). If the adsorption is irreversible, the impurity is incorporated in the crystal and if it is reversible there is no incorporation of impurities (Raul *et al*., 2000).

Results of the nickel content of the final powder (Table 3.3) show that the adsorption of iron is reversible and that hydrolysis (which is thought to initiate nucleation) occurs on the surface of the seed, since hydrolysis was found to be absent in highly buffered solutions in the absence of seed particles (Mackiw *et al*., 1957; Elmarghani and Sliepcevich, 1986).

The evolution of the m_0, m_2, nickel depletion rates (Figs. 3.4a, 3.6 and Table 3.2 respectively) and comparison of the G_0 values at Fe=0 and 6 mg/L showed that iron promotes both growth and nucleation. The dominant particle rate process was found to be dependent on the concentration of iron in solution. Growth was favoured over nucleation up to an iron concentration of 6mg/L and thereafter nucleation became dominant. Nucleation and growth promotion in the presence of high shear rates (typical of those employed in nickel reduction systems) create conditions that favour rapid aggregation (Mumtaz and Hounslow, 2000). This phenomenon was revealed in the evolution of the m_2 and m_0 (Figs. 3.6 and 3.4a respectively). Since aggregation is size dependent, above a certain critical size (approximately $\overline{L}_{1.0}$=10 μm and *D(4.3)*=66 μm) aggregation ceased. Previous population balance modelling studies of plant data have found no evidence of aggregation for volume based particles sizes above 50 μm (Lewis and Hounslow, 2005; Taty Costodes *et al.*, 2006). However, the sharp increase in the *D(4.3)* towards the end of the cycle and the general decrease in surface area shows that aggregation of larger particles plays a major role in size enlargement.

These particle rate processes were confirmed by comparing the morphology of the seed and powder obtained (Fig. 3.8), which revealed that the size of the aggregating particles became finer above iron levels of 6 mg/L, which gives evidence of nucleation. The smooth surface morphology of nickel powder at Fe= 6 mg/L is typical of size enlargement by growth in the presence of a growth promoter (Evans, 1968).

3.4 Conclusion

Iron has been found to alter the precipitation behaviour and morphology of nickel powder by acting as both a growth promoter and nucleation agent. Nucleation and growth promotion have been found to occur through reversible adsorption and possibly hydrolysis to mixed hydroxides of Fe(II)-Ni(II), thus insignificant amounts of iron were incorporated in the powder.

The effect of iron was found to be concentration dependant, with growth being preferentially favoured over nucleation up to a concentration of 6 mg/L. Based on the analysis of previous plant data, it was observed that iron levels of less than 3 mg/L do not significantly affect the precipitation behaviour of nickel. However, a value of 6 mg/L was considered a critical concentration based on previous industrial experience with nickel reduction plants, which indicated no appreciable change in the precipitation behaviour of nickel at Fe concentrations of up to 6 mg/L. Hence this concentration is used commercially as a level where action needs to be taken to reduce Fe levels in the reduction solution.

With further increases in iron concentration above 6 mg/L, nucleation became more favourable and the extent of nucleation increased with increasing iron concentration up to 200 mg/L. Nucleation and growth promotion in the presence of high shear rates resulted in rapid aggregation which ceased at approximately $\overline{L}_{1.0}$=10μm and *D(4.3)*=66 μm. The particle size was found to be largely determined by aggregation of larger particles with growth serving mainly as a bridge to cement the particles together.

Thus, there is evidence to suggest that iron is one of the factors responsible for the production of nickel powder with undesirable morphology. An examination of the powder with undesirable morphology reveals that the surface morphology is smooth and continuous or is slightly fragmented (Fig. 1.1). Both these effects have been demonstrated to occur in the presence of iron. Thus, to ensure that powder with the desirable morphology is produced, the recommended levels of iron in the reduction solution based on laboratory scale experiments, was found be below 6 mg/L.

4. EFFECTS OF A MORPHOLOGY MODIFIER

4.1 Introduction

In this part of the study the effect of a morphology modifier used as an additive in the nickel reduction process was investigated on a pilot plant scale. While this modifier is used to produce the desired powder morphology, which is spherical and open ("botryoidal") as opposed to closed powder (Fig. 1.1), its mechanism of action was not well understood. Industrial observations suggest that increasing the modifier dosage increases the powder porosity, resulting in higher catalytic surface area for reduction and shorter reduction times. However, previous plant experience demonstrates that increasing the modifier dosage beyond a certain point does not always yield the desired effect.

Previous studies on the effect of additives have mainly focussed on comparing the effects of different additives on the physical properties of the powder, and the effect of specific additives on the precipitation mechanisms were not explored (Kunda *et al.*, 1965; Kunda *et al.*, 1968). Since the additives were tested at a fixed concentration, based on previous industrial experience, the effect of concentration of additive on the physical properties of the powder and precipitation mechanisms were not investigated. In addition, most of the results were based on samples collected in one batch reduction, termed densification, or samples collected at the beginning and end of successive densifications. Thus, the effect of the additive over a number of densifications or over each successive densification was not investigated. This factor is critical in understanding the effect of the additive on the precipitation process as conducted on a commercial scale where the number of densifications performed before discharging the powder (termed a cycle) is between 50-60. It has also been shown that the major particle rate processes depend on the particle size distribution (PSD), which is governed by the number of densifications conducted and the amount of nickel precipitated (Mackiw *et al.*, 1957).

Thus, in order to effectively employ this additive and understand its effects on powder morphology, its mechanism of action at different concentrations needs to be determined. The range of modifier dosages studied (0.25 - 5 vol %) was based on preliminary studies and previous plant experience. Below a modifier dosage of 0.25 vol %, reduction could not be completed within a period of 30 min and 5 vol % is the maximum dosage used on an industrial scale.

The mechanism of action of the additive, including the active particle rate processes, were identified by transforming the PSD data into moments (Hounslow *et al.*, 1988) and from the BET surface area results. Evidence for the identified active particle rate processes and additive mechanism of action was obtained from the scanning electron micrographs. Furthermore, the active particle rate processes were identified over a number of densifications in a single cycle.

4.2 Experimental

4.2.1 Apparatus and reagents

Experiments were conducted on a pilot plant scale using a 75 L lagged stainless steel autoclave fitted with steam coils, draft tube and a dual impeller configuration. A 0.125 m six bladed Rushton turbine was used as the lower impeller with an off-bottom clearance of 0.1 m. An axial flow impeller of diameter 0.125 m was used as the upper impeller. Temperature and pressure in the autoclave were regulated using automatic controllers. Feed solutions were prepared in a 200 L vessel fitted with an axial flow impeller and steam heating coils. Sampling was conducted through a discharge flash tank fitted with a 220 ml steel sampling cup for sample collection. The experimental set up is shown in Fig. 4.1.

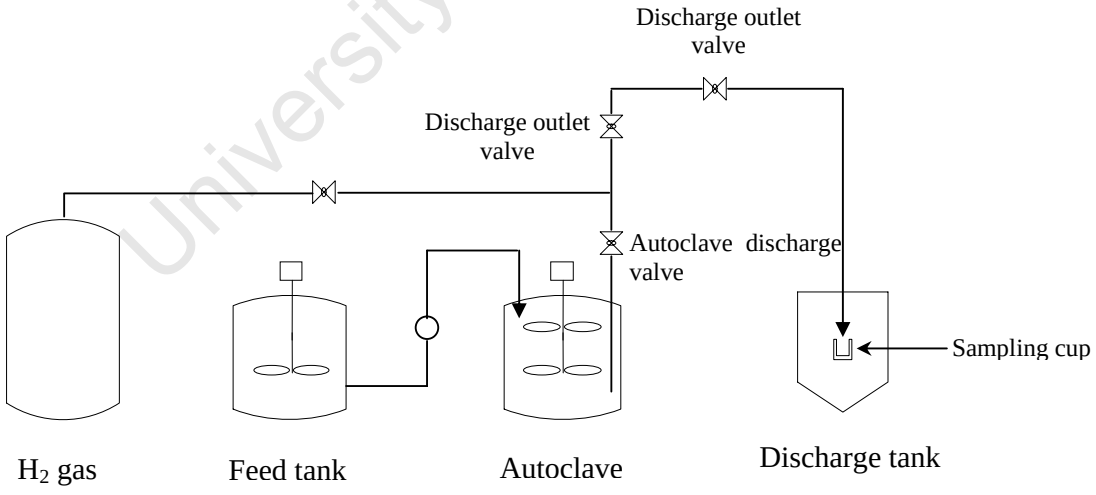

Figure 4.1 Set up of equipment used to conduct the experiments

Feed solutions were obtained from the leach section of a base metal refinery by leaching a Ni-Cu matte in $CuSO_4$ – H_2SO_4 (copper winning spent electrolyte) using oxygen as the oxidizing agent followed by removal of iron to generate a feed solution containing between 55-65 g/L of total metals and 350-400 g/L of $(NH_4)_2SO_4$. Analytical grade ammonia solution was used to adjust the NH_3/Ni molar ratio to 2.2. Nucleation solution was prepared by adding the following nucleating catalysts to the unbuffered feed solution (not containing $(NH_4)_2SO_4$): aerosol C61, acrysol A3 and aluminium sulphate.

Modifier N9300 (a polyacrylic acid derivative) supplied by Chemserve Technical Products was used as an additive. High purity hydrogen gas (minimum assay 99.8 % H_2) was used as a reducing agent. Samples were collected in 250 ml plastic containers, and after separation, the powder was dried on aluminium pans using a magnetic hot plate. The volume of the reduction end solution was measured using a 1 L volumetric flask. A laser diffraction Malvern Mastersizer (Model S-Long bench) was used to measure the PSD of the nickel powder and a Leica electron optics (Leo) scanning electron microscope (Model SS 440) was used to capture electron micrographs of the powder. Powder purity was determined using a surface analyser for trace elements (SAFT) and the nickel concentration in the reduction solution was measured by inductively coupled plasma optical emission spectroscopy (ICP - OES).

4.2.2 Procedure

56 L of preheated nucleation solution was pumped from the feed tank into the autoclave in order to generate the seed needed for subsequent reduction. Agitation and heating were commenced by setting the agitator and temperature controllers to 580 rpm and 180 ^oC respectively. To avoid saturating the headspace with steam before commencing reduction the autoclave was pressurised with hydrogen to 2800 kPa when a temperature of 170 ^oC was attained. Timing was started as soon as hydrogen was introduced into the autoclave in order to note the reduction time. Hydrogen was automatically introduced when the pressure dropped below 2800 kPa as a result of hydrogen utilisation during reduction. Reduction was deemed to be complete when the autoclave pressure remained constant at 2800 kPa for more than 30 s indicating that hydrogen consumption due to reduction had stopped. The reduction time was noted immediately and heating and flow of hydrogen was stopped by changing the temperature controller setting to 0 ^oC and closing the hydrogen inlet valve from the control panel respectively.

To confirm that nucleation had occurred, a sample from the autoclave was obtained by opening the discharge outlet valves to the flash tank. The autoclave discharge valve was slowly and slightly opened, while the remaining two discharge valves were fully opened. Care was taken to avoid discharging all the powder in the autoclave during sampling as a result of the large pressure difference between the autoclave (2800 kPa) and flash tank (atmospheric pressure). The presence of fine black nuclei in the nucleation end solution indicated that nucleation was successful. Agitation was then stopped and the powder allowed to settle for 1 h. Thereafter the nucleation end solution was discharged from the autoclave by fully opening all the discharge valves.

The reduction solution was prepared by pumping the metal solution from the leach section into the feed tank and the molar ratio of NH_3:Ni was adjusted to between 1.95-1.98 by addition of ammonia solution and under agitation. Titration of the reduction solution with 0.1 N H_2SO_4 was used to measure the concentration of NH_3 in solution and the nickel concentration was measured as total metals by EDTA titration. If the correct molar ratio was obtained, a predetermined amount of additive was then added depending on the desired dosage. Dosage levels ranged from 0.25 - 5 vol %. The reduction solution was kept at temperatures around 90 ^oC and continuously agitated before being reduced. 56 L of reduction solution were then pumped into the autoclave and reduction was conducted using a procedure similar to that used for nucleation. A solution colour change from dark blue to light green indicated that reduction was complete and this was confirmed by measuring the residual nickel concentration. Settling times were 30 min for the first three densifications, thereafter 10 min. Samples were collected after every densification and were transferred from the sampling cup into 250 mL plastic beaker where there were allowed to cool before being transferred into sample containers. The powder and solution were separated by decantation and the volume and nickel concentration in the reduction end solution were measured using a measuring cylinder and ICP-OES respectively.

Powder samples were washed three times with hot water, with the water being decanted at each washing stage and dried on an aluminium pan using a magnetic hot plate set at 100 ^oC. Drying was stopped when the powder particles began to swirl under the influence of the magnetic field, indicating that the powder was dry. However, samples obtained on nucleation and the first initial densifications were gelatinous and therefore difficult to wash and dry.

As a result the PSD of these samples was not analysed. The powder was allowed to cool, weighed on an analytical balance and then transferred into a 100 mL plastic bottle for storage.

Nickel content and impurities in the powder were measured using a surface analyser for trace elements (SAFT) and the powder morphology was observed from the SEM micrographs.

4.3 Results and Discussion

The experiments to check for reproducibility have been repeated under similar conditions but on a laboratory scale using a 0.5 L stainless autoclave. However, nucleation was done on a plant scale and the seed introduced to the laboratory reactor for further batch reductions. The same ratios of seed:total metal feed were used on the plant, pilot plant and laboratory scale. Findings from these experiments indicate a high degree of reproducibility in terms of the evolution of particle size distribution and the derived moments. Results of these laboratory experiments are presented in Section 3.3.1 of this thesis.

These results and those produced on the plant scale indicate that reduction experiments are reproducible provided the reduction conditions i.e. amount of seed, composition and concentration of feed solution and modifier dosage remain unchanged.

4.3.1 Attainable number of densifications

The attainable number of densifications was defined as the number of batch reductions that could be completed within a reduction time of less than 30 min. Generally reduction times ranged from 10 min in the initial stages of the cycle to 25 min at the end of the cycle. The attainable number of densifications increased when the modifier dosage was increased from 0.25 vol % to 1 vol % and thereafter decreased with further increases in modifier dosage (Table 4.1 and Fig. 4.2). Thus, the optimum modifier dosage needed to achieve the maximum number of densification at the lowest modifier dosage lies between 0.25 - 3 vol %.

Table 4.1
Attainable number of densifications achieved as function of modifier dosage

Modifier dosage (vol %)	Attainable densifications
0.25	5
1	11
3	10
5	7

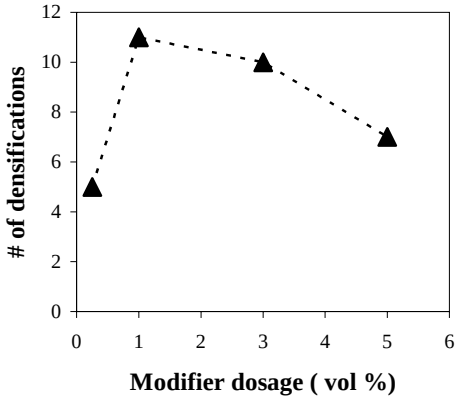

Figure 4.2 Attainable number of densifications as a function of modifier dosage

4.3.2 Nickel depletion rate

The nickel depletion rate increased with modifier dosage up to a dosage of 3 vol % and decreased thereafter (Fig. 4.3). Depletion rates generally decreased with increase in the number of densifications within each cycle.

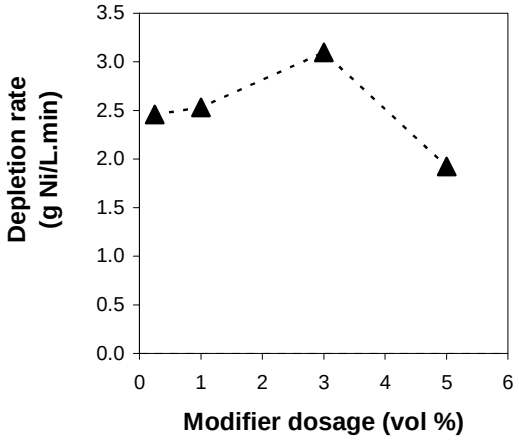

Figure 4.3 Variation of nickel depletion rate with modifier dosage

4.3.3 Evolution of PSD of nickel powder

The evolution of the PSD on a volume % basis at different modifier levels is shown in Fig. 4.4.

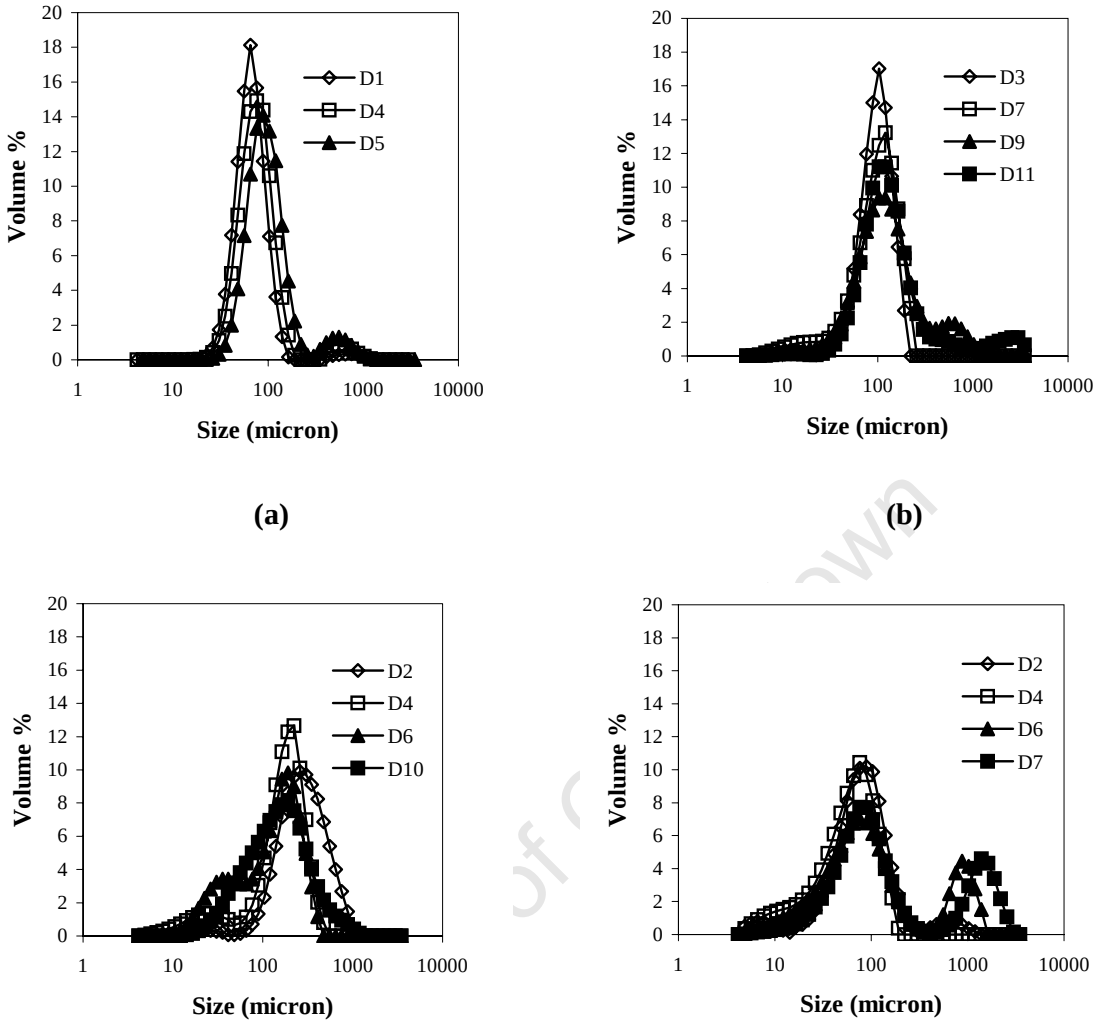

Figure 4.4 Evolution of the PSD at different modifier levels: (a)- 0.25 vol %; (b)- 1 vol %; (c)- 3 vol % and (d)- 5 vol %

The PSD at all the modifier dosages was bimodal with modal sizes of approximately 100 μm and 1000 μm with the exception of the modifier dosage of 3 vol % where modal sizes were approximately 20 μm and 100 μm.

Similar trends were observed in the evolution of the PSD at 0.25 vol % and 1 vol %, suggesting that the active particle rate processes were similar in both cases. The gradual shift in modal side at the 100 μm peak indicates molecular growth of these particles, while the decrease in volume % with each successive densification suggests the presence of aggregation.

The maximum primary crystal size that can be achieved by molecular growth alone can be calculated from equation 3.1 by inserting the appropriate values i.e. $V_m = 6.6 \times 10^{-3}$ m^3 mol^{-1}, $\Delta c = 6.65$ mol m^{-3} (based on total mass deposited over eleven densifications) and $N_o \sim 10^{13}$ m^{-3} (estimated from Fig. 4.5a). The calculated d_{max} value is 20.3 μm thus, it is unlikely that the particles at the 100 and 1000 μm modal sizes were formed by molecular growth alone, suggesting that aggregation played a major role in the formation of these particles.

The gradual shift of the modal size to smaller sizes observed at modifier dosage of 3 vol %, suggests that breakage was a dominant mechanism and there was a decrease in the extent of aggregation.

At 5 vol %, the modal size at approximately 100 μm remains nearly unchanged indicating that there is no significant molecular growth occurring.

A more detailed investigation of the particle size enlargement and reduction mechanisms follows and hereafter the particle size distributions are represented in their moment forms only.

4.3.4 Moments evolution

The PSD data was transformed into moments and de-normalised based on the liquor mass balance obtained from the charge volume and measured nickel concentration before and after reduction. The evolution of the m_0 and the number based mean size ($L_{1.0}$) of the powder at each densification in a given cycle are shown in Fig. 4.5.

A slight decrease in the value of m_0, corresponding to a decrease in the number of particles (from 6.72 to 4.9e11), was noted in the entire cycle for a modifier dosage of 0.25 vol %. As the modifier dosage was increased above 0.25 vol %, an increase in the number of particles was noted in the early stages of the cycle, followed by a decrease in the number of particles as noted at modifier dosages of 3 and 5 vol % (Fig. 4.5a). The trend was less defined at a modifier dosage of 1 vol % where there was a periodic increase and decrease in the number of particles.

Since, aggregation results in a decrease in the number of particles; nucleation and breakage in an increase in the number of particles; and growth does not affect particle number, the active particle rate processes can be identified from the evolution of the zeroth moment. However, nucleation has been shown to be absent under normal reduction conditions (Sheritt Gordon Mines, 1958).

Thus, the increase in particle number could only be due to breakage. Thus, it appears that aggregation was the major particle rate process at modifier dosage of 0.25 vol % with breakage becoming apparent at higher modifier dosage levels. Overall, the total number of particles in the system increased with modifier dosage (Fig. 4.5a).

This factor was reflected in the number based mean size, which decreased with increasing modifier dosage (Fig. 4.5b).

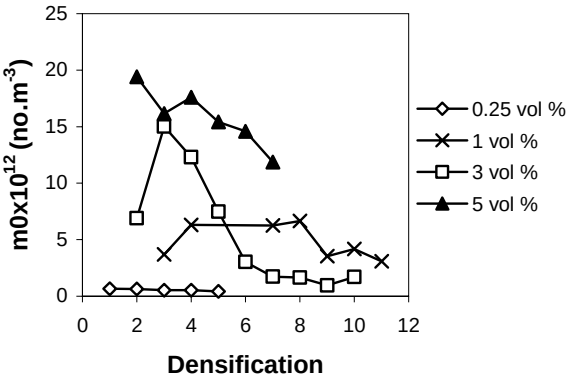

(a)

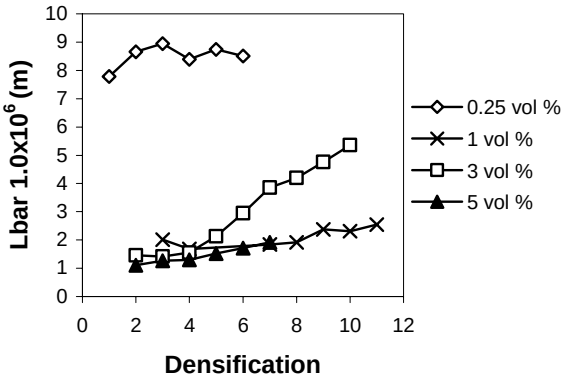

(b)

Figure 4.5 Evolution of: (a) the zeroth moment; (b) the number based mean size

Thus, the evidence is that increasing modifier dosages above 0.25 vol % increased the extent of breakage, resulting in an increase in the number of particles and decrease in number-based mean size. A modifier dosage of 0.25 vol % was found to be the minimum dosage required to achieve appreciable reduction within a period less than 30 min. This is essential to ensure that the process becomes economic to operate commercially, thus this dosage was used as the starting reference value.

The evolution of the m_3 and the volume or mass moment mean *D(4.3)* is shown in Fig. 4.6. The m_3 reflects the change in volume or mass (for particles with constant density) of the particles as result of precipitation of salt or metal from solution. In nickel precipitation systems this occurs through the deposition of nickel metal from solution onto the surface of the metal, a process known as growth or plating.

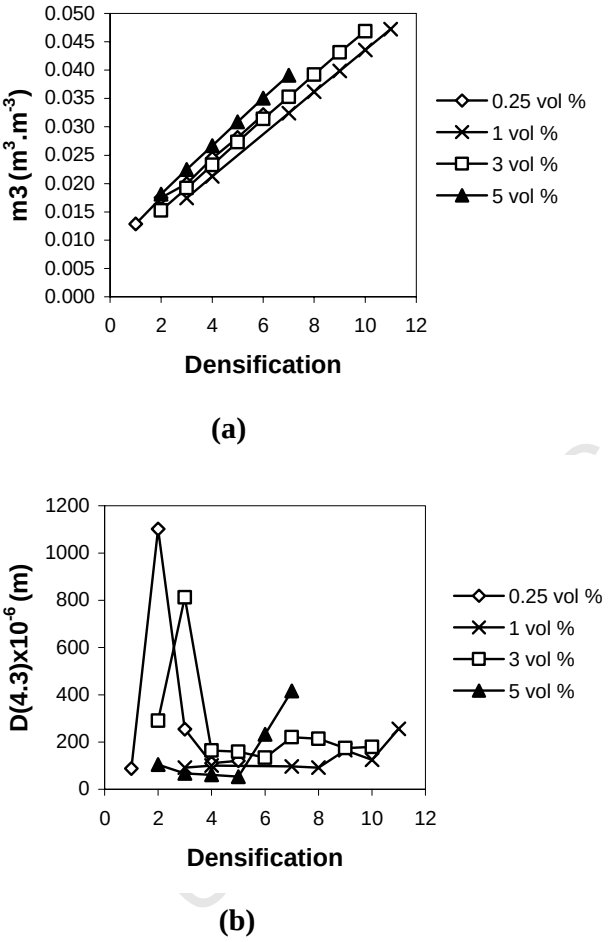

Figure 4.6 Evolution of: (a) the third moment; (b) the volume based moment mean

Growth was an active particle rate processes at all modifier dosages and the growth rate was constant, as indicated by the linear relationship between m_3 and the densification number (Fig. 4.6a). The *D(4.3)* for modifier dosages of 0.25 and 3 vol % were characterised by erratic behaviour at the beginning of each cycle. However, the total mass deposited increased slightly with modifier dosage. This was reflected by the D(4.3) at the end of each cycle, which was highest at a modifier dosage of 5 vol % and lowest at 0.25 vol % (Fig. 4.6b).

The evolution of the m_2 is shown in Fig. 4.7. The behaviour of m_2 was erratic at modifier dosages of 1 and 3 vol %, however, clear trends were observed at 0.25 and 5 vol % dosage levels. The surface areas at the end of each cycle were more influenced by the modifier dosage as opposed to the number of densifications conducted.

Thus, while there was an increase in the number of attainable densification with increase in modifier dosage up to 1 vol % and a decrease thereafter, the surface area at the end of each cycle increased with increase in modifier dosage.

Overall, there was a decrease in m_2 at 0.25 vol % and an increase at higher dosage levels. Decrease in m_2, corresponding to a decrease in surface area, is a clear indication of aggregation. Cementation of primary particles during aggregation results in a decrease in surface area as the area between the particle bridges becomes unavailable as reduction sites.

In the absence of nucleation, the increase in m_2 can either be due to growth or breakage. Based on the evolution of the PSD on a volume % basis and the mass deposition rate, no significant molecular growth was observed at a modifier dosage of 5 vol %. Furthermore, if growth was the dominant mechanism one would expect a parabolic increase in m_2, this shows that the process is dominated by aggregation as further evidenced by the decrease in m_0 (Fig. 4.5a). Thus, the linear increase in m_2 from D5 to D7 at a modifier dosage of 5 vol % can be largely attributed to breakage by fragmentation (Fig. 4.7). Aggregation of larger particles can also be noted from the sharp increase in the *D(4.3)* at a modifier dosage of 5 vol % from D5 to D7 (Fig. 4.6b). Since breakage is more intense for large particles, fragmentation of these particles would result in a sharp increase in m_2.

The m_2 at the end of each cycle increased with increase in modifier dosage (Fig. 4.7), indicating that the extent of aggregation decreases with increase in modifier dosage. Similarly, from the increase in m_2, it can be concluded that the particles aggregates become more prone to breakage as the modifier dosage is increased.

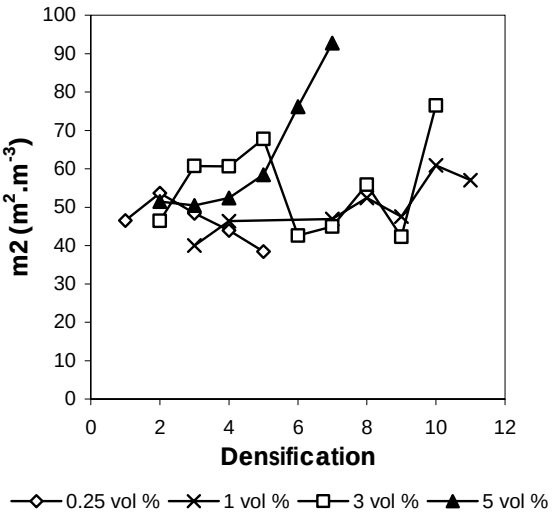

Figure 4.7 Evolution of the *m2* at different modifier dosages

4.3.5 BET surface area

BET surface area results of the powder at the initial stages and end of the cycle are shown in Fig. 4.8. The surface area decreased with each successive densification within a cycle and generally increased with increase in modifier dosage (Fig. 4.8).

At a dosage of 5 vol %, the cycle could not be extended beyond seven densifications despite the fact that the surface area at the end of the cycle was comparable to that at the initial stages of cycles with modifier dosages of 0.25 and 1 vol % (Fig. 4.8). The decrease in surface area was sharper at 0.25 and 5 vol % as indicated by the slope of the curves. Since BET measurements detect external area plus pore area, the decrease in surface area may be due to decrease in pore area, as an overall increase in m_2 was noted at modifier dosages greater than 0.25 vol %. Comparison of the BET surface area and the m_2 reveals that the modifier increases the external surface area as opposed to increasing the pore area, contrary to industrial observations that it increases powder porosity. For the complex morphology of particles shown in Fig. 3.9, the pore area may be significantly larger than external area.

The decrease in nickel depletion rates with increase in the number of densifications is largely due to the overall decrease in BET surface area as each cycle progresses.

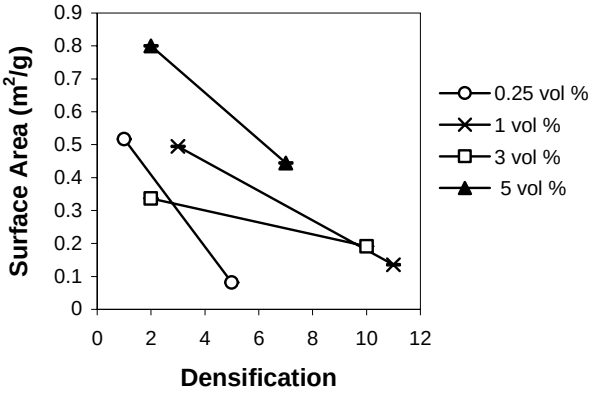

Figure 4.8 BET surface area results at the beginning and end of each cycle

4.3.6 SEM and SAFT results

SEM micrographs of the powder at the beginning and end of each cycle are shown in Fig 4.9. The powder began as fine spherical particles, which aggregated as the cycle progressed. Compact aggregated powder was formed at modifier dosages of up to 3 vol % and at 5 vol % the powder was loose and porous (Fig. 4.9).

Thus, increasing the modifier dosage beyond 3 vol % appears to promote breakage. The SEM micrographs confirm the findings obtained both the PSD and BET surface area results.

The nickel content of the powder from each cycle as measured by the SAFT method is shown in Table 4.2. There was no appreciable difference in the nickel content of the powder for modifier dosages between 0.25 and 3 vol %, however, the nickel content dropped slightly at a modifier dosage of 5 vol %. These results confirm that powder formed was mostly nickel with cobalt being the major impurity.

Table 4.2
Purity of nickel powder obtained at selected modifier dosages

Modifier dosage (vol %)	% Nickel in powder
0.25	99.8
1	99.9
3	99.7
5	99.4

(a) 0.25 vol %

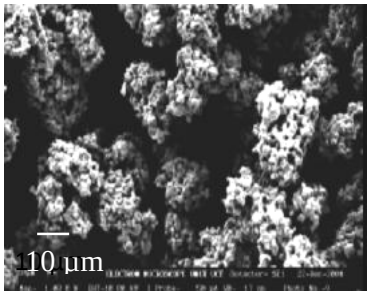

D1

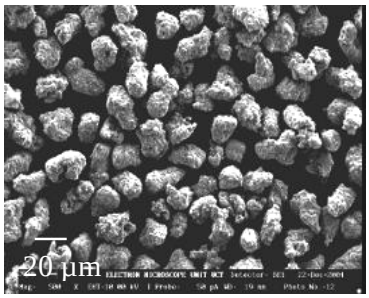

D5

(b) 1 vol %

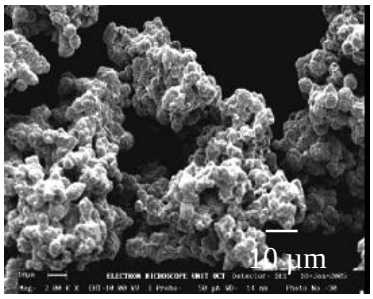

D3

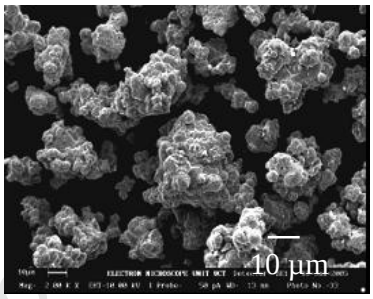

D11

(c) 3 vol %

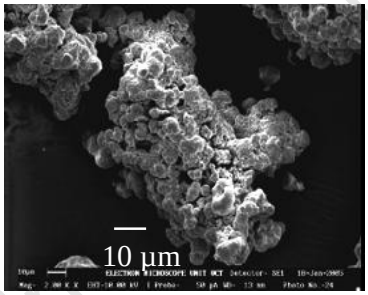

D2

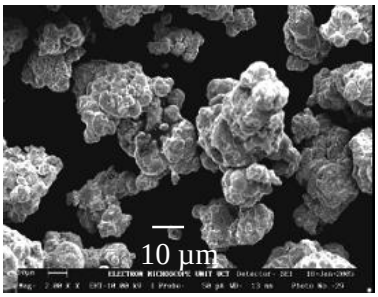

D10

(d) 5 vol %

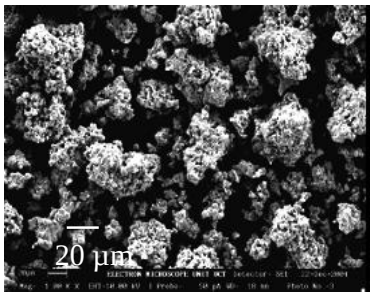

D1

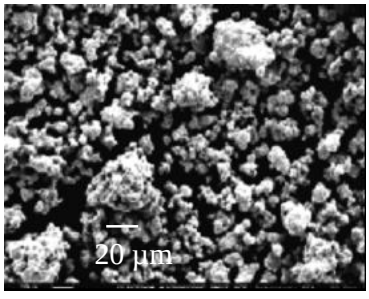

D7

Figure 4.9 SEM micrographs of the powder at the initial stages and end of the cycle at specified modifier dosage

4.3.7 Proposed mechanism of action of the modifier

Based on evidence from the evolution of the PSD, moments, nickel depletion rates, BET surface area and SEM micrographs, increase in modifier dosage retards growth and leads to weaker agglomerate bonds. Weaker agglomerate bonds make the particles more prone to shear induced breakage due to intensive agitation employed in reduction autoclaves to ensure adequate suspension of the dense nickel particles. Thus, the modifier can be considered to act as an anti-agglomerating agent. This proposal is consistent with observation from the evolution of the PSD and SEM micrographs, which revealed that increasing the modifier dosage results in an increase in the total number of particles and the formation of loose porous particles as opposed to compact aggregates. The generation of more primary particles leads to an increase in the surface area, which in turn should result in an increase in the number of attainable densifications. This is so because the rate of reduction was found to be proportional to surface area of nickel particles (Needes and Burkin, 1975). However, the results obtained indicate that the number of attainable densifications only increase when the modifier dosage is increased from 0.25 to 1 vol % and decreases thereafter. This indicates that the increase in the number of attainable densifications as a result of the increase in surface area, induced by modifier addition, is only effective up to a modifier dosage of 1 vol %. This suggests that the modifier retards growth. If it promoted growth then an increase in modifier dosage would lead to an increase in the number of attainable densifications. While there is an increase in the nickel depletion rate up to a modifier dosage of 3 vol %, there is no corresponding increase in number of attainable densifications.

BET results show that the surface area of the powder at the end of the cycle at a modifier dosage of 5 vol % is comparable to that of the powder at the initial stages of cycles with modifier dosages of 0.25 and 1 vol %. However, appreciable reduction was not realised within 30 min. This indicates that while adequate surface area was available, reduction did not occur possibly as a result of surface deactivation by the modifier. Since the modifier has to first adsorb on the surface in order to interfere with reduction, the extent of deactivation depends on the amount of modifier added. Thus, selective deactivation of the particle surface area is desirable in order to avoid excessive aggregation, which decreases the effective surface area available for reduction. However, deactivation of the entire particle surface is undesirable as it terminates reduction. Thus, the optimum modifier dosage for this system lies between 0.25 and 1 vol %, further experiments would need to be conducted in this region to refine the estimate for the optimum dosage for the system.

4.4 Conclusion

The modifier dosage has been found to greatly influence the number of attainable densifications in a cycle, nickel depletion rate, the evolution of the PSD and the morphology of the powder obtained. Maximum number of attainable densifications was obtained at 1 vol % and decreased with further increases in modifier dosage. Nickel depletion rates increased up a modifier dosage of 3 vol % and decreased thereafter. The number of particles increased while the number based mean size decreased with increases in modifier dosage, while the mass/volume based mean size was highest at 5 vol % and lowest at 0.25 vol %.

The evolution of the m_0, m_2 and m_3 revealed that aggregation and growth were the major particle rate processes at modifier dosage of 0.25 vol %, with breakage becoming apparent at higher dosage levels. Evidence of the presence of aggregation and breakage was further confirmed by the evolution of the volume % distribution.

The modifier was found to act as an anti-agglomerating agent by inhibiting growth, resulting in an increase in the surface area available for reduction. This increase in surface area increased the number of attainable densifications up to a modifier dosage of 1 vol %, thereafter the effect of increased surface area was negated by the growth inhibiting effect of the modifier.

5. KINETIC MODELLING OF NICKEL REDUCTION

For metallic powders, the properties of the individual particles (e.g. size, shape and microstructure) and the bulk properties (e.g. chemical composition, PSD, specific surface and apparent density) are important in powder metallurgy. All these parameters are determined by the overall precipitation kinetics which are governed by the relative rates and mechanisms of the kinetic processes of nucleation, growth, aggregation and breakage (Söhnel and Garside, 1992). Thus, in order to control the powder properties one needs to identify the kinetic processes active during the precipitation process.

In the previous chapters, the active particle rate processes were identified from the evolution of the moments of the PSD. The objective of this chapter is to verify these mechanisms by means of mathematical models based on the moment form of the population balance equation. The following models were tested based on conclusions drawn from the moments evolution of the experimental PSD data: (i) aggregation-only; (ii) aggregation and growth; (iii) nucleation and aggregation; (iv) nucleation and growth and (v) aggregation and breakage.

5.1 Mathematical Models

The mathematical models used in this work are based on the moment transformation of the population balance (equation 2.23) coupled with the kinetics of the particular particle rate process. Previous investigators have used a differential technique based on the discretised population balance as described by Hounslow *et al*., (1988) to identify the active particle rate processes during nickel reduction (Lewis and Hounslow, 2005; Taty Costodes *et al*., 2006).

Based on the evolution of the PSD of the powder on a plant scale, Lewis and Hounslow (2005) tested four models namely; (i) growth-only, (ii) nucleation and growth, (iii) nucleation and aggregation and (iv) aggregation and growth. They found that none of these models generates satisfactory matches for the experimental data, indicating that the process is complex and different mechanisms are active to varying degrees in each cycle. However, the process was demonstrated to be dominated by aggregation and breakage.

Similar findings were obtained by Taty Costodes *et al.*, (2006) who tested the growth only model and found that it only predicts the growth shift in the middle densifications, indicating that growth is not the only mechanism active during nickel reduction.

The approach adopted in this study is based on the evolution of the PSD on a laboratory and pilot plant scale and the moment form of the population balance. The different models used in this study are presented below.

5.1.1 Aggregation

The aggregation process is characterised by the aggregation rate constant or kernel (β_o). For size-independent aggregation in a batch system using length as the internal coordinate, Hounslow *et al.*, (1988) derived equation 5.1 as an expression for the moments of the distribution as a function of time.

$$m_j(t) = m_j(t_o)\left(\frac{2}{N_o\beta_o t + 2}\right)^{1-j/3} \tag{5.1}$$

Differentiating equation 5.1 with respect to time, gives the birth and death terms of the moment equation for size-independent aggregation (equation 5.2).

$$\overline{B_{aj}} - \overline{D_{aj}} = -\frac{1}{2}(1 - j/3)\beta_o m_o(t) m_j(t) \tag{5.2}$$

This equation agrees with that derived by Hulburt and Katz (1964) for the 0^{th} and 3^{rd} moment of the PSD.

5.1.2 Aggregation and growth

The nickel precipitation process was described by a size- independent growth rate (G) and aggregation kernel. The moment form of the PBE is given by equation 5.3.

$$\frac{dm_j}{dt} - jGm_{j-1} = -\frac{1}{2}(1 - j/3)\beta_0 m_0(t) m_j(t) \tag{5.3}$$

For the 0^{th} and 3^{rd} moments equation 5.3 reduces to:

$$\frac{dm_0}{dt} = -\frac{1}{2}\beta_o m_0(t)^2 \tag{5.4}$$

$$\frac{dm_3}{dt} = 3Gm_2 \tag{5.5}$$

5.1.3 Nucleation and aggregation

The nickel precipitation process was described by a nucleation rate (B^o), which gives the rate of appearance of nuclei at a size l_o and a size-independent aggregation kernel. The moment form of the PBE is given by equation 5.6.

$$\frac{dm_j}{dt} = B^0 l_0^j - \frac{1}{2}(1 - j/3)\beta_0 m_0(t) m_j(t) \tag{5.6}$$

For the 0th and 3rd moment equation 5.6 reduces to:

$$\frac{dm_0}{dt} = B^0 - \frac{1}{2}\beta_0 m_0(t)^2 \tag{5.7}$$

$$\frac{dm_3}{dt} = B^0 l_0^3 \tag{5.8}$$

Equation 5.7 is a nonlinear differential equation and can be solved analytically (Chen *et al.*, 2003) to yield:

$$m_0 = \frac{1}{\beta_0 \tau}\frac{1 - \exp(-t/\tau)}{1 + \exp(-t/\tau)} \tag{5.9}$$

The precipitation time constant (τ) is defined by equation 5.10.

$$\tau = \frac{1}{\sqrt{2B^o\beta_0}} \tag{5.10}$$

5.1.4 Nucleation and growth

For nucleation and growth the moment form of the PBE is given by equation 5.11.

$$\frac{dm_j}{dt} - jGm_{j-1} = B^0 l_0^j \tag{5.11}$$

For the 0th moment, only the nucleation term remains in equation 5.11.

5.1.5 Aggregation and breakage

The PBE for aggregation and breakage using length as the internal co-ordinate is defined by equation 5.12 (Schaer *et al.*, 2001). This equation has no analytical solution and has to be solved numerically or transformed into its moment form to a simpler relationship that can be solved analytically. The moment transformation of the PBE for breakage gives the birth and death functions in equation 5.13 by substituting $2^{1/3}L = l$ in the breakage term in equation 5.12 (Schaer *et al.*, 2001).

$$\frac{\partial n(L,t)}{\partial t} = \frac{L^2}{2}\left(\int_0^L \frac{\beta\left(\left(L^3-\lambda^3\right)^{1/3},\lambda\right)n\left(\left(L^3-\lambda^3\right)^{1/3},t\right)n(\lambda,t)}{\left(L^3-\lambda^3\right)^{2/3}}d\lambda\right) + n(L,t)\left(\int_0^\infty \beta(L,\lambda)n(\lambda,t)d\lambda\right) + 2^{4/3}k_{bo}\left(2^{1/3}L\right)^a n(2^{1/3}L) - k_{bo}L^a n(L) \tag{5.12}$$

$$\overline{B_{bj}} - \overline{D_{bj}} = (2^{((3-j)/3)} - 1)k_{bo}m_{j+a} \tag{5.13}$$

The size independent factor of the breakage frequency (k_{bo}) is related to the breakage frequency (k_b) by equation 5.14, where *u* is the volume of the particles (Randolph and Larson, 1988).

$$k_b(u) = k_{bo}u^{a'} \tag{5.14}$$

Using a constant breakage frequency (a' = 0 and a = 0) the moment form of the PBE for breakage yeilds:

$$\frac{dm_j}{dt} = \left(2^{(3-j)/3} - 1\right)k_{bo}m_j \tag{5.15}$$

The final moment model for aggregation and breakage is obtained by combining equation 5.15 and 5.2 to yield:

$$\frac{dm_j}{dt} = \left(2^{(3-j)/3} - 1\right)k_{bo}m_j - \frac{1}{2}(1-j/3)k_a m_0(t)m_j(t) \tag{5.16}$$

For the 0th moment and 3rd moment this equation reduces to:

$$m_0 = \frac{e^{tk_{bo}}\left(k_{bo}m_0(0) - C\right) + C}{k_{bo}} \text{ ; where } C = \frac{1}{2}\beta_o m_0(0)^2 \quad (5.17)$$

$$m_3 = m_3(0) \quad (5.18)$$

5.2 Results and Discussion

The first section of the results seeks to identify the active mechanisms of the precipitation process under normal reduction conditions, based on standard industrial plant operating conditions. Under standard operating conditions, commercial systems operate with a free NH_3: Ni^{2+} molar ratio of between 2.0-2.5 in the presence of high strength ammonium sulphate ($(NH_4)_2SO_4$: Ni^{2+} molar ratio of 1.8-4.5) at elevated temperature (180-210 ^oC) and pressure (2800-3500 kPa). To achieve appreciable reduction within a reasonable time an additive is added in dosages between 0.3-0.35 for the morphology modifier and Fe levels in the reduction solution are usually less than 3 mg/L.

Data generated from laboratory scale studies is presented first, followed by that generated on a pilot plant scale. Results obtained from repeatability studies conducted on a laboratory scale using experimental conditions simulating those on an industrial scale (presented in Section 3.3.1) were used in the modelling work. This information was used to identify the active particle rate processes expected under standard operating conditions.

The second section identifies the active mechanisms in the presence of iron and is based on laboratory scale data presented in Chapter 3.

The last section identifies the active particle rate processes in the presence of varying amounts of the morphology modifier based on data generated on a pilot plant scale, presented in Chapter 4. For purposes of consistency the moments are expressed as a function of the densification number instead of time.

5.2.1 Reduction under standard operating conditions

Since nucleation has been found to be absent under normal reduction conditions (Sherrit Gordon Mines, 1958), therefore the aggregation-only, aggregation and growth, and aggregation and breakage models were tested.

Of these three models only the aggregation and growth model gave a satisfactory fit to the experimental 0^{th} and 3^{rd} moment (Fig 5.1). The average experimental value of βo and G based on the aggregation and growth model were $3.87(\pm 0.35)\times 10^{-16}$ $m^3.\#^{-1}.s^{-1}$ and $4.00(\pm 0.65)\times 10^{-9}$ $m.s^{-1}$ respectively. These values were calculated from the experimental measured moments by solving the differential equations 5.4 and 5.5.

The aggregation-only model only fits the 0^{th} moment (Fig 5.1a) and underestimates the 2^{nd} moment and 3^{rd} moment (Fig 5.2). Since volume is conserved during aggregation, the 3^{rd} moment is expected to remain constant.

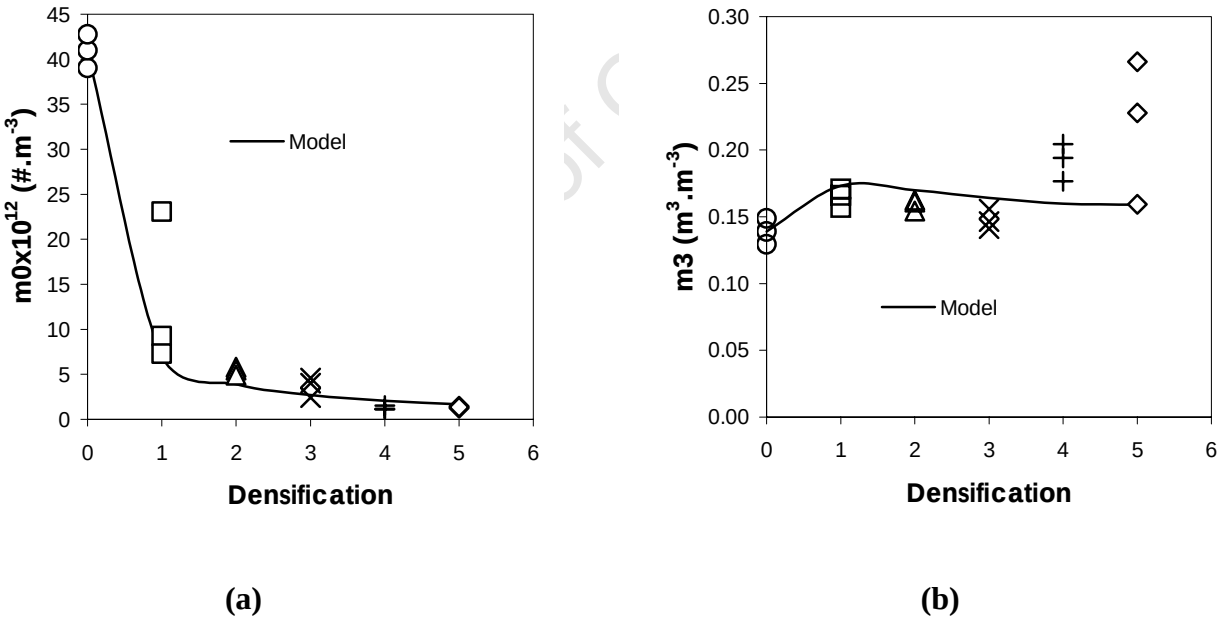

(a) **(b)**

Figure 5.1 Normalised experimental and simulated moments for batch growth and aggregation (a) 0^{th} moment and (b) 3^{rd} moment

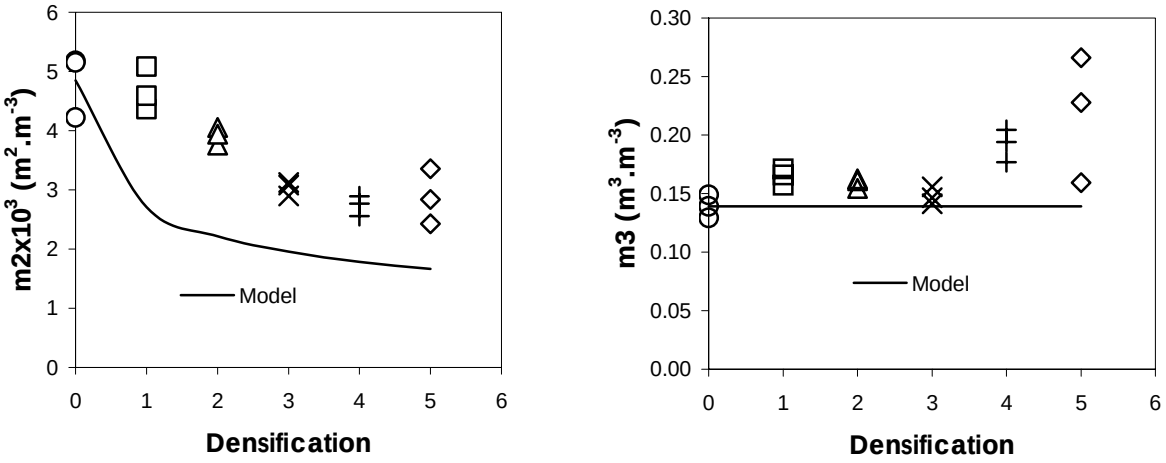

(a) **(b)**

Figure 5.2 Normalised experimental and simulated moments for batch aggregation (a) 2nd moment and (b) 3rd moment

Thus, it can be concluded that aggregation is not the only active particle rate process and in the absence of nucleation, growth is only mechanism that can account for the difference between experimental and simulated values for the 2nd and 3rd moments.

The aggregation and breakage model gives negative breakage rates until D4, indicating that breakage only becomes significant for larger particles (i.e. *D(4.3)* approximately 100 µm, estimated from Fig. 3.2). In the final stages of the cycle (D4-D5), one can assume negligible aggregation based on the fact that there is no significant change in the 0th moment (Fig. 5.1a) and the calculated k_{bo} in the absence of aggregation was found to be $3.38(\pm 1.43) \times 10^{-4}$ s^{-1}.

Based on these results the nickel reduction process under standard operating conditions is considered to be largely dominated by aggregation and growth in the early stages of the cycle with breakage and growth becoming significant in the later stages of the cycle when larger particles have been formed. The "Agglomeration Tendency", defined as the ratio of the number of seed crystals N_s to the number of product crystals N_p (Derenzo *et al.*, 1996) is approximately 25, indicating that this process exhibits a very high agglomeration tendency.

5.2.2 Reduction in the presence of iron

Four models were tested namely; aggregation and growth, nucleation and aggregation, nucleation and growth, and aggregation and breakage.

In the absence of Fe, only the aggregation and growth model gave a satisfactory fit to the 0th and 3rd moments (Fig. 5.3) confirming the results obtained with the repeatability studies, since reduction was conducted under standard operating conditions. However, the fit in the 3rd moment was poor towards the end of the cycle. This factor is largely due to the fact that the precision in the experimental 3rd moment decreases drastically towards the end of the cycle (Fig. 3.2).

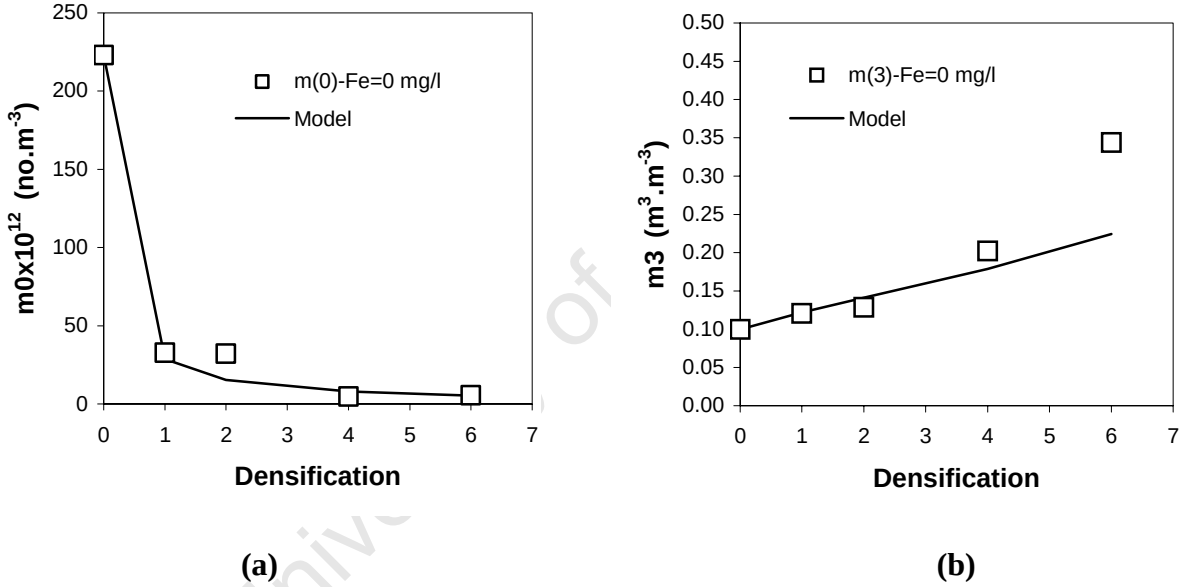

(a) **(b)**

Figure 5.3 Normalised experimental and simulated moments for batch aggregation and growth in the absence of Fe (a) 0th moment and (b) 3rd moment

Results for the growth and aggregation model in the presence of Fe are shown in Figure 5.4. The model gave a satisfactory fit of the 0th moment as from D2 at Fe=6 mg/L with the fit becoming poor with increasing concentration of Fe (Fig 5.4a). The model gave a satisfactory fit to the 3rd moment at Fe=6 mg/L except towards the end of the cycle, as noted in the absence of Fe. At higher Fe levels the difference between the simulated and experimental values increased, however, the difference became smaller towards the end of the cycle (Fig 5.4b).

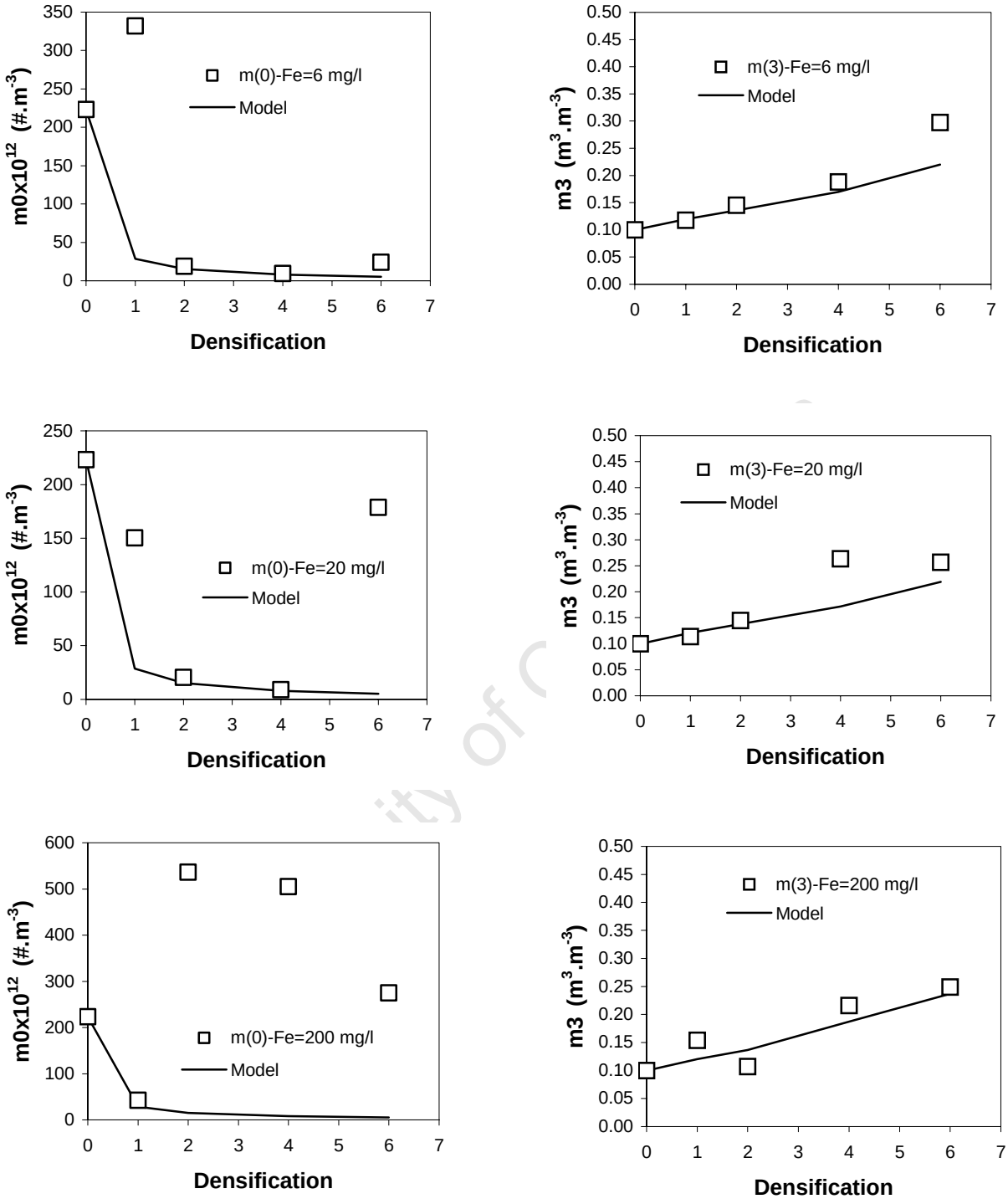

(a) **(b)**

Figure 5.4 Normalised experimental and simulated moments for batch aggregation and growth in the presence of Fe (a) 0^{th} moment and (b) 3^{rd} moment

The average experimental value of βo in presence of Fe, based on the aggregation and growth was $1.45(\pm 0.77)\times 10^{-16}$ $m^3.\#^{-1}.s^{-1}$ and the G values are given in Table 5.1.

Table 5.1
Values of *G* used in the aggregation and growth model

Fe concentration in reduction solution (mg/L)	$G \times 10^{-9} (m.s^{-1})$
0	4.70
6	4.76
20	5.06
200	4.77

Thus, it can be concluded that growth and aggregation are not the only active mechanisms in the presence of Fe and that, as the Fe concentration is increased beyond 6 mg/L, growth and aggregation cease to be dominant mechanisms.

The nucleation and aggregation model does not give a satisfactory fit to the 0^{th} moment at Fe= 6 mg/L and 200 mg/L, however, this model predicts the 0^{th} moment at the end of the cycle at Fe levels of 200 mg/L (Fig 5.5a). At Fe=20 mg/L, a satisfactory fit in the 0^{th} moment was only observed at the initial stages of the cycle and the model nearly predicted the 0^{th} moment at the end of the cycle.

The model underestimates the 3^{rd} moment at all Fe levels and the difference between the simulated and experimental values increases as the cycle progresses. Since the 3^{rd} moment evolves as a result of growth and/or nucleation, from Fig. 5.5b it can be concluded that the evolution of the 3^{rd} moment is largely determined by molecular growth as opposed to nucleation. The experimental value of B^o based on the nucleation and aggregation model was; 2.13×10^{12}, 1.71×10^{12} and 6.49×10^{12} $m^{-3}s^{-1}$ for Fe levels of 6, 20 and 200 mg/L respectively. The βo value used was similar to that found for the aggregation and growth model in the presence of Fe.

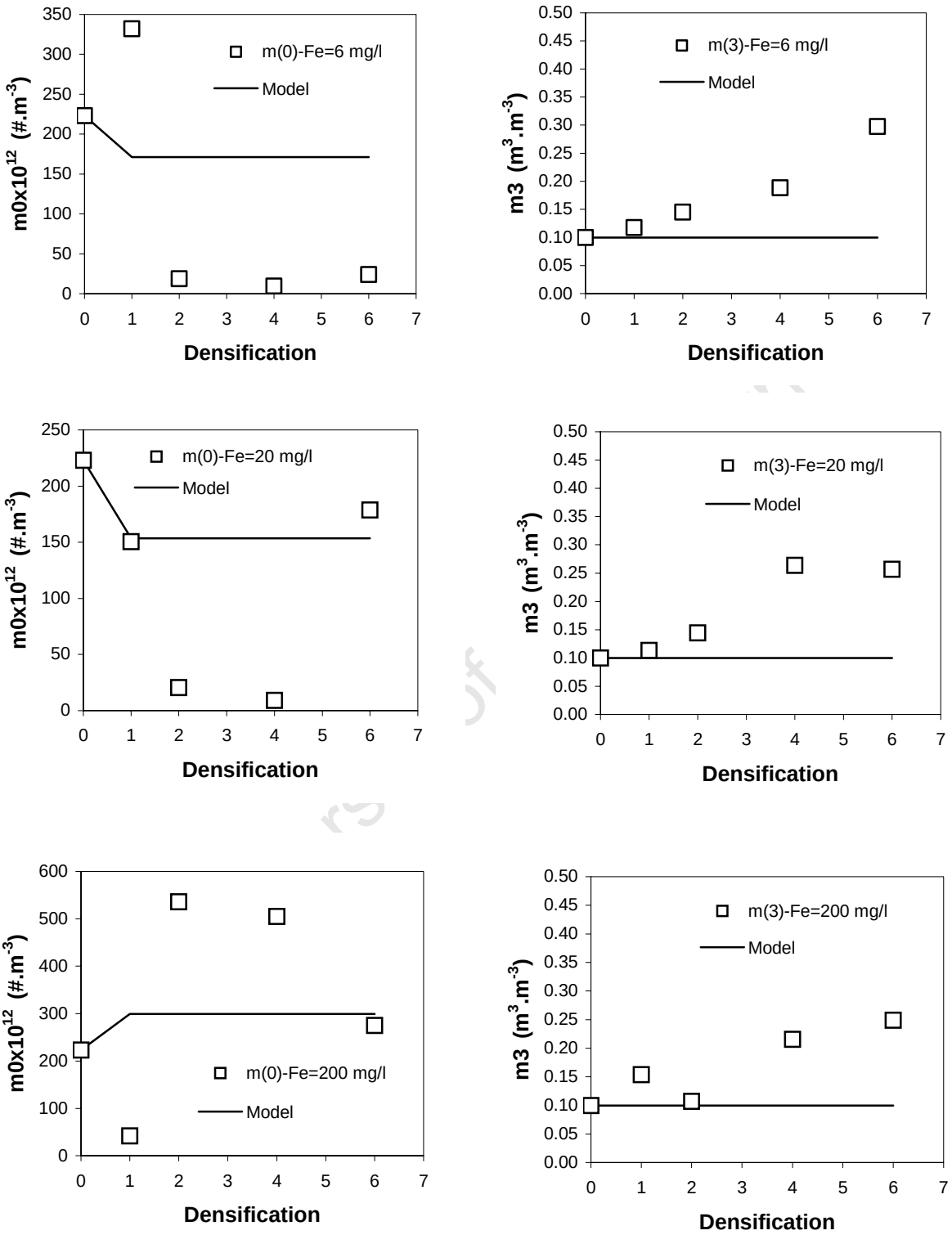

(a) **(b)**

Figure 5.5 Normalised experimental and simulated moments for batch nucleation and aggregation in the presence of Fe (a) 0^{th} moment and (b) 3^{rd} moment

The nucleation and growth model overpredicts 0th moment. A sample of the results at Fe= 6 mg/L is depicted in Fig. 5.6a, with a similar trend observed at the other Fe levels. If nucleation does occur, this result suggests that the aggregation process is highly efficient or the nucleation rate is not constant throughout the cycle. As has been demonstrated for the nucleation and aggregation model, nucleation did not have a significant effect on the 3rd moment thus, the evolution of the 3rd moment is expected to be similar to that shown in Fig. 5.4b for the aggregation and growth model. Therefore, this model was considered inappropriate for modelling the experimental data.

For aggregation and breakage, the model fails to fit the 0th and 3rd moment. A sample of the results for the 0th moment at Fe= 6 mg/L is depicted in Fig. 5.6b. A similar trend was observed at the other Fe levels. The 3rd moment remains constant at its initial value since volume is conserved on aggregation and breakage, thus the model does not fit the experimental values. The breakage model used assumes that k_{bo} is a function of the hydrodynamic conditions. Therefore, since similar hydrodynamic conditions were used, the k_{bo} used in the aggregation and breakage model is similar to that derived from reduction under standard conditions. Since breakage has already been demonstrated to be negligible for particles with a *D(4.3)* less that 100 µm, therefore the initial sharp increase in the 0th moment in the presence of iron can only be attributed to nucleation.

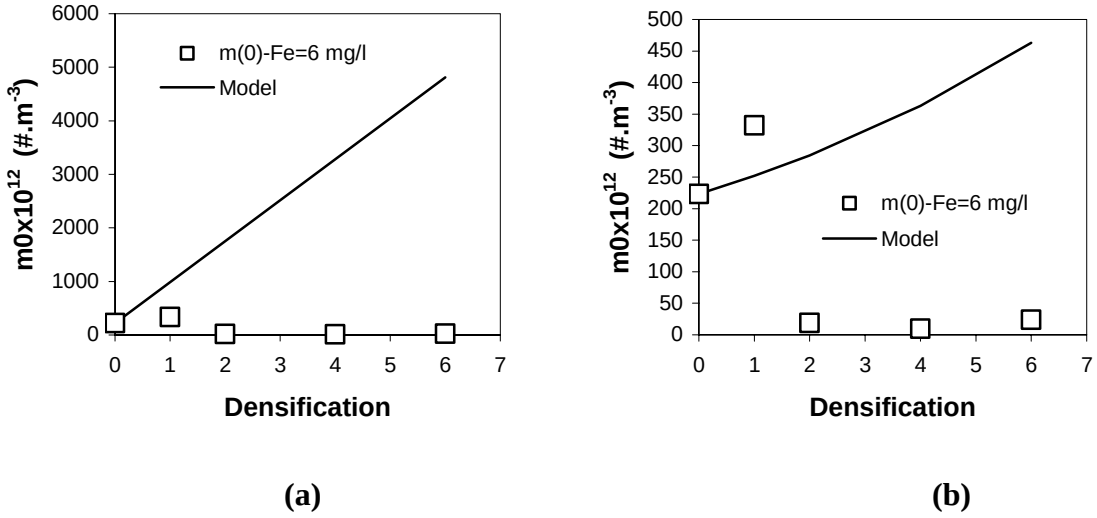

Figure 5.6 Normalised experimental and simulated moments at Fe= 6 mg/L (a) nucleation and growth model (b) aggregation and breakage

From the results obtained above it can be seen that when Fe is introduced into the reduction solution the process becomes complex and can not be explained by a single model. The Agglomeration Tendency decreases rapidly from approximately 40 in the absence of Fe to 0.8 at Fe=200 mg/L, indicating a strong tendency towards secondary nucleation or breakage as the Fe concentration is increased. However, since supersaturation is depleted in the process, the decrease in the Agglomeration Tendency is largely attributed to secondary nucleation.

Thus, it is clear that Fe induces secondary nucleation; however, it appears the nucleation rate is not constant throughout the cycle as assumed in the modelling work. The nucleation rate appears to vary depending on the surface area available for reduction. Comparison of the 2^{nd} and 0^{th} moments in the presence of Fe reveals that nucleation becomes significant when there is a significant drop in surface area i.e. initial stages of the cycle for Fe= 6 and 200 mg/L and towards the end of the cycle for Fe= 20 mg/L (Fig. 3.6 and Fig. 5.4a). Thus, a significant drop in surface area enhances surface nucleation by directing supersaturation release on nucleation since the available seed surface area becomes inadequate to deplete supersaturation by molecular growth. This is further confirmed by the fact that the aggregation model fits the experimental 0^{th} moment in cases where nucleation is not significant (Fig. 5.4a). These results confirm the surface nucleation mechanism which was proposed to occur in the presence of Fe.

Nucleation was found to have a negligible effect on the 3^{rd} moment and growth alone successfully predicted the 3^{rd} moment. Based on the kinetic parameters used to model growth (Table 5.1) it can be concluded that Fe does have an effect on the growth rate.

Thus, reduction in presence of Fe can be characterised by a size-independent aggregation and growth model with varying degrees of nucleation depending on the Fe concentration and available surface area, with breakage occurring towards the end of the cycle when larger particles have been formed. These findings confirm the conclusions reached in Chapter 3, although, further studies are required to study the nucleation mechanism in detail. The variation of the nucleation rate with seed surface area still needs to be established.

5.2.3 Reduction in the presence of a morphology modifier

Since nucleation has been demonstrated not to occur in buffered solutions and in the absence of nucleating agents (Sheritt Gordon Mines, 1958) only three models were tested, namely, aggregation only, aggregation and growth, and aggregation and breakage.

The aggregation only model gave a satisfactory fit to the experimental 0^{th} moment only at a modifier dosage of 0.25 vol % and at 3 vol % towards the end of the cycle (Fig. 5.7).

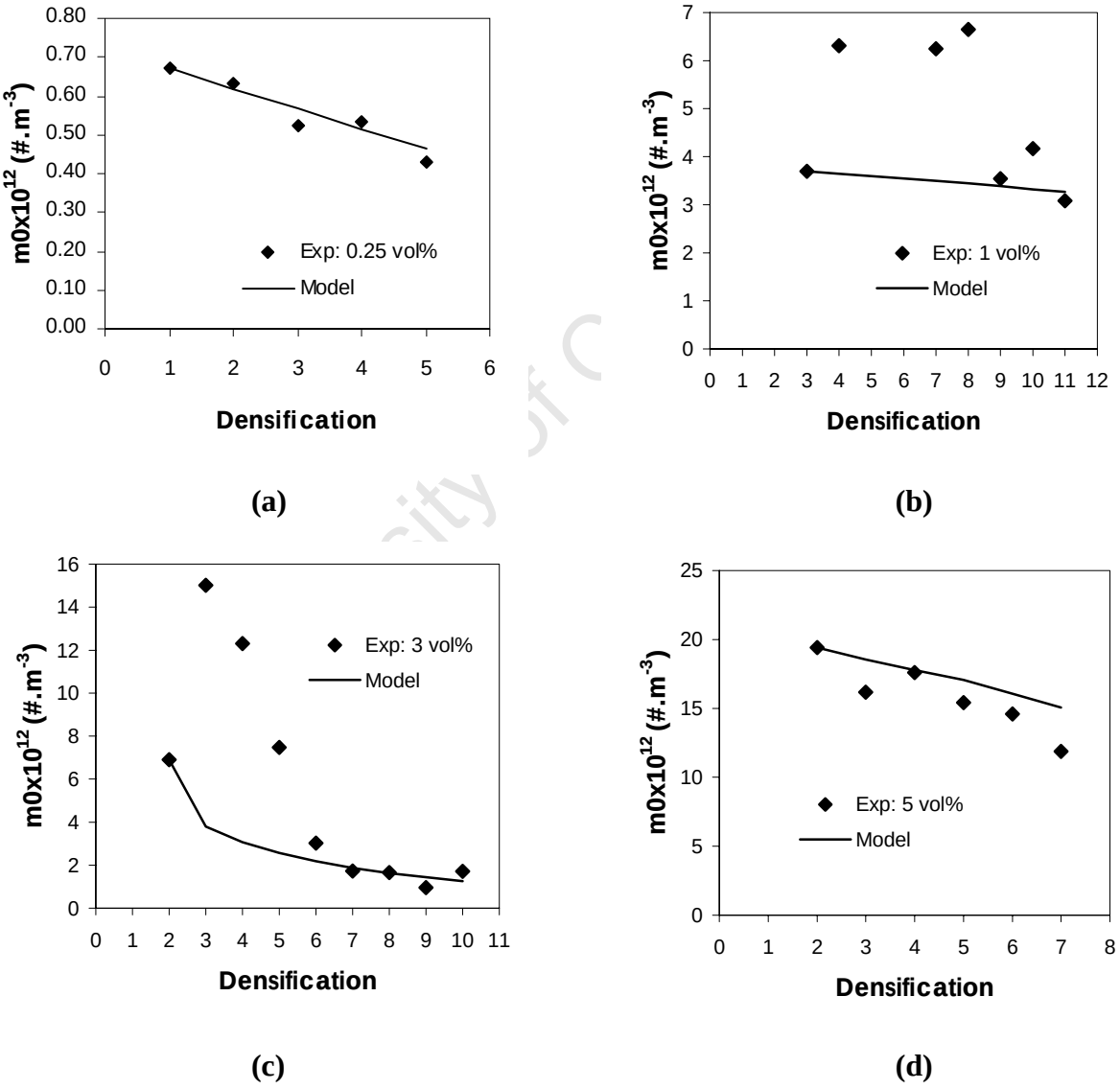

Figure 5.7 Normalised experimental and simulated 0^{th} moment for batch aggregation with increasing modifier dosage (a) 0.25 vol % (b) 1 vol % (c) 3 vol % (d) 5 vol %

A satisfactory fit in the 2nd moment was obtained towards the end of the cycle at a modifier dosage of 0.25 vol %, while the model underestimated the 2nd moment at higher modifier dosages (Fig. 5.8).

Since volume is conserved on aggregation, the model underestimates the 3rd moment at all modifier dosages, as there is an increase in the 3rd moment as the cycle progresses (Fig. 5.9).

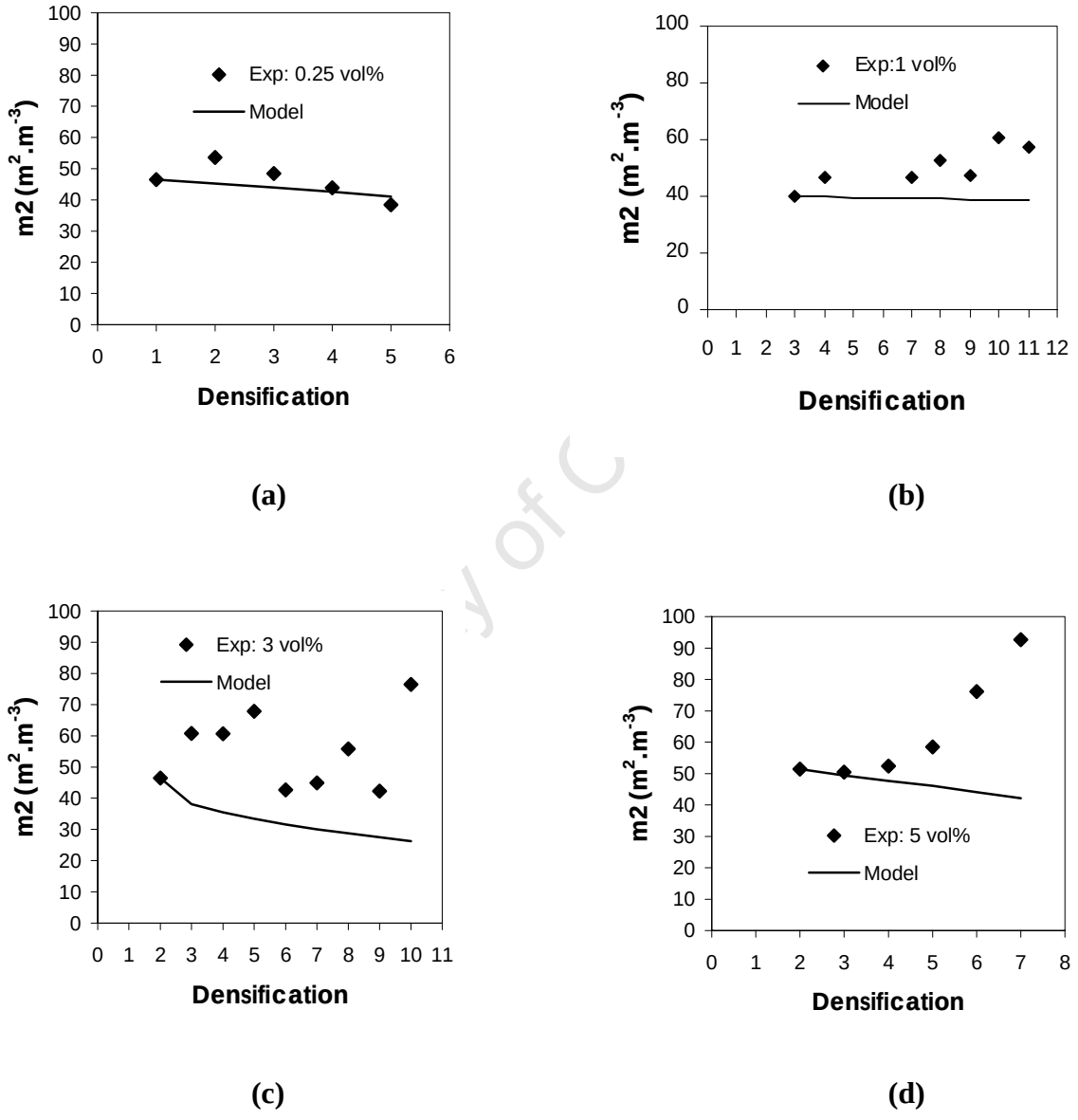

Figure 5.8 Normalised experimental and simulated 2nd moment for batch aggregation with increasing modifier dosage (a) 0.25 vol % (b) 1 vol % (c) 3 vol % (d) 5 vol %

The average experimental values of βo used in the aggregation only model are given in Table 5.2.

Thus, it can be concluded that aggregation is not the only active particle rate process and it ceases to be a dominant mechanism at modifier dosages greater than 0.25 vol %.

Table 5.2
Values of βo used in the aggregation only model

Modifier dosage in reduction solution (vol %)	$\beta o \times 10^{-16}$ $(m^3.\#^{-1}.s^{-1})$
0.25	3.63
1	0.0990
3	2.33
5	0.131

For the growth and aggregation model the trend in the 0^{th} moment is similar to that for the aggregation model since particle number is conserved when only growth occurs (Fig 5.7). The model slightly under-predicts the 3^{rd} moment in most instances, but overall gives an acceptable reflection of the experimental 3^{rd} moment when one takes into account the error associated with each measurement of the 3^{rd} moment (Fig. 5.9). The model input values of G are given in Table 5.3.

Table 5.3
Values of G used in the aggregation and growth model

Modifier dosage in reduction solution (vol %)	$G \times 10^{-9}$ $(m.s^{-1})$
0.25	1.02
1	0.470
3	0.757
5	0.268

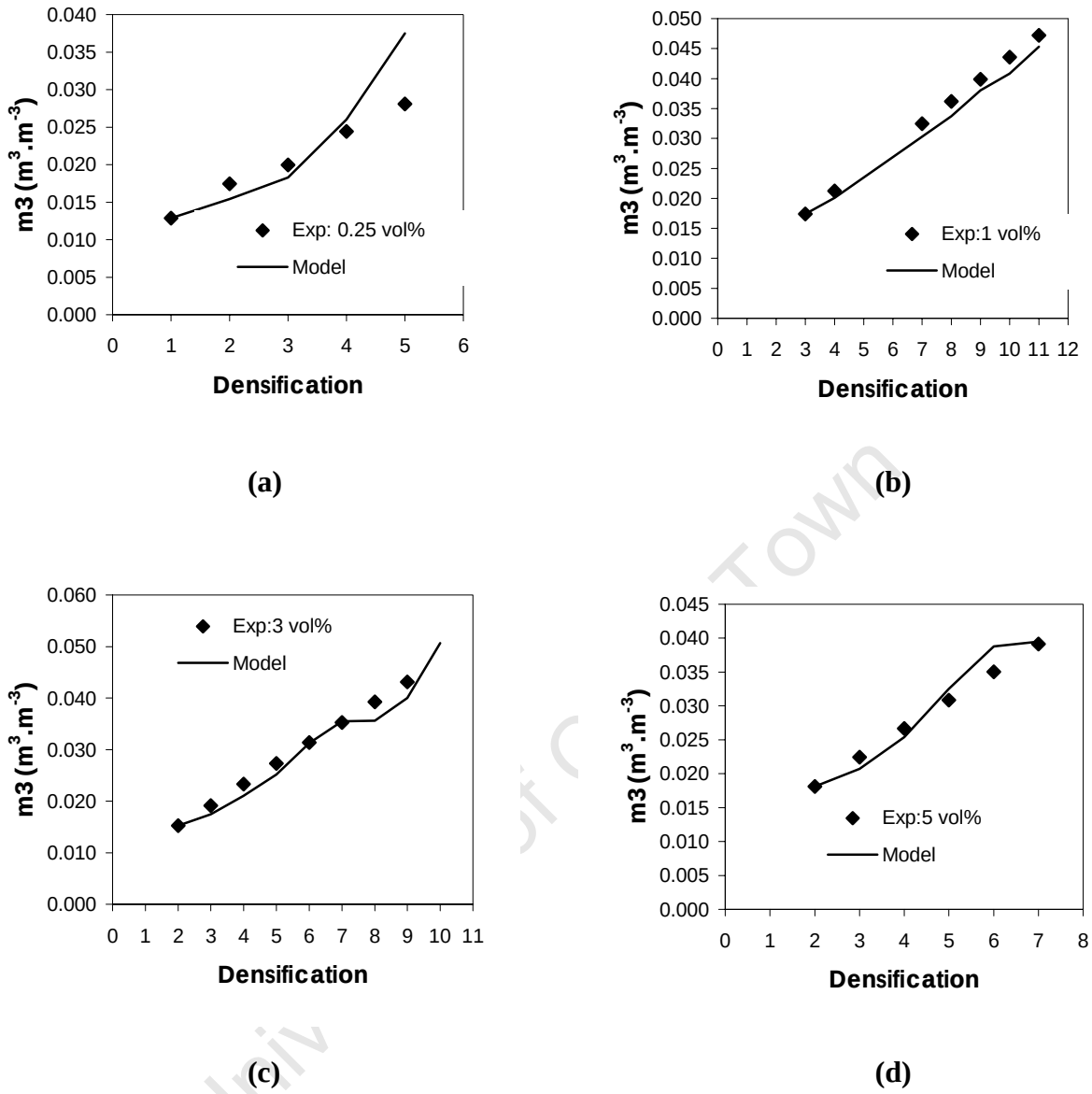

Figure 5.9 Normalised experimental and simulated 3rd moment for batch aggregation and growth with increasing modifier dosage (a) 0.25 vol % (b) 1 vol % (c) 3 vol % (d) 5 vol %

While the growth and aggregation model gives a good reflection of the 3rd moment, it fails to give a satisfactory prediction of the 0th moment at modifier levels greater than 0.25 vol % indicating that aggregation and growth are not the only active particle rate processes.

The aggregation and breakage model gives a satisfactory fit to the 0th moment at modifier dosages of 0.25 and 5 vol % (Fig. 5.10).

At 1 vol % modifier dosage the model only predicts the 0^{th} moment in the initial stages of the cycle and overestimates it thereafter. A similar trend was observed when using the breakage only model (Fig. 5.11a).

The model did not work at a modifier dosage of 3 vol %; however, the breakage only model does give a satisfactory prediction of the 0^{th} moment in the initial stages of the cycle (Fig. 5.11b).

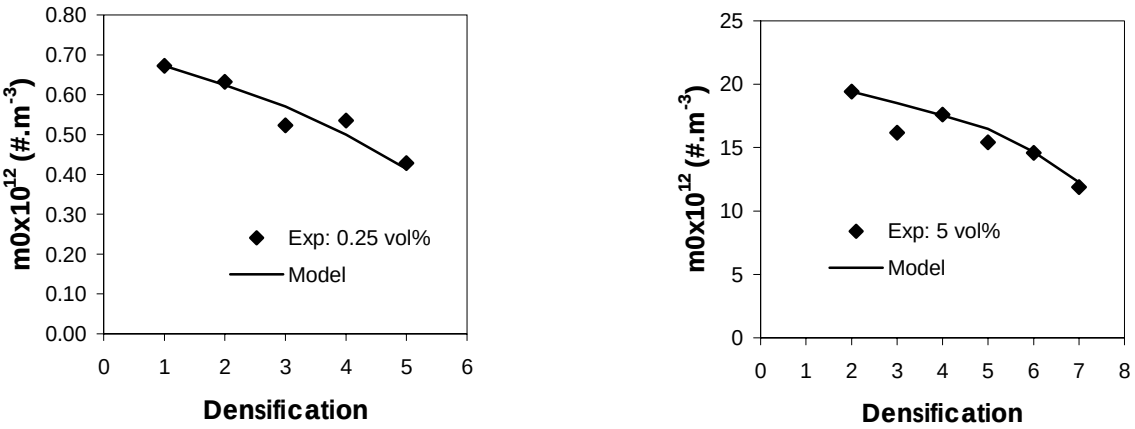

(a) **(b)**

Figure 5.10 Normalised experimental and simulated 0^{th} moment for batch aggregation and breakage with increasing modifier dosage (a) 0.25 vol % (b) 5 vol %

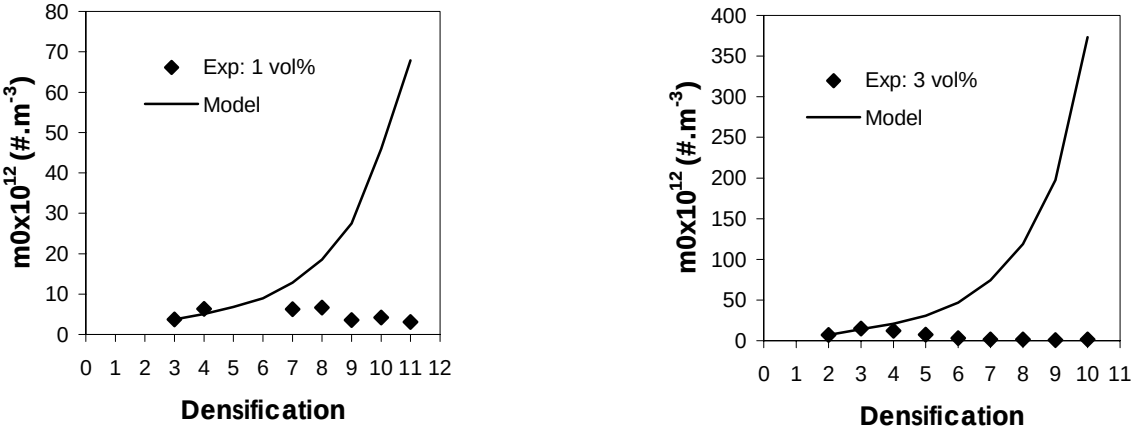

(a) **(b)**

Figure 5.11 Normalised experimental and simulated 0^{th} moment for breakage with increasing modifier dosage (a) 1 vol % (b) 3 vol %

Since volume is conserved on aggregation and breakage this model will underestimate the 3rd moment. The values of βo used in the aggregation and breakage model are similar to those in Table 5.2, while the k_{bo} values are given in Table 5.4.

Table 5.4
Values of k_{bo} used in the aggregation and breakage model

Modifier dosage in reduction solution (vol %)	$k_{bo} \times 10^{-4}$ *(s^{-1})*
0.25	0.232
1	4.08
3	7.07
5	0.835

From the results presented above, it can be seen that aggregation, growth and breakage adequately predicts the 0th and 3rd moments at modifier dosages of 0.25 and 5 vol %. The situation becomes complex at modifier dosages of 1 and 3 vol % and different mechanisms become active at different stages in each cycle. In the initial stages of the cycle the process is largely dominated by breakage and growth, while aggregation and growth become dominant towards the end of the cycle. Thus, conclusive evidence of the effect of the morphology modifier can be drawn by comparing the results obtained at modifier dosages of 0.25 and 5 vol %.

The modifier can be described as increasing the breakage rate since k_{bo} generally increases with modifier dosage and decreasing the aggregation rate since βo decreases with increase in modifier dosage. Based on the number of particles at the end of each cycle, the Agglomeration Tendency decreased sharply with increasing modifier dosage. This decrease in the extent of aggregation is largely attributed to the decrease in the molecular growth rate as the modifier dosage is increased (Table 5.3). These conclusions are in agreement with those reached in Chapter 4, which described the modifier as an anti-agglomerating agent as a result of inhibiting growth, resulting in an increase in surface area available for reduction.

However, at modifier dosages greater than 1 vol % the increase in surface area available for reaction is negated by the growth inhibiting effect of the modifier.

5.3 Particle formation

Based on the modelling work it can be concluded that, under standard operating conditions, particle formation occurs mainly by growth and aggregation. Calculations based on the mass deposition rates have shown that the final particle size is largely determined by aggregation with growth providing the crystalline neck cementing the particles together. However, the degree of aggregation decreases significantly towards the end of the cycle (Fig. 5.1) and the number of particles remains nearly constant. This factor, coupled with the absence of a sharp rise in either the number or volume based mean size towards the end of the cycle (Fig. 3.2), indicates that there is a critical size beyond which aggregation ceases. If more densifications are conducted beyond this stage, as is the practice on a commercial scale where a minimum of 50 densifications are conducted per cycle, size enlargement will occur mainly by growth. Beyond this stage, breakage also becomes noticeable and significant breakage has been shown to occur for particles with a *D(4.3)* greater than 100 µm. Thus, it can be concluded that the final particle morphology is largely determined by the growth mechanism and the particle size by aggregation.

Scanning electron micrograph cross-sections of the spherical, open powder (Fig. 5.12) show that the particles are polycrystalline and the dendrites arise from a central precursor and grow in a multi-radial direction.

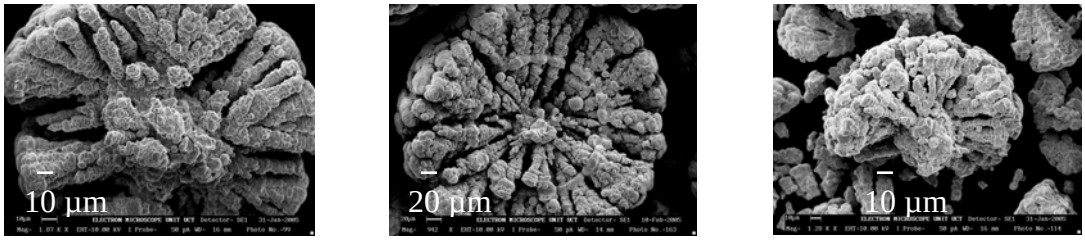

Figure 5.12 Scanning electron micrographs of the spherical, open powder

This mechanism is similar to that proposed for spherulitic particles formed in the presence of foreign particles (Gránásy *et al.*, 2005).

Furthermore, the internal radial growth pattern is characteristic of the spherulitic growth mode. However, since growth alone in the absence of aggregation cannot account for the PSD, the particles were not formed from the nucleated primary crystals as observed in other spherulitic growth systems such as vaterite spherulites (Andreassen, 2001, Andreassen, 2005). Although there is no general accepted theory of spherulitic crystallisation, the most prevalent theory suggests it occurs as a result of secondary nucleation of crystal grains at the crystal growth front (Gránásy et al., 2005). This process known as growth front nucleation (GFN) arises as a result of static heterogeneities (due to impurities or molecular defects) and/or dynamic heterogeneities (when reorientation of molecules is slow relative to interface propagation).

Thus, the spherical, open particle is considered to occur through the formation of a precursor as a result of secondary aggregation followed by spherulitic growth as a result of impurity action (i.e. morphology modifier). The modifier selectively deactivates growth sites on the nickel particle surface resulting in the spherulitic growth mode.

When iron is introduced into the reduction system, it induces surface nucleation which creates new growth sites on the particle surface. This increases the surface activity of the powder resulting in more compact spherulites (Fig 1.1b and c). A similar change in morphology has been noted in spherulitic growth systems when supersaturation was increased, which in turn increases the growth rate (Beck *et al.*, 2007). Based on phase field modelling, Gránásy *et al.*, (2005) also observed that as the supersaturation is increased, there is an increased branching frequency yeiding more space filling patterns. Formation of crystals on the surface of the solid phase has also been reported to result in the formation of dendrites which can grow on the surface and subsequently break off the crystal (Söhnel and Garside, 1992).

From the modelling work, iron was found to increase the molecular growth rate up to a concentration of 20 mg/L, with nucleation becoming more pronounced with increasing iron concentrations beyond 6 mg/L. Above iron levels of 20 mg/L the nuclei formed by surface nucleation do not appear to undergo further growth as evidenced by the SEM micrographs of the powder (Fig. 3.8e).

Thus, compact spherulites are expected to be formed in the presence of iron up to a concentration of 20 mg/L with the degree of compactness increasing with increasing iron concentration. A certain degree of compactness is normally beneficial for spherulitic particles which are normally fragile as a result of their open structure.

Thus, iron levels below 6 mg/L may be beneficial in terms of making the spherulites more compact, reducing particle breakage while not significantly changing the particle morphology and powder purity. Iron levels below 6 mg/L have been demonstrated not to significantly alter the desired particle morphology.

Formation of closed, spherical particles is therefore proposed to be induced by any growth promoting impurity which is capable of activating the nickel particle by creating new growth sites as a result of surface nucleation.

Similar findings were obtained by Kunda and Evans (1968) who observed that additives that appeared to promote growth resulted in the production of spherical shaped compact powder, while additives that appeared to inhibit growth produced irregular shaped dendritic powder.

5.4 Conclusion

Kinetic modelling of laboratory scale reduction experiments conducted under standard operating conditions suggest that the process is dominated by aggregation and growth in the early stages of the cycle. Growth and breakage become significant in the later stages of the cycle when larger particles (i.e. ~100 μm) have been formed. The process was found to have a very high Agglomeration Tendency. It was also demonstrated, based on the mass deposition rate, that particle size enlargement in the early stages of the cycle is largely due to aggregation, with growth serving to cement the particles together. The magnitude of the growth rate is of the order of 10^{-9} $m.s^{-1}$, indicating that growth is a slow process requiring several densifications in order to increase particle size.

Reduction in the presence of Fe was characterised by a size independent aggregation and growth model with varying degrees of nucleation depending on the Fe concentration and available surface area. Iron was found to increase the growth rate up to a concentration of 20 mg/L.

The variation of the nucleation rate with Fe concentration and seed surface area has not yet been established.

An aggregation, growth and breakage model was found to satisfactorily predict the 0^{th} and 3^{rd} moments at modifier dosages of 0.25 and 5 vol % for experimental data generated on a pilot-plant scale. These results are in agreement with the findings of Lewis and Hounslow (2005) who found that on a plant scale the process was largely dominated by aggregation and breakage. Based on these results it was found that increasing the morphology modifier dosage results in an increase in the breakage rate and a decrease in the aggregation rate, which was largely attributed to the decrease in the molecular growth rate.

Both the morphology modifier and Fe were found to change the particle morphology by having an effect on the molecular growth rate.

Spherically shaped nickel powder was proposed to be formed through the formation of a precursor by secondary aggregation followed by spherulitic growth. The degree of compactness of the spherulites was proposed to be determined by the number of active growth sites on the particle surface.

The morphology modifier was found to act as a growth inhibitor, decreasing the number of growth sites, leading to more open spherulites. Iron was found to increase the number of growth sites by inducing surface nucleation leading to more compact spherulites.

Thus, by adequately controlling the proportion of growth promoters and inhibitors it is possible to control particle morphology. Since iron is frequently present in most nickel ores and is converted to ferrous sulphate during leaching, it presents an inherent source of catalyst material. While in commercial practice, reduction is never carried out in the absence of an anti-agglomerating agent, these additives are expensive and are normally employed in minute quantities. They are however, critical in maintaining appreciable reduction rates by maintaining adequate surface area for reduction making the process more economic to operate. They also reduce plastering on the autoclave walls and impellers reducing downtime required for leaching, thus increasing productivity. Since iron levels of less than 20 mg/L have been shown not significantly affect powder purity, thus iron levels can be effectively controlled to achieve the required particle design at minimal cost.

6. CONCLUSIONS

The effects of the morphology modifier and iron on the precipitation behaviour of nickel produced by high-pressure hydrogen reduction have been investigated. The motivation behind the study was to determine the factors responsible for the formation of powder with undesirable morphology and to develop a fundamental understanding of the precipitation mechanisms responsible for powder formation. In nickel precipitation by hydrogen reduction, two product morphologies have been observed: the spherical, open powder (desirable) and the spherical, closing/closed powder (undesirable).

Under standard operating conditions, the process was characterised by a high agglomeration tendency and agglomeration ceased when the limiting aggregate size (D_{max}) of approximately 100 μm was reached. Based on the evolution of the volume and number based mean sizes there was no evidence that particles greater than 100 μm aggregate together. Calculations based on the mass deposition rate demonstrated that the formation of particles with a volume mean size greater than 100 μm was a result of aggregation and that growth alone could not account for such particle sizes. The magnitude of the growth rate was of the order of 10^{-9} $m.s^{-1}$, indicating that growth is a slow process requiring several densifications in order to increase particle size.

Breakage was apparent when particles reached a volume mean size greater than 100 μm and the fines generated aggregated back into the main population. After the limiting aggregate size was reached size enlargement occurred mainly by molecular growth. Thus, it was proposed that the mechanism of molecular growth determines the final morphology of the particles and aggregation their final size. The evolution of the experimental 0^{th} and 3^{rd} moment were successfully modelled by a size-independent aggregation and growth model, validating the conclusions originally proposed.

Based on these findings and evidence from SEM micrographs (i.e. polycrystallinity and the internal radial growth pattern) the formation of the spherical, open powder was proposed to occur through the formation of a precursor by secondary aggregation followed by spherulitic growth.

While the mechanism of spherulitic growth is still not fully understood, a prevalent theory suggests it occurs through growth front nucleation as a result of static and/or dynamic heterogeneties. In the case of nickel reduction it is proposed static heterogeneities caused by the action of the morphology modifier is largely responsible for the formation of the spherulites.

However, at this stage it is not possible to establish the variation of the growth rate with respect to supersaturation. The widely used definition of supersaturation in terms of solubility has limited application to this process since the nickel metal precipitated is not soluble in the reduction solution. The use of the overpotential as a measure of supersaturation was proposed based on the electrochemical nature of the process; however, this approach is still being explored. This information is essential if the mechanism of growth is to be fully understood.

The morphology modifier was found to act as an anti-agglomerating agent by inhibiting growth, resulting in an increase in the surface area available for reduction. Growth inhibition leads to the formation of weaker agglomerate bonds making the particles more prone to shear-induced breakage. This increase in surface area increased the number of attainable densifications up to a modifier dosage of 1 vol %. While the BET surface area at the end of the cycle conducted with a modifier dosage of 5 vol % was comparable to that at the initial stages of the cycles conducted with modifier dosages of 0.25 and 1 vol %, appreciable reduction could not be obtained within a reduction time of 30 min. Thus, the effect of increased surface area as a result of the anti-agglomeration effect of the morphology modifier is negated by growth inhibition at modifier dosages greater than 1 vol %. Comparison of the BET surface area and the 2^{nd} moment revealed that increasing the modifier dosage increases the external surface area as opposed to increasing the pore area, contrary to industrial observations that it increases powder porosity. For complex morphologies, such as those obtained in nickel reduction, the pore area may be significantly larger than the external area. Powder purity was not significantly affected by modifier dosage up to a dosage of 3 vol %. Further increases in modifier dosage to 5 vol % reduced the nickel content of the powder from 99.7% to 99.4%.

The evolution of the 0^{th} and 3^{rd} moments at modifier dosages of 0.25 and 5 vol % was adequately predicted by a size-independent aggregation and growth model coupled with a constant breakage frequency model. At modifier dosages of 1 and 3 vol % different mechanisms become active at different stages in each cycle with the process largely dominated by breakage and growth in the initial stages of the cycle, while aggregation and growth become dominant towards the end.

Thus, conclusive evidence of the effect of the morphology modifier was drawn by comparing the results obtained at modifier dosages of 0.25 and 5 vol %.

From these results, increasing the modifier dosage was found to decrease the growth and aggregation rates, while the breakage rate was increased. These results are in agreement with the proposed mechanism of action of the modifier.

Iron has been found to alter the precipitation behaviour of nickel by inducing surface nucleation, thus promoting growth. Growth was found to be preferentially favoured over nucleation up to a concentration of 6 mg/L. Above this concentration, nucleation became more prominent and its extent increased with increasing Fe concentration up to 200 mg/L. While homogenous nucleation has been previously demonstrated to be absent in the presence of ferrous sulphate in buffered nickel ammine sulphate solutions, heterogeneous nucleation has been demonstrated to occur in the presence of nickel seed even in buffered solutions. While the mechanism of nucleation is still not well understood, it is thought to occur through the formation of mixed hydroxides of Fe(II)-Ni(II), suggesting that the nickel seed surface promotes hydrolysis of basic sulphates of iron and nickel. Powder purity was not affected by the presence of Fe up to a concentration of 20 mg/L.

Reduction in the presence of Fe was characterised by a size-independent aggregation and growth model with varying degrees of nucleation depending on the Fe concentration and available surface area. Iron was found to increase the growth rate up to a concentration of 20 mg/L. The agglomeration tendency decreased rapidly from approximately 40 in the absence of Fe to 0.8 at Fe=200 mg/L, indicating a strong tendency towards secondary nucleation as the Fe concentration was increased. Comparison of the 0^{th} and 2^{nd} moments in the presence of Fe indicated a strong relationship between the nucleation rate and the surface area available for reduction. Nucleation became apparent only when there was a significant drop in surface area. As the available area became insufficient to consume supersaturation by growth, supersaturation release was directed towards surface nucleation. This was further confirmed by the fact that the size-independent aggregation model gave a satisfactory fit to the 0^{th} moment when nucleation was not apparent. However, the variation of the nucleation rate with seed surface area and the mechanism of nucleation still require further investigation.

Both the morphology modifier and iron have been found to affect the morphology of the nickel particles by their effect on growth.

The morphology modifier has been proposed to promote less compact spherulites by reducing the number of growth sites on the nickel particle as a result of growth inhibition. Iron has been found to promote more compact spherulites by creating additional growth sites as a result of surface nucleation.

Previous studies have noted that the degree of compactness of the spherulites was found to increase with increasing supersaturation, which in turn increases the growth rate. However, a certain degree of compactness has been found to be desirable in order to reduce shear-induced breakage normally experienced with more fragile open spherulites.

Thus, by characterising a particular impurity as either promoting or inhibiting growth it is possible to manipulate and predict the final morphology of the nickel powder spherulites. Based on these findings, a modifier dosage of less than 1 vol % and Fe levels of less than 6 mg/L are recommended if spherical, open particles are desired. Since iron is frequently present in most nickel ores and becomes part of the reduction solution during leaching, it presents an inherent source of catalyst material. This factor, coupled with the fact that powder purity was unaffected by the presence of Fe up to a concentration of 20 mg/L, makes iron (ferrous sulphate) an economical catalyst. However, in commercial practice, reduction is never carried out in the absence of a morphology modifier (or an anti-agglomerating agent) because the high agglomeration tendency of nickel drastically reduces the nickel depletion rate to a point where the process becomes uneconomical. Due to the high cost of these additives, they are used in very minute quantities, normally not exceeding 1 vol % in dosage.

Thus, manipulating Fe levels in the reduction solution presents a great opportunity for achieving cost effective particle design.

7 SUGGESTIONS FOR FUTURE WORK

The work presented in this thesis sheds light on one of the complex problems encountered in the operation of nickel powder reduction plants i.e. the impact of foreign substances on the precipitation behaviour of nickel. However, further work on the fundamental aspects of the precipitation process needs to be conducted to enable process development. The powder reduction process technology has remained nearly unchanged for the past half a century since its inception, largely due to limited research work being conducted in this field of study.

More extensive electrochemical and experimental precipitation studies are needed in order to determine the exact rate equation and the precipitation mechanisms involved. To date there is no universal accepted rate equation for the reduction process although a number of studies have been conducted. With the recent developments in high temperature sensors (e.g. for hydrogen, pH and potential) and mixing devices most of the limitations previously encountered in experimental studies can now be easily resolved.

It is now possible through the use of moment transformation of the PSD and application of the population balance equation to identify the particulate processes responsible for powder formation. However, a fundamental understanding of the respective mechanisms of nucleation and growth is still limited. Most empirical expressions used to describe nucleation and growth requires a measurement of supersaturation. However, the convectional definition of supersaturation in terms of solubility has limited application to this system since the nickel metal precipitated is not soluble in the reduction solution. Thus, the driving force should be expressed in electrochemical terms and the overpotential which is the driving force in electrodic reactions should be equated to supersaturation as in chemical reactions. While the use of the Butler-Volmer equation for electrodic reactions is recommended as the starting point the major challenge is to measure or calculate the exchange current density (i_o) of the nickel reduction system.

Despite this challenge, this approach would yield a true measure of the driving force as opposed to surface area especially in systems where impurities can affect the surface activity of the particles.

8. REFERENCES

Agrawal, A., Kumar, V., Pandey, B.D and Sahu, K.K. (2006) "A comprehensive review on the hydro metallurgical process for the production of nickel and copper powders by hydrogen reduction," *Materials Research Bulletin*, 41, p879-892

Andreassen, J-P. (2005) "Formation mechanism and morphology in precipitation of vaterite-nano-aggregation or crystal growth," *Journal of Crystal Growth*, 274, p256-264

Andreassen, J-P. (2001) "Growth and aggregation phenomena in precipitation of calcium carbonate," *PhD Thesis*, Norwegian University of Science and Technology, Norway

Beck, R., Malthe-Sørenssen, D and Andreassen, J-P. (2007) "The onset of polycrystalline growth in precipitation of L-glutamic acid compared to an aromatic amine derivative," *In* A.E. Lewis and C. Olsen, (eds), *14th International Workshop on Industrial Crystallization*, Cape Town, South Africa, 9-11th September, p177-184

Bockris, J.O.'M and Reddy, K.N. (1970), *Modern Electrochemistry*: *An introduction to an interdisciplinary area*, Volume 2, Plenum/Rosetta Press, New York, Chapter 8.6., p986-990

Boyd, W and Essen, J.V. (2000) "Precipitation of nickel metal by hydrogen reduction- A New Perspective," *Presented at ALTA 2000 Ni/Co Conference*, Perth, 15-17 May 2000

Brugman, C.F and Kerfoot, D.G. (1986) "Treatment of nickel-copper matte at Western Platinum by the Sheritt acid leach process," *25th Annual Conference of Metallurgists*, 17-20 August 1986

Burkin, A.R. (1987) "Hydrometallurgy of nickel sulphides," In: *Extractive metallurgy of nickel, Critical reports on Applied Chemistry* 17, Ed. Burkin, A.R., Society of Chemical Industry, John Wiley and Sons, 1987, p99-150

Bramley, A.S., Hounslow, M.J and Ryall, R.L. (1996) "Aggregation during precipitation from solution: A method for extracting rates from experimental data," *Journal of Colloid and Interface Science*, 183(0530), p155-165

Chen, P.-C., Liu, S.M., Jang, C.J., Hwang, R.C., Yang, Y.L., Lee, J.S and Jang, J.S. (2003) "Interpretation of gas-liquid reactive crystallization data using a size-independent agglomeration model," *Journal of Crystal Growth*, 257, p333-343

Derenzo, S., Shimizu, P.A and Giulietti, M. (1996) "On the behaviour of adipic acid aqueous solution batch cooling crystallization," *American Chemical Society*, p145-150

Dobrokhotov, G.N and Onuchkina, N.I. (1962), *Izv. Vuzov, Tsvetnaya Metallurgiya*, 5, p72-78

Elmarghani, M.A and Sliepcevich, C.M. (1986) "Continuous nickel reduction from ammoniacal nickel sulphate solutions by hydrogen in a tubular reactor," *The Reinhart Schuhmann International Symposium. Metallurgical Soceity*, Nov 1986, p1047-1055

Evans, D.J.I. (1968) "Production of metals by gaseous reduction from solution- Processes and Chemistry," *Advances in Extractive Metallurgy*, Institution of Mining and Metallurgy, London, UK, p831-907

Gránásy, L, Puszatai, T., Tegze, G., Warren, J.A. and Douglas, J.F. (2005) "Growth and form of spherulites," *Physical review, E* 72, p011605-011615

Hounslow, M.J., Ryall, R.L and Marshall, V.R. (1988) "A discretized population balance for nucleation, growth, and aggregation," *AIChE Journal*, Volume 34, No. 11, p1821-1832

Hulburt, H.M and Katz, S. (1964) "Some problems in particle technology. A statistical mechanical formulation," *Chemical Engineering Science*, 19, p555-574

Jackson, E. (1986), *Hydrometallurgical Extraction and Reclamation*, Ellis Horwood Limited, Chapter 4, p147-200

Jones, A.G. (1993) "Particle breakage, abnormal growth and agglomeration during industrial crystallisation," *Analytical Proceedings*, Volume 30, p456-457

Jones, A.G. (2002), *Crystallization Process Systems*, Butterworth and Heinemann, Chapter 8, p215-257

Kolhinen, T and Jalkanen, H. (2005) "Thermodynamic modelling of ammoniacal nickel sulphate solutions," *Scandinavian Journal of Metallurgy* 34, p334-339

Kunda, W., Evans, D.J.I and Mackiw, V.N. (1965) "Effects of Addition Agents on the Properties of Nickel Powders produced by Hydrogen Reduction," *Presented at International Powder Metallurgy Conference*, New York, USA, 14- 17 June 1965

Kunda, W and Evans, D.J.I. (1968) "Controlling the properties of nickel powders produced by the hydrogen reduction of nickel ammine sulphate solution," *Presented at Second European Symposium on Powder Metallurgy*, Stuttgart, Germany, 7-10 May 1968

Lewis, A.E. and Hounslow, M.J. (2005) "Identifying mechanisms of nickel precipitation in a hydrogen reduction process," In: *16th Industrial Crystallisation Conference* (ed. J. Ulrich), Dresden, Germany, 11-14th September 2005, p391-398

Lewis, A.E and Ntuli, F. (2005) "An investigation into the crystallisation behaviour of nickel through reduction with hydrogen," *Research Report to Impala Refineries*, Chemical Engineering Department, University of Cape Town, 11 May 2005, p1-22

Lewis, A.E., Taty-Costodes, C.T., Ntuli, F and Nathoo, J. (2004) "An investigation into the crystallisation behaviour of nickel through reduction with hydrogen," *Research Report to Impala Refineries*, Chemical Engineering Department, University of Cape Town, 10 March 2004, p1-23

Mackiw, V.N., Lin, W.C and Kunda, W. (1957) "Reduction of nickel by hydrogen from ammonical nickel sulphate solutions," *Journal of Metals*, p786-794

Mason, T.F and Burkin, A.R. (1975) "Kinetics of reduction of aqueous cupric acetate," In: *Leaching and Reduction in Hydrometallurgy* (ed. Burkin, A.R.), IMM, London, UK, p102-109

Meddings, B and Mackiw, V.N. (1964) "The gaseous reduction of metals from aqueous solution," In: *Unit processes in hydrometallurgy* (eds. Wadsworth, M.E and Davis, F.T.), Gordon and Breach, New York, p345-384

Mullin, J.W. (2001), *Crystallization*, 4th Edition, Butterworth and Heinemann, Chapter 8, p323-324

Mumtaz, H.S and Hounslow, M.J. (2000) "Aggregation during precipitation from solution: an experimental investigation using Poiseuille flow," *Chemical Engineering Science*, 55, p5671-5681

Nagai, T and Sato, M. (1972) "An electrochemical aspect on pressure precipitation of nickel," In: *International Symposium on Hydrometallurgy* (eds. Evans, D.J.I and Shoemaker, R.S.), AIME, New York, p16-41

Needes, C.R.S. and Burkin, A.R. (1975) "Kinetics of reduction of nickel in aqueous ammoniacal ammonium sulphate solutions by hydrogen," In *Leaching and reduction in hydrometallurgy*, London: IMM, p91-96

Ntuli, F and Lewis, A.E. (2006) "The effect of a morphology modifier on the precipitation behaviour of nickel powder," *Chemical Engineering Science*, 61, p5527-5533

Ntuli, F and Lewis, A.E. (2007) "The influence of iron on the precipitation behaviour of nickel powder," *Chemical Engineering Science*, 62, p3756-3760

Ochieng, A and Lewis, A.E. (2006) "Nickel solid concentration distribution in stirred tanks," *Minerals Engineering*, Volume, 19(2), p180-189

Osseo-Asare, K. (2003) "Hydrogen reduction of metal ions: an electrochemical model," In: Hydrometallurgy 2003- Fifth International Conference in Honour of Prof. Ian Ritchie, Vol 2: Electrometallurgy and Environmental Hydrometallurgy (eds. Young, C.A., Alfantazi, A.M., Anderson, D.B., Dreisinger, D.B., Harris, B and James A.), *The Minerals, Metals & Materials Society*, p1151-1165

Randolph, A.D., Larson, M.A. (1988) *Theory of particulate processes*, Second edition. Academic Press, New York

Raul, M., Bartosch, K., Kind, M., Kuch, St., Lacmann, R., Mersmann, A. (2000) "The influence of impurities on crystallization kinetics-A case study on ammonium sulphate," *Journal of Crystal Growth*, 213, p116-128

Saarinen, T., Lindfors, L.E and Fugleberg, S. (1998) "A review of the precipitation of nickel from salts solutions by hydrogen reduction," *Hydrometallurgy*, Volume 47, p309-324

Schaer, E., Ravetti, R and Plasari, E. (2001) "Study of silica particle aggregation in a batch agitated vessel," *Chemical Engineering and Processing*, 40, p277-293

Schaufelberger, F.A and Yonkers, N.Y. (1956) "Recovery of Elemental Metal Powder from Salt Solutions," *United States Patent Office*, 2,734,821, 14 Feb 1956, p1-30

Schaufelberger, F.A. (1956) "Precipitation of metal from salt solution by reduction with hydrogen," *Journal of Metals, Trans AIME*, p695-704

Sangwal, K. (1996) "Effect of impurities on crystal growth processes," *Progress in Crystal Growth and Characterization*, 32, p3-43

Sangwal, K. (1998) "Growth kinetics and surface morphology of crystals grown from solutions: Recent observations and their interpretation," *Progress in Crystal Growth and Characterization*, 36(3), p163-248

Sherritt Gordon Mines. (1958) "The manufacture and properties of metal powders produced by the gaseous reduction of aqueous solutions," *Powder Metallurgy*, 12, p40-52

Sobol, S.I. (1993) "The problems of study of thermodynamics and kinetics of nickel and cobalt reduction by hydrogen from solutions," In: The Paul E. Queneau International Symposium, Extractive Metallurgy of copper, nickel and cobalt, Vol I. Fundamental Aspects, (eds. Reddy, R.G. & Weizenbach, R.N.), *The Minerals, Metals & Materials Society*, p803-812

Söhnel, O and Garside, J. (1992), *Precipitation*: *Basic Principles and Industrial Applications*, Butterworth and Heinemann, Oxford

Söhnel, O and Mullin, J.W. (1991) "Aggregation in batch precipitated suspension, Particle design via Crystallization," *AIChE Symposium Series*, 284, Vol 87, p182-189

Taty Costodes, V.C., Mausse, C.F., Molala, K and Lewis A.E. (2006) "A simple approach for determining particle size enlargement mechanisms in nickel reduction," *International Journal of Mineral Processing*, 78, p93-100

Zhang, Y.F and Lewis, A.E. (2006) "Effect of crystallisation on the reaction kinetics of nickel reduction by hydrogen," Shorter Communication, *Chemical Engineering Science* 61, p4120-4125

Zubryckyj, N., Kunda, W and Evans, D.J.I. (1969) “Extra-high-purity powder from nickel sulphate solution by hydrogen reduction,” *Journal of the Electrochemical Society*: *Electrochemical Technology*, 16(4), p542-546